NASA CR-2595

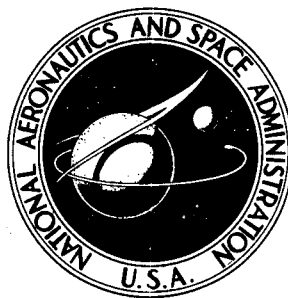# NASA CONTRACTOR REPORT

NASA CR-2595

CONTROL OF SHOCK WAVE - BOUNDARY LAYER INTERACTIONS BY BLEED IN SUPERSONIC MIXED COMPRESSION INLETS

Michael K. Fukuda, Warren G. Hingst, and Eli Reshotko

Prepared by
CASE WESTERN RESERVE UNIVERSITY
Cleveland, Ohio 44106
for Lewis Research Center

NATIONAL AERONAUTICS AND SPACE ADMINISTRATION • WASHINGTON, D. C. • AUGUST 1975

1. Report No. NASA CR-2595	2. Government Accession No.	3. Recipient's Catalog No.
4. Title and Subtitle CONTROL OF SHOCK WAVE - BOUNDARY LAYER INTER- ACTIONS BY BLEED IN SUPERSONIC MIXED COMPRESSION INLETS		5. Report Date August 1975
		6. Performing Organization Code
7. Author(s) Michael K. Fukuda, Warren G. Hingst, and Eli Reshotko		8. Performing Organization Report No. FTAS/TR-75-110
		10. Work Unit No.
9. Performing Organization Name and Address Case Western Reserve University 2040 Adelbert Road Cleveland, Ohio 44106		11. Contract or Grant No. NGL-36-027-038
		13. Type of Report and Period Covered Contractor Report
12. Sponsoring Agency Name and Address National Aeronautics and Space Administration Washington, D.C. 20546		14. Sponsoring Agency Code

15. Supplementary Notes

Final Report. Project Manager, Bernhard H. Anderson, Wind Tunnel and Flight Division, NASA Lewis Research Center, Cleveland, Ohio

16. Abstract

An experimental investigation was conducted to determine the effect of bleed on a shock wave - boundary layer interaction in an axisymmetric mixed-compression supersonic inlet. The inlet was designed for a free-stream Mach number of 2.50 with 60-percent supersonic internal area contraction. The experiment was conducted in the NASA Lewis Research Center 10- by 10-Foot Supersonic Wind Tunnel. The effects of bleed amount and bleed geometry on the boundary layer after a shock wave - boundary layer interaction were studied. The effect of bleed on the trans-formed form factor H_{tr} is such that the full realizable reduction in H_{tr} is obtained by bleeding off a mass flow equal to about one-half of the incident boundary layer mass flow. More bleeding does not yield further reduction in H_{tr}. Bleeding upstream or downstream of the shock-induced pressure rise is preferable to bleeding across the shock-induced pressure rise since, for the latter, bleed flow from the high pressure side of the interaction can detrimentally reenter the boundary layer on the upstream low pressure side. Differences between upstream and down-stream bleeding are detectable but slight and do not seem significant. Slanted holes yield lower values of H_{tr} and of compressible displacement and momentum thicknesses than normal holes. Two bleed hole sizes were tested, and no difference in performance was detected.

17. Key Words (Suggested by Author(s)) Turbulent boundary layer Supersonic inlet Boundary layer bleed Shock - boundary layer interaction	18. Distribution Statement Unclassified - unlimited STAR category 02 (rev.)	
19. Security Classif. (of this report) Unclassified	20. Security Classif. (of this page) Unclassified	21. No. of Pages 143	22. Price* $5.75

* For sale by the National Technical Information Service, Springfield, Virginia 22161

TABLE OF CONTENTS

LIST OF FIGURES

LIST OF TABLES

LIST OF SYMBOLS

a_o Coefficient for inlet contour equations

a_1 Coefficient for inlet contour equations

a_2 Coefficient for inlet contour equations

a_3 Coefficient for inlet contour equations

A_c Inlet capture area (1757 cm^2)

AS   Across the shock bleed configuration

c_p Specific heat at constant pressure

DS   Downstream of shock bleed configuration

h   Enthalpy

H_c Compressible form factor ($\delta*/\theta$)

H_{tr} Transformed form factor
$$H_c - (\gamma-1/2)M_e^2)/((T_w/T_o)(1+(\gamma-1/2)M_e^2))$$

M   Mach number

M_e Mach number at edge of boundary layer

$\dot{M}_{BL_1}$ Probe 1 boundary layer mass flow (.242 kg/sec)

$\dot{M}_{BL_5}$ Probe 5 boundary layer mass flow (.486 kg/sec)

$\dot{M}_{BLEED}$ Bleed mass flow

$\dot{M}_C$ Capture mass flow (13.52 kg/sec)

$\dot{M}_{CB}$ Total centerbody bleed mass flow

$\dot{M}_{COWL}$ Cowl bleed mass flow

$\dot{M}_{FCB}$	Centerbody bleed mass flow in first interaction region
$\dot{M}_{TB}$	Total centerbody and cowl bleed mass flow
$\dot{M}_{TOTAL}$	Total centerbody bleed
p	Static pressure
p_o	Freestream stagnation pressure ($M = 2.50$)
p_{oc}	Compressor face stagnation pressure
Pr	Prandtl number
R_c	Cowl lip radius (23.65 cm)
T	Temperature
T_e	Temperature at edge of boundary layer
T_o	Freestream stagnation temperature ($M = 2.50$)
T_w	Wall temperature
u	velocity
u_e	velocity at edge of boundary layer
US	Upstream of shock bleed configuration
x	Axial coordinate measure along inlet centerline
y	Coordinate normal to body surface
γ	Ratio of specific heats
δ	Boundary layer thickness
$\delta *$	Compressible displacement thickness
θ	Compressible momentum thickness
ρ	Density
ρ_e	Boundary layer edge density

CONTROL OF SHOCK WAVE - BOUNDARY LAYER INTERACTIONS

BY BLEED IN SUPERSONIC MIXED COMPRESSION INLETS

by Michael K. Fukuda, Warren G. Hingst,[*] and Eli Reshotko

CHAPTER I

INTRODUCTION

The growth of boundary layers on the internal surfaces of super-
sonic inlets may play a major role in the overall performance of such
inlets. Several of the ways in which boundary layers influence inlet
performance are: the modification of the external flow field due to
decreasing the amount of inviscid flow area, the forward shifting of
the shock structure, and possibly, the separation of the boundary layer
which may cause inlet unstart.

Boundary layer separation is usually associated with adverse
pressure gradients and/or shock-boundary layer interactions which are
necessarily present in supersonic inlets. Thus the characteristics of
boundary layer growth on the internal surfaces of a supersonic inlet
may cause changes, sometimes very drastic ones, in the performance
of such an inlet.

To control the growth of the boundary layer on the internal
surfaces of an inlet, a system of bleeding the boundary layer at
various locations may be incorporated into the inlet. The bleed
system usually removes the low momentum portion of the boundary layer
through porous sections, slots or scoops. In this way, the size and
characteristics of the boundary layer are in some way controlled.

[*]NASA Lewis Research Center, Cleveland, Ohio

A penalty is incurred, however, in maintaining a 'healthy' (non-separating) boundary layer by bleeding. The bleed mass flow is not usually reinjected into the inlet, so part of the captured mass flow is lost. To compensate for this loss in mass flow, a larger nacelle may be needed which would increase the friction drag and inlet weight. In addition, the bleed flow is usually vented overboard through bleed exits, a phenomenon which also incurs a drag penalty. Thus it is desirable to minimize the amount of boundary layer bleed while still providing good internal aerodynamic performance.

Experiments incorporating bleed systems in a supersonic inlet have been performed previously by Cubbison et al[1], Hingst and Johnson[2], and Smeltzer and Sorensen[3]. There have also been studies by Kilburg and Kotansky[4] and Strike and Rippey[5] on shock-boundary layer interactions with and without bleed in simpler geometries. There has also been a study by McLafferty and Ranard[6] on the effect of bleed for a given geometry and the effect of the bleed system geometry on the bleed mass flow. These types of information have ultimately been used to design supersonic inlets with bleed systems to obtain optimum performance as in Smeltzer and Sorensen[7] and Syberg and Koncsek[8].

The purpose of this experiment was to further clarify and quantify the effects of bleed on the characteristics of a boundary layer through a shock-boundary layer interaction in a supersonic inlet. With this aim, several types of bleed configurations have been studied. These configurations included variation of bleed hole size, angle of bleed holes to the surface normal and bleed hole pattern. In addition to

the porous or discrete hole type of bleed, a scoop was also used.
Each of the configurations was tested over a range of bleed mass
flows. The Reynolds number and shock positions were also varied.

In order to best reproduce the Mach number and pressure variations
encountered in mixed compression inlets as well as to study the effects
of bleed on successive shock-boundary layer interactions, the study
was conducted on an actual inlet tested in the NASA-Lewis Research
Center 10 x 10 Foot Supersonic Wind Tunnel. The supersonic inlet used
for this experiment was a mixed compression axisymmetric inlet having
a design Mach number of 2.5 and with 60% of the supersonic area con-
traction occuring internally. The inlet was operated with a cold-
pipe choked plug assembly instead of an engine. It was basically the
same inlet used in the previously cited studies of references 1 and 2
with the exceptions of new external cowl pieces to control the bleed
mass flow rate and a bleed region in place of a solid wall in the
first centerbody shock-boundary layer interaction region.

The bleed configurations investigated in this test were chosen
based on the experimental results reported in references 1, 2 and 5
as well as on computations using the methods of references 9 to 12.

These tests were conducted at a freestream Mach number of 2.50.
Total pressure measurements were made upstream and downstream of the
shock impingement points on the cowl and centerbody. Static pressure
measurements were also made along cowl and centerbody forces. In
addition, bleed flow rates were measured for cowl and centerbody bleed

3

systems. Data are reported for a unit Reynolds number of 8.2×10^{6}

per meter.

CHAPTER II

APPARATUS AND PROCEDURE

Section 2.1 Inlet Geometry

An axisymmetric mixed compression inlet with a design Mach number of 2.50 was used in this study. At the design condition, 40% of the supersonic area contraction was external and 60% was internal. The inlet had a capture radius, R_c, of 23.65 cm and a capture area, A_c, of 1757 square cm. The capture mass flow at the design condition was 13.52 kg/sec. The inlet was tested with a cold-pipe choked plug assembly in place of an engine. A photograph of the inlet mounted in the test section of the NASA-Lewis 10' x 10' Supersonic Wind Tunnel is shown in Figure 2.1.

The external compression was accomplished with a 12.5° half angle cone which remained conical to a non-dimensional inlet station, $\frac{x}{R_c}$, of 2.88. The distance x is measured along the centerline of the centerbody from the spike up. At the design Mach number, the oblique shock wave generated by the cone tip passed just over the cowl lip and 0.25% of the capture mass flow was spilled. Figure 2.2 shows a schlieren photograph of the cone tip shock passing over the cowl lip. At the design condition, the angle from the cone tip to cowl lip was 26.47° and the shock angle was 26.72°. The cowl lip began at an

Section 2.3 Bleed System

To study the behavior of the boundary layer under varying bleed conditions, different bleed sections were used. The different types of bleed sections were 'porous' bleed, consisting of discrete rows of holes, and a scoop. Each of the porous sections had a different hole diameter or angle to the surface. The angles were 20° and 90° to the surface tangent and the hole diameters were 0.318 cm and 0.159 cm. The rows of holes were staggered to provide a more uniform bleed distribution.

The model was constructed to permit easy removal and interchange of the bleed sections. These interchangeable sections were in the forward centerbody section, around the first shock-boundary layer interaction region, and in the forward cowl section, around the first cowl shock-boundary layer interaction region. Bleed was also incorporated into the aft centerbody region around the geometric throat of the inlet. The aft centerbody bleed was of the porous type and was not changed during the experiment. The aft centerbody bleed was primarily used to prevent inlet unstart due to boundary layer separation.

Each of the porous interchangeable sections consisted of rows of holes of equal diameter with the holes in each row being equally spaced circumferentially. There weren't any bleed sections in which the hole diameters or angles were mixed. In addition, the distance between the rows of bleed holes for a given bleed section remained constant and the measurements of length of a bleed section was from the center of the first row of holes to the center of the last row of

8

holes.

In the forward centerbody interaction region, the 20° slanted

holes and the scoop types of bleed configurations were used. The data

of McLafferty and Ranard[6] indicated that a larger amount of mass flow

could be extracted by using slanted holes in place of normal ones.

Since the forward centerbody bleed mass flow was not physically

separated from the aft centerbody bleed mass flow, the largest plenum

pressure recovery bleed configuration for the forward centerbody bleed

was needed. The data of reference 6 indicated that slanted hole bleed

sections would have a much higher plenum pressure recovery than normal

hole bleed sections and this was the motivation for using the slanted

hole bleed configuration in the forward centerbody interaction region.

In addition, a nozzle directed downstream was attached to the aft

centerbody bleed region to try and alleviate mixing between the for-

ward and aft centerbody bleed and possible recirculation of the aft

centerbody bleed through the forward centerbody bleed region. The

nozzle and aft centerbody bleed region are shown in Figure 2.6.

The two minor axes of holes used in the forward centerbody inter-

action region were 0.318 cm and 0.159 cm and these were at 20° to the

surface tangent. The 0.159 cm hole bleed region consisted of 10 rows

of holes in an alternating pattern with 180 holes per row. This bleed

section encompassed the $\frac{x}{R_c}$ distance from 2.72 to 2.92 as measured from

the center of the first row of holes to the center of the last row

of holes. The 0.318 cm hole bleed region consisted of 5 rows of holes

in the alternating pattern from $\frac{x}{R_c} = 2.73$ to $\frac{x}{R_c} = 2.92$ with 360 holes per row. These bleed sections are shown in Figure 2.7a and b.

An axisymmetric scoop was also used in the forward centerbody interaction region. The scoop height was 0.127 cm and the leading edge was located at an $\frac{x}{R_c}$ location of 2.84. The scoop is shown in Figure 2.7c.

The aft centerbody bleed consisted of 5 rows of 0.318 cm diameter normal holes with 221 holes per row in an alternating pattern. This bleed section was located from $\frac{x}{R_c} = 3.37$ to 3.44. Again, the aft centerbody bleed region was not changed during the experiment and was used mainly to prevent boundary layer separation and inlet unstart. A nozzle was attached to this bleed section as explained previously and shown in Figure 2.6.

Bleed on the cowl was used in the vicinity of the first reflected shock interaction region. Three different bleed sections used were: (1) 10 rows of 0.318 cm diameter holes normal to the surface with 300 holes per row, (2) 20 rows at 0.159 cm diameter holes normal to the surface with 600 holes per row and (3) 6 rows at 0.318 cm minor axis holes at 20° to the surface tangent with 300 holes per row with all bleed sections having rows in an alternating pattern. The 0.318 cm diameter normal hole bleed section ran from an $\frac{x}{R_c}$ location of 3.05 to 3.29, the 0.159 cm diameter normal bleed section from $\frac{x}{R_c} = 3.12$ to 3.28 and the 0.3175 cm minor axis slanted holes from $\frac{x}{R_c} = 3.123$ to 3.29. The cowl bleed regions are shown in Figures 2.8a, b, and c.

10

To control the amount of bleed on the cowl and centerbody an apparatus used by Sanders and Mitchell[13] was also used in this experiment. This apparatus consisted of two pairs of pipes that were fitted over the bleed exit passages. The amount of mass flow through each pipe was controlled by remotely actuated calibrated conical exit plugs and there was one pair of pipes each for cowl and centerbody. The centerbody bleed pipes were 17.47 cm in diameter and the cowl pipes had a diameter of 25.60 cm. One set of these pipes is shown in Figure 2.1.

The effect of bleed location, relative to the shock location, on the boundary layer was investigated by opening or closing rows of holes. Three general bleed hole patterns were used in determining the effectiveness of bleed location relative to the shock location. These three general patterns were rows of holes opened upstream of the shock reflection, those opened downstream of the shock reflection and those opened across the shock reflection. The three types were not mixed and the number of rows of holes opened was primarily determined by trying to obtain a significant range of bleed mass flow rates.

A list of the locations of the center of the bleed holes in a row for bleed sections on the centerbody and cowl are presented in Tables 2-IV and 2-V respectively.

Section 2.4 Pressure Measurements

Static pressure measurements were made along cowl and centerbody surfaces with the wind tunnel's DAMPR (Digital Automatic Multiple

11

Pressure Recorder) system. The system basically consists of a pressurized tank on which tubing from the static taps is attached. A capsule connected to an electric sensing system is placed between the static pressure line on the outside of the tank and high pressure in the interior of the tank. The tank is slowly depressurized and when the unknown static pressure equals the tank pressure, an electric circuit is broken. The time of the current breakage is then recorded and stored. After all capsule circuits are broken, the data is recovered and pressures are calculated. The basic DAMPR system consisted of 2 tanks with a capacity of measuring 160 pressures each. Additional information on the DAMPR system may be found in reference 14.

Most of the static pressure measurements were made on the bottom centerline of the inlet with static pressure taps in the bleed regions staggered circumferentially so not to be directly behind a bleed hole. The $\frac{x}{R_c}$ locations of the individual pressure taps on the centerbody and cowl are given in Tables 2-VI and 2-VII respectively. Note that the number of static taps for the different bleed sections may not be the same.

Total pressure surveys were taken at the compressor face to measure the total pressure recovery of the inlet. There were 6 rakes which contained 12 total pressure taps per take at an $\frac{x}{R_c}$ station of 7.40. The position of the compressor face rakes are shown in Figure 2.3.

The crux of the experiment was the measurement of boundary layer

profiles before and after the shock-boundary layer interaction regions. Surveys of the boundary layers were made with a total of seven traversing total pressure probes. Four of these probes were located on the centerbody and three on the cowl. The centerbody probe tips were located at $\frac{x}{R_c}$ stations of 2.68, 3.04, 3.30 and 3.55 and are referred to as Probes 1 to 4 respectively. The cowl probe tips were located at $\frac{x}{R_c}$ stations of 3.01, 3.36 and 3.55 and are referred to as Probes 5 to 7 respectively. All probe tips were flattened with an inner height of 0.010 cm and an outer height of 0.020 cm with a width of 0.096 cm. A schematic of a single probe is shown in Figure 2.9 and a view of probe locations relative to the theoretical shock impingement points is shown in Figure 2.5. A photograph showing Probes 1 and 2 as well as the centerbody bleed regions is presented in Figure 2.10. Surface measurements of static pressures at each axial probe tip location were made as well as surface temperature measurements by thermocouples also at these locations.

The traversing boundary layer probes were made to step twenty-five times through a given distance, taking twenty-six data points. The total distance of travel was determined before the experiment began by the approximate boundary layer thickness. The approximate total travel distance for Probes 1, 2 and 5 was 0.95 cm, for Probes 3 and 4, 0.76 cm and for Probes 6 and 7, 1.27 cm. The probe step sizes for the first five steps were approximately half the size of the last twenty steps. The step size of the last twenty steps remained relatively constant for a given probe.

13

The first data point actually taken corresponded to the probe tips resting on the wall. To determine whether the probes were actually resting on the wall, an electrical contact method was used which gave a visual indication when the probe touched the wall.

The boundary layer probes were placed in different circumferential locations to avoid wake effects from other probes. The circumferential positions of the respective probes are indicated in Table 2-VIII where 0° was the top centerline of the inlet.

Since a pitot tube was used in measuring the total pressure profile in the boundary layer, it was necessary to ascertain the effects of the shear layer and the presence of the wall on the pressure measurements. Specifically, was the pressure measured that on the axis of the pitot tube? There have been studies done on the behavior of pitot tubes in incompressible flow by Young and Maas[15] and McMillan[16], and in compressible flow by Allen[17], Wilson[18], and Wilson and Young[19]. The studies in compressible flow have been somewhat conflicting and have yet to be fully resolved. Several of the researchers have given corrections to the actual measurement point which involved defining a new measurement point, which was usually higher than the center of the probe. This correction was used instead of trying to correct the measured pressure to that at the probe center. In all cases considered, the measured pressure corresponded to a pressure somewhere within the probe opening. In particular, Wilson and Young[19] have concluded that at Mach 2.0 the aerodynamic interference of a pitot tube was negligible when the outside diameter of the pitot tube was

less than 6% of the boundary layer thickness.

After examining the data presented it was decided to make a correction to the probe measurement point. The correction used was to add 0.00152 cm to the probe centerline and this was used as the measurement point. It should be noted that in all cases except for extremely large bleed rates on the cowl, the outside height of the pitot tube was less than 6% of the boundary layer thickness and that the correction used had very little effect on computation of boundary layer parameters.

Section 2.5 Testing Procedure and Inlet Operation

The experiment was conducted in the NASA-Lewis Research Center 10-by 10-Foot Supersonic Wind Tunnel at a test section Mach number of 2.50. Data were taken at two unit Reynolds numbers of 8.2 and 5.75 x 10^6 per meter although only the data for the higher Reynolds number will be presented.

The inlet was operated in two modes of terminal shock position. In the supercritical mode, the terminal shock was positioned downstream of the geometric throat while in the critical mode the terminal shock was held at the geometric throat. Most of the data were taken in the supercritical mode because the terminal shock was much more stable for low bleed rates. The difference between the two modes was that the shock waves were allowed to reflect past the geometric throat in the supercritical mode while the shock system terminated at the throat in the critical mode.

15

The testing procedure was to set the bleed pipe exit plugs to obtain maximum mass flow through the bleed regions once the inlet was at the design Mach number. Then the centerbody bleed pipe exit plugs were gradually closed and data were taken. The procedure was repeated until either inlet unstart was imminent or else there was no bleed mass flow. The centerbody bleed mass flow was then increased and the same procedure was followed on the cowl.

Section 2.6 Data Reduction Procedure

The data were acquired and reduced using the NASA-Lewis Research Center automatic data reduction system together with the data reduction computer program used by prior investigators (ref. 1 and 2) but modified slightly for the needs of the present task. The data handling system included digitizing and permanently recording all the data. Pressure measurements were made by the DAMPR system, explained in section 2.4, and were automatically digitized and recorded by the CADDE (Central Automatic Digital Data Encoder) system. Data taken by voltage measurements were first digitized by the AVD (Automatic Voltage Digitizer) system then recorded by CADDE. The CADDE system permanently recorded the digitized information on magnetic tape and these data were in turn sent to an IBM 360 Digital Computer to be processed. More information on the automatic data reduction system is presented in reference 14.

The digitized data recorded by CADDE and processed on the IBM 360 could then be sent back to the researchers and displayed by

16

means of a Fax-plotter and tabulated by an automatic typewriter. In addition, key pressure and model parameter measurements were duplicated and the results displayed. These were totally independent of the automatic data reduction system and were obtained as a safe-guard against a failure in that system.

After the data were taken, digitized and recorded for a given test condition, it was sent from CADDE to the digital computer. As full on line data reduction and printing were very cumbersome and time consuming, the data were selectively reduced and these results were printed by a remote terminal. The selective data reduction computation options included preselected static and total pressures, boundary layer Mach number and velocity profiles and integral para-meters.

After all of the data for a given bleed geometry had been taken, they were inputted into the digital computer to be reduced. A complete output of all calculations was then received for close inspection.

The data reduction program computed and printed:

    (1)   Static and total pressures
    (2)   Boundary layer Mach number, temperature and velocity profiles
    (3)   Boundary layer integral parameters
    (4)   Compressor face total pressure recovery and distortion
    (5)   Model parameters (such as angle of attack)
    (6)   Wind Tunnel parameters (such as unit Reynolds number)
    (7)   Inlet and Bleed Mass Flows

The assumptions made in the boundary layer calculations are enumerated in Appendix A. Also, the compressor total pressure recovery calcul-ations were done by a mass flow weighted averaging.

TABLE 2-I

INLET CONTOUR EQUATIONS

$$R = a_o + a_1 \left(\frac{x}{R_c}\right) + a_2 \left(\frac{x}{R_c}\right)^2 + a_3 \left(\frac{x}{R_c}\right)^3$$

Centerbody Coefficients

a_o	a_1	a_2	a_3	Minimum Axial Distance
0	0.22169	0	0	0
-.11756	-.068682	0.24482	-.045077	2.873
-80.1714	67.683	-18.849	1.7467	3.435
9.0579	-6.3711	1.6356	-0.14195	3.650
-.54987	0.9722	-0.23265	0.016264	4.079
-1.0072	1.1198	-0.23362	0.014197	4.724

Cowl Coefficients

1.000	0	0	0	2.009
0.63207	0.33541	-0.087699	0.0049357	2.397
0.79107	0.21454	-0.061232	0.0036622	2.883
6.3449	-4.24523	1.1257	-0.10095	3.543
7.3753	-4.5529	1.07795	-0.085642	3.865
2.3502	-0.86963	0.17807	-0.012557	4.079
1.3465	-8.2013	1.7846	-0.012943	4.294
-0.051811	0.6415	-0.014378	0.010736	4.863

TABLE 2-II

METHOD OF CHARACTERISTICS PRESSURE DISTRIBUTION ON THE CENTERBODY

$\dfrac{x}{R_c}$	M	$\dfrac{p}{p_o}$	$\dfrac{x}{R_c}$	M	$\dfrac{p}{p_o}$
2.082	2.21	.092	3.128	1.61	.229
2.162	2.21	.093	3.152	1.60	.231
2.239	2.20	.093	3.175	1.59	.235
2.311	2.20	.093	3.197	1.58	.240
2.380	2.20	.093	3.217	1.57	.244
2.445	2.20	.093	3.237	1.56	.248
2.507	2.20	.093	3.257	1.55	.251
2.566	2.20	.093	3.276	1.54	.254
2.622	2.20	.093	3.296	1.53	.257
2.674	2.20	.093	3.316	1.54	.255
2.724	2.20	.094	3.336	1.55	.250
2.771	2.20	.094	3.356	1.57	.244
2.815	2.20	.094	3.376	1.58	.239
2.857	2.20	.094	3.396	1.59	.234
2.879	1.70	.201	3.416	1.60	.231
2.916	1.69	.204	3.436	1.61	.229
2.952	1.70	.202	3.456	1.64	.218
2.986	1.70	.200	3.476	1.13	.438
3.017	1.71	.198	3.496	1.18	.411
3.047	1.69	.203	3.517	1.18	.411
3.075	1.64	.218	3.537	1.18	.415
3.102	1.62	.227	3.557	1.14	.433

TABLE 2-III

METHOD OF CHARACTERISTICS PRESSURE DISTRIBUTION ON THE COWL

$\frac{x}{R_c}$	M	$\frac{p}{p_o}$	$\frac{x}{R_c}$	M	$\frac{p}{p_o}$
2.009	2.17	.099	3.093	1.72	.196
2.091	2.12	.105	3.118	1.71	.199
2.171	2.09	.110	3.141	1.70	.203
2.248	2.07	.115	3.164	1.68	.207
2.321	2.04	.119	3.185	1.67	.211
2.391	2.02	.123	3.205	1.66	.215
2.457	2.01	.126	3.224	1.64	.220
2.521	1.96	.136	3.243	1.63	.224
2.582	1.93	.142	3.262	1.23	.392
2.640	1.91	.147	3.285	1.23	.395
2.696	1.88	.152	3.308	1.25	.384
2.748	1.86	.159	3.332	1.25	.386
2.798	1.83	.165	3.355	1.22	.400
2.845	1.81	.171	3.379	1.21	.404
2.871	1.80	.175	3.404	1.20	.407
2.910	1.78	.180	3.429	1.19	.416
2.943	1.76	.185	3.454	1.21	.402
2.977	1.75	.187	3.478	1.23	.392
3.009	1.75	.189	3.504	1.24	.390
3.039	1.74	.191	3.523	1.26	.380
3.067	1.73	.193	3.542	1.27	.373
			3.561	1.29	.361

TABLE 2-IV

CENTERBODY BLEED HOLE POSITIONS

Small Slanted Holes (0.159 cm diameter)

Row	$\dfrac{x}{R_c}$
1	2.715
2	2.741
3	2.765
4	2.789
5	2.813
6	2.837
7	2.862
8	2.886
9	2.910
10	2.934

Large Slanted Holes (0.318 cm diameter)

1	2.728
2	2.777
3	2.825
4	2.873
5	2.922

Scoop at $\dfrac{x}{R_c}$ location of 2.84.

The $\dfrac{x}{R_c}$ positions are given for the center of the bleed hole.

TABLE 2-V

COWL BLEED HOLE DISTRIBUTION

Large Normal Holes (0.318 cm diameter)

Row	$\dfrac{x}{R_c}$
1	3.125
2	3.142
3	3.160
4	3.177
5	3.195
6	3.212
7	3.230
8	3.247
9	3.264
10	3.282

Small Normal Holes (0.159 cm diameter)

Row	$\dfrac{x}{R_c}$
1	3.125
2	3.134
3	3.142
4	3.151
5	3.160
6	3.168
7	3.177
8	3.186
9	3.195
10	3.203
11	3.212
12	3.221
13	3.230
14	3.238
15	3.247
16	3.256
17	3.264
18	3.273
19	3.282
20	3.291

Table 2-V, cont'd.

Slanted Holes (0.318 cm minor axis)

Row	$\frac{x}{R_c}$
1	3.050
2	3.098
3	3.146
4	3.195
5	3.243
6	3.291

The $\frac{x}{R_c}$ positions are given for the center of the bleed hole.

TABLE 2-VI

CENTERBODY STATIC TAP LOCATIONS

Tap Number	$\frac{x}{R_c}$	Tap Number	$\frac{x}{R_c}$
1	2.524	17	3.201
2	2.578	18	3.222
3	2.621	19	3.224
4	2.728	20	3.265
5	2.774	21	3.316
6	2.825	22	3.334
7	2.873	23	3.351
8	2.922	24	3.369
9	2.943	25	3.387
10	2.965	26	3.404
11	2.986	27	3.421
12	3.008	28	3.440
13	3.061	29	3.459
14	3.115	30	3.502
15	3.158	31	3.523
16	3.179	32	3.588

PROBE STATIC TAP LOCATION

Probe	$\frac{x}{R_c}$
1	2.686
2	3.039
3	3.303
4	3.547

Static tap locations only given for scoop and small slanted hole bleed pieces.

TABLE 2-VII

COWL STATIC TAP LOCATIONS

Tap Number	$\frac{x}{R_c}$ (A)	$\frac{x}{R_c}$ (B)
1	2.818	2.818
2	2.872	2.872
3	3.034	3.034
4	3.088	3.074
5	3.125	3.122
6	3.142	3.170
7	3.160	3.219
8	3.177	3.267
9	3.194	3.315
10	3.212	3.362
11	3.229	3.405
12	3.247	3.426
13	3.264	3.448
14	3.281	3.469
15	3.362	3.491
16	3.405	3.512
17	3.426	3.534
18	3.448	3.676
19	3.469	3.724
20	3.491	3.745
21	3.512	
22	3.534	
23	3.676	
24	3.724	
25	3.745	

PROBE STATIC TAP LOCATIONS

Probe	$\frac{x}{R_c}$
1	3.008
2	3.394
3	3.555

Column A gives the $\frac{x}{R_c}$ locations for both normal hole bleed regions while Column B gives the $\frac{x}{R_c}$ location for the slanted hole bleed region.

25

TABLE 2-VIII

AXIAL AND CIRCUMFERENTIAL PITOT PROBE LOCATIONS

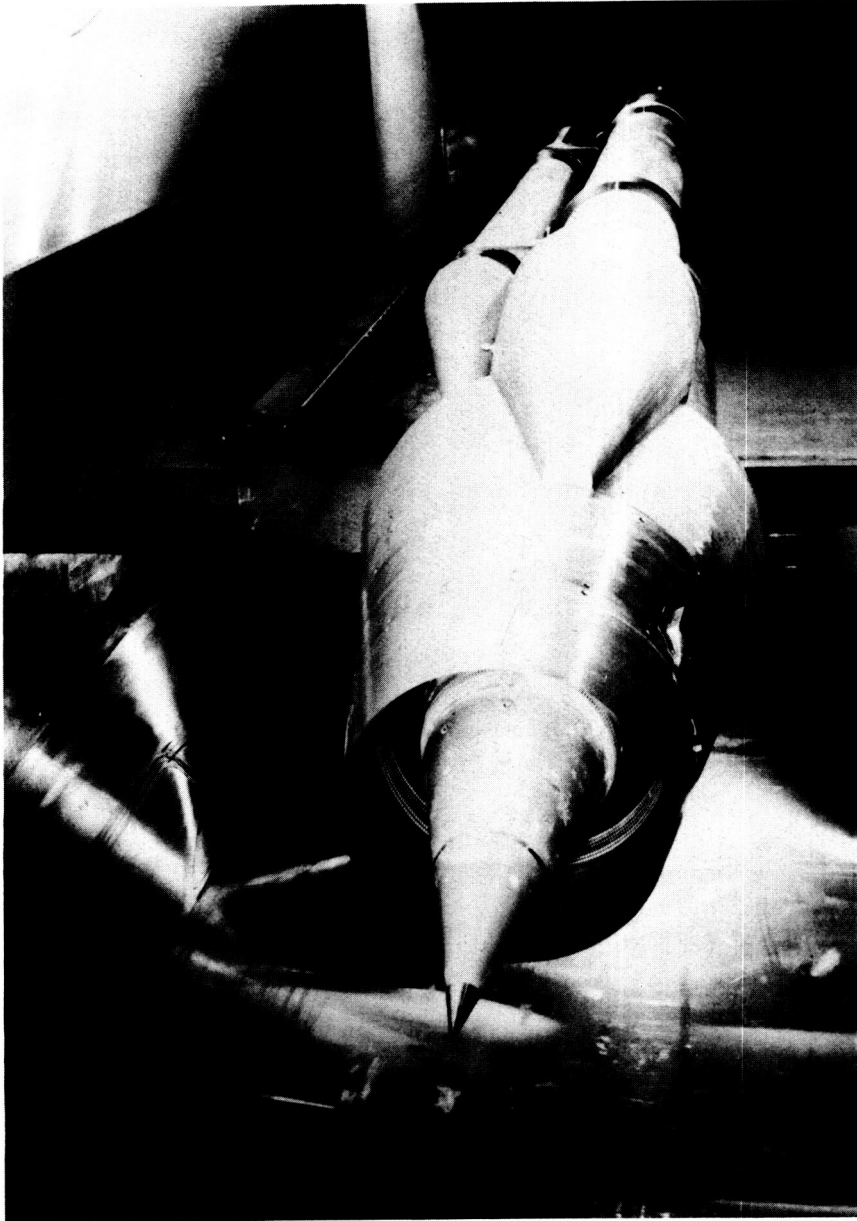| Probe	Axial Locations $(\frac{x}{R_c})$	Angular Location
1	2.686	345
2	3.039	0
3	3.303	180
4	3.547	167.5
5	3.008	146.25
6	3.394	168.75
7	3.555	191.25

Figure 2.1 Photograph of Inlet Mounted in the Test Section
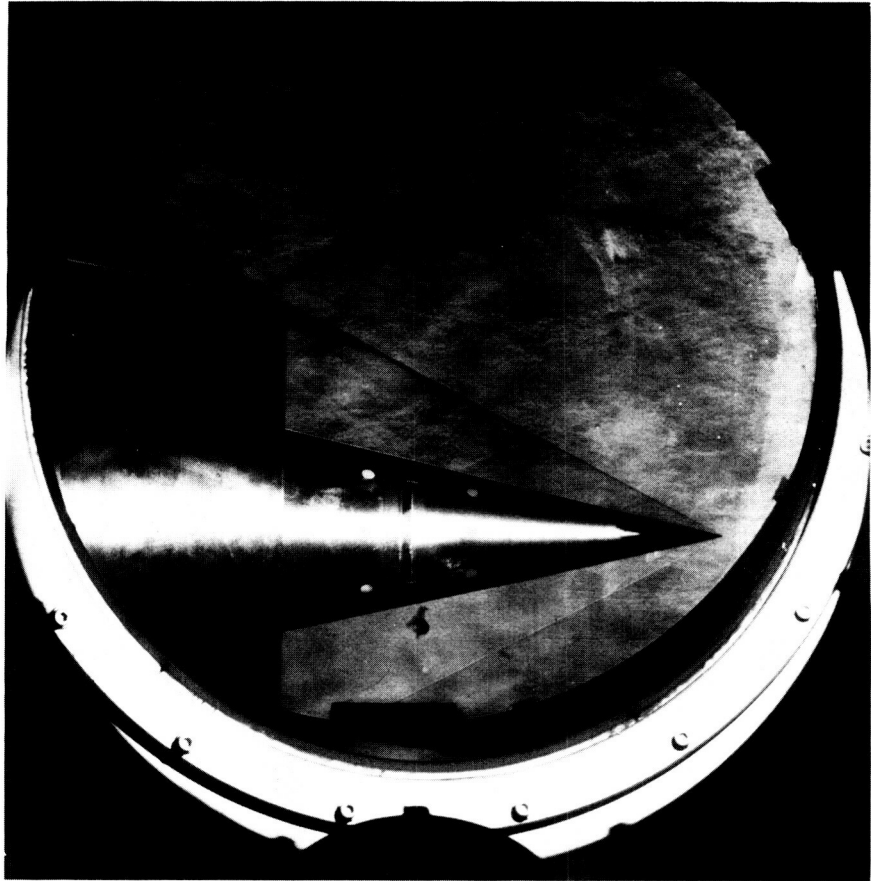
Figure 2.2   Schlieren Photograph of the Inlet Showing
the Cone Tip and Cowl Lip Shock Waves

support struts

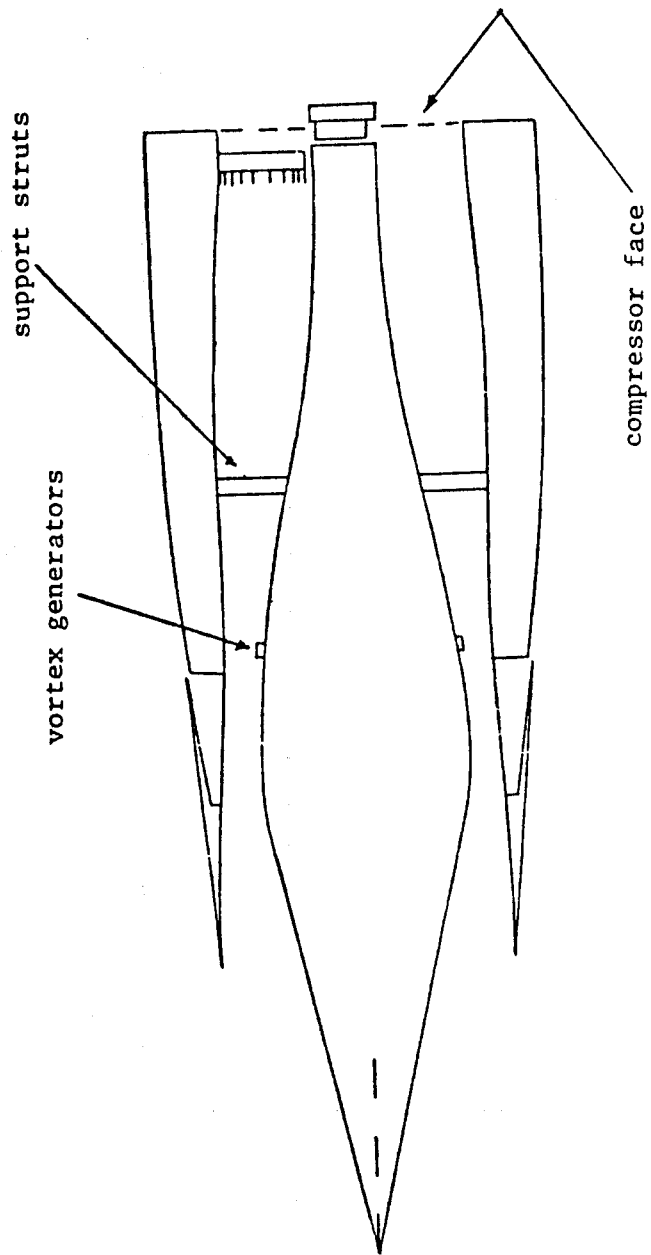vortex generators

compressor face
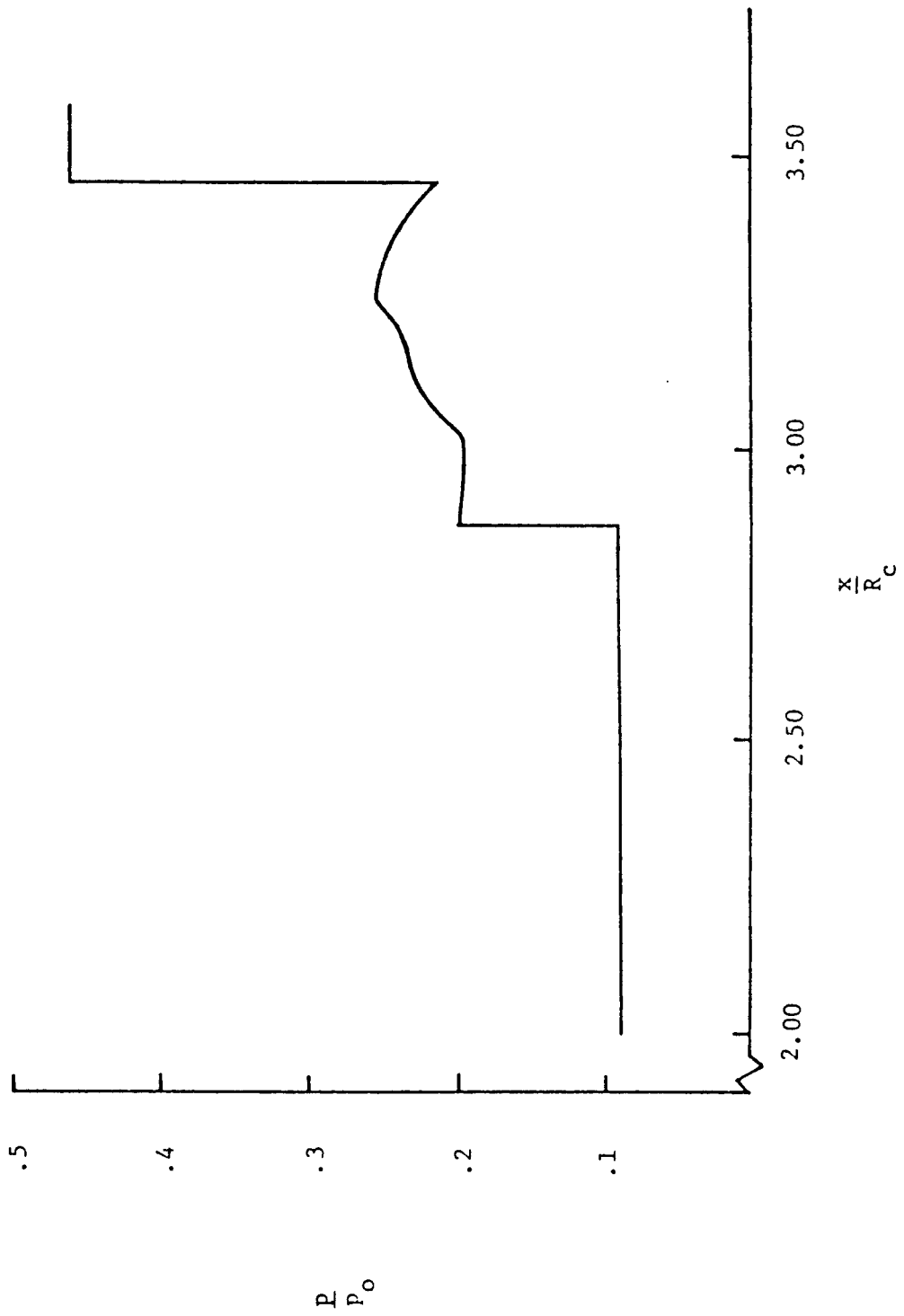
Figure 2.3   Inlet Schematic
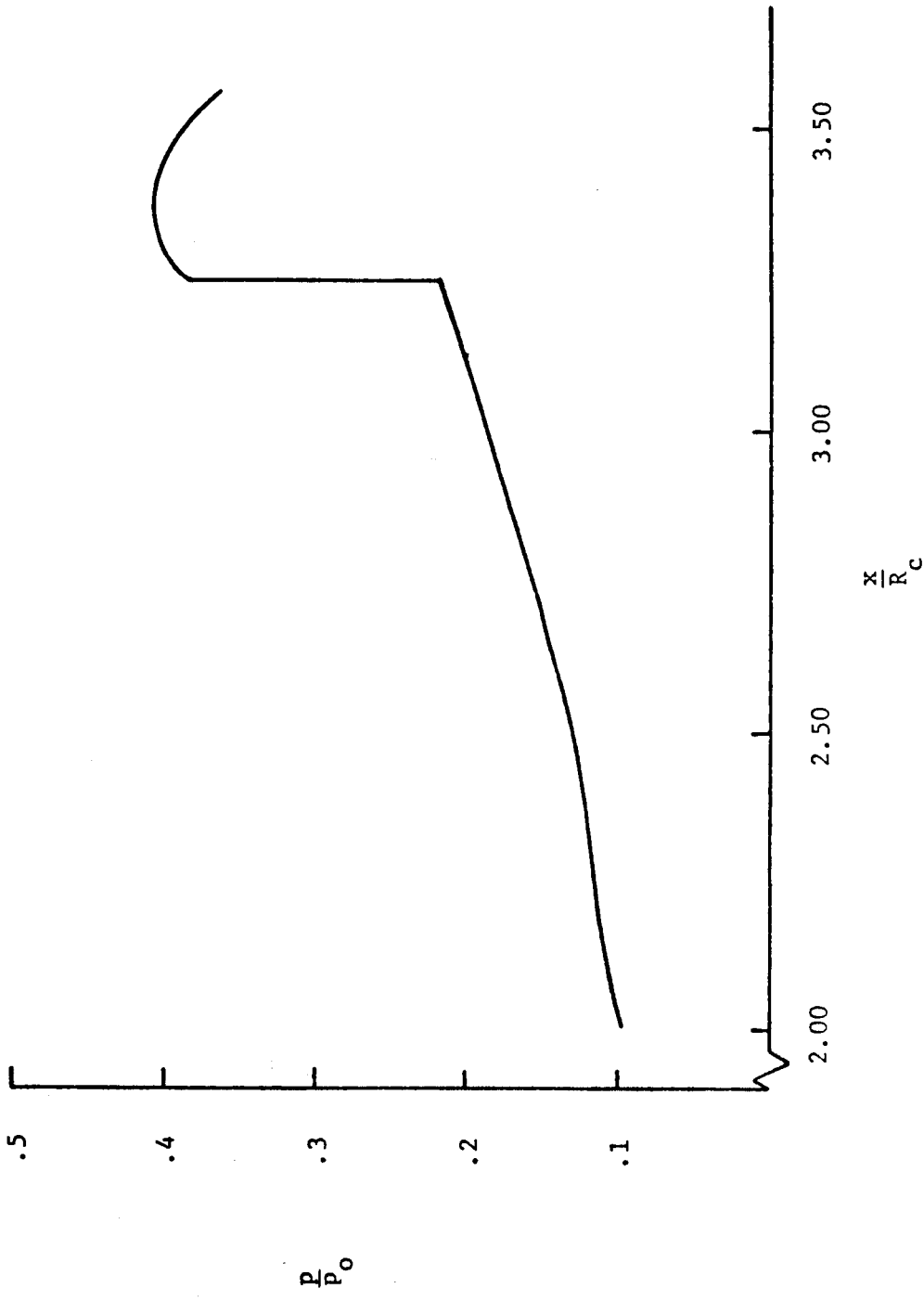
Figure 2.4a Theoretical Centerbody Static Pressure Distribution

Figure 2.4b Theoretical Cowl Static Pressure Distribution

Method of characteristics solution

δ^* added solution

Probe 7
$\dfrac{x}{R_c} = 3.555$

Probe 6
$\dfrac{x}{R_c} = 3.394$

Probe 5
$\dfrac{x}{R_c} = 3.006$

Probe 4
$\dfrac{x}{R_c} = 3.557$

Probe 3
$\dfrac{x}{R_c} = 3.303$

Probe 2
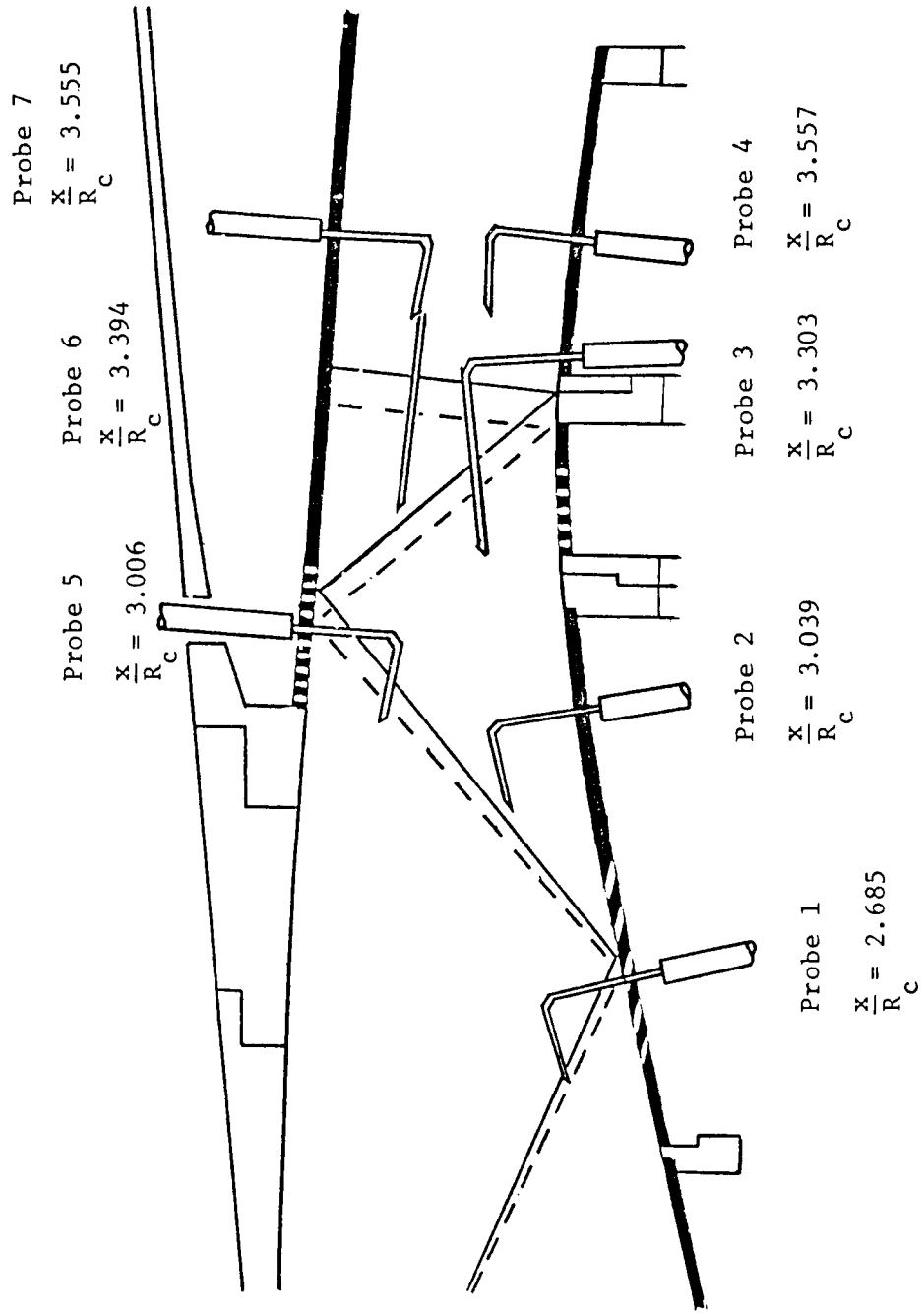$\dfrac{x}{R_c} = 3.039$

Probe 1
$\dfrac{x}{R_c} = 2.685$

Figure 2.5 Comparison of Method of Characteristics and δ^* Added Shock
Impingement Locations
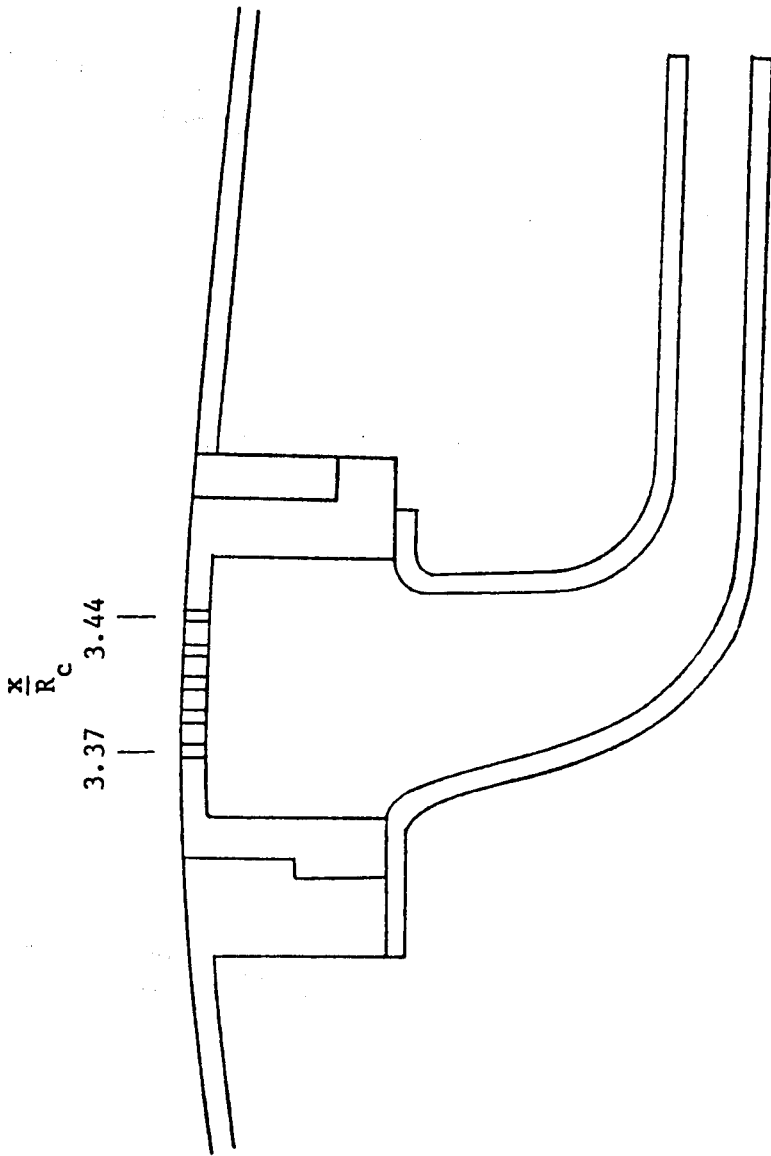
Figure 2.6   Schematic of Aft Centerbody Bleed and Nozzle

33

.318 cm   .238 cm

$\frac{x}{R_c} = 2.92$

$\frac{x}{R_c} = 2.73$
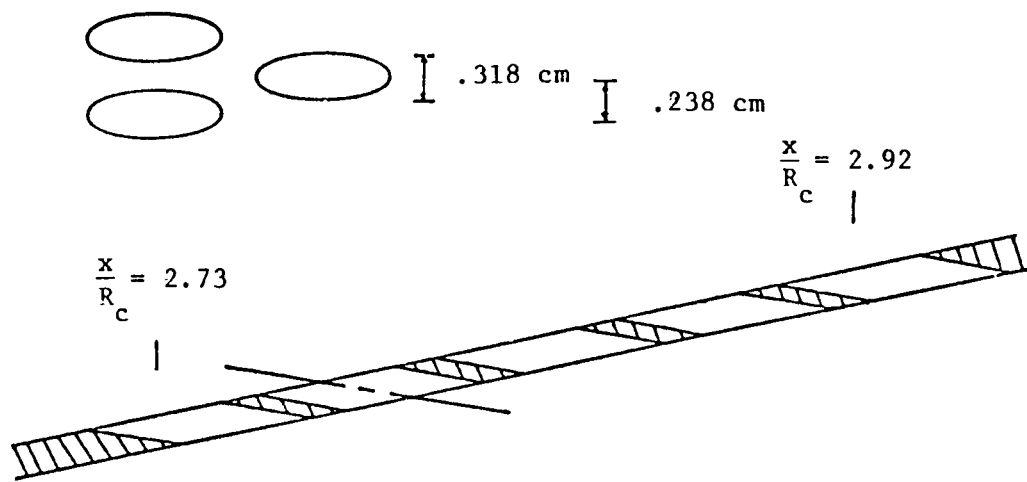
Figure 2.7a   Forward Centerbody Bleed Region (Large Slanted Holes)

.159 cm   .119 cm

$\frac{x}{R_c} = 2.93$

$\frac{x}{R_c} = 2.72$
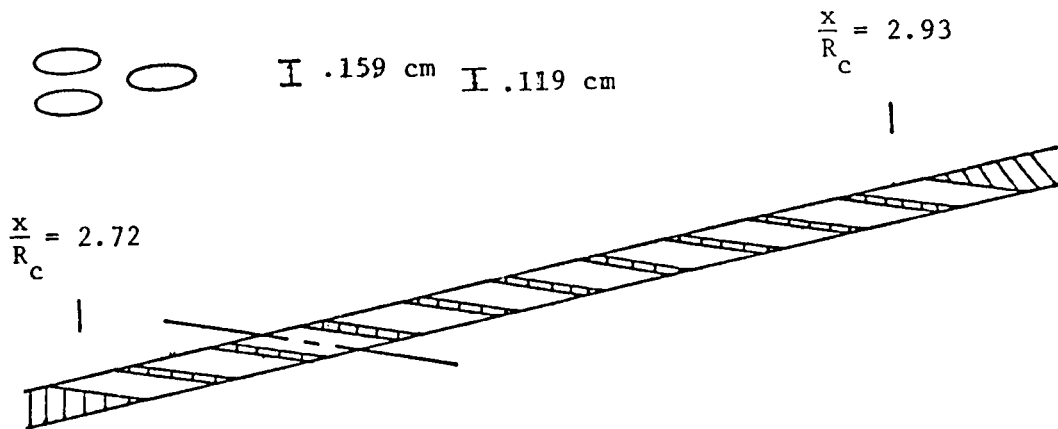
Figure 2.7b   Forward Centerbody Bleed Region (Small Slanted Holes)

$$\frac{x}{R_c} = 2.84$$

.127 cm
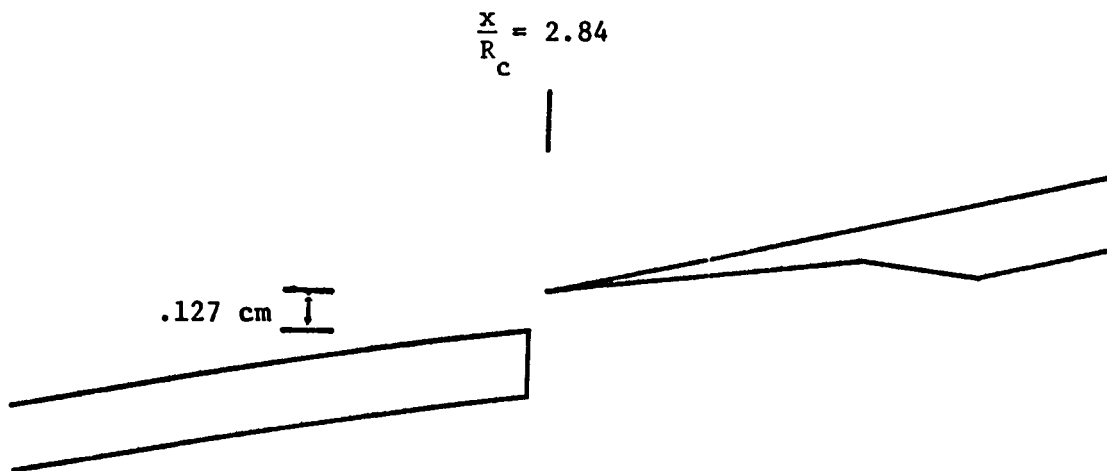
Figure   Figure 2.7c   Forward Centerbody Bleed Region (Scoop)

.318 cm   .238 cm

$$\frac{x}{R_c} = 3.13$$

$$\frac{x}{R_c} = 3.28$$
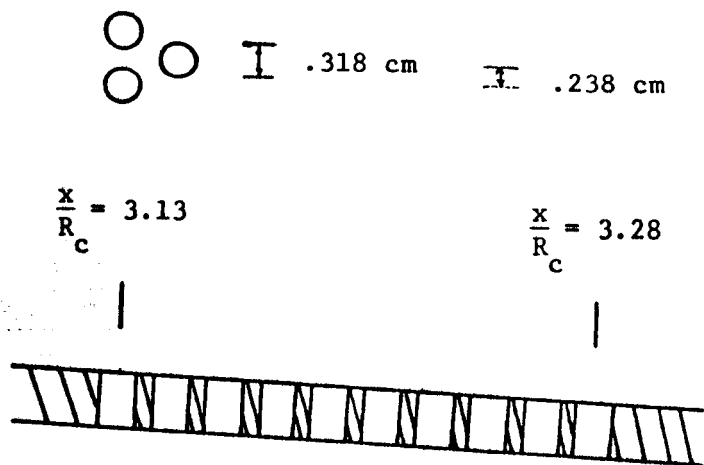
Figure 2.8a   Cowl Bleed Region (Large Normal Holes)

.159 cm   .119 cm

$\dfrac{x}{R_c} = 3.13$ $\dfrac{x}{R_c} = 3.29$
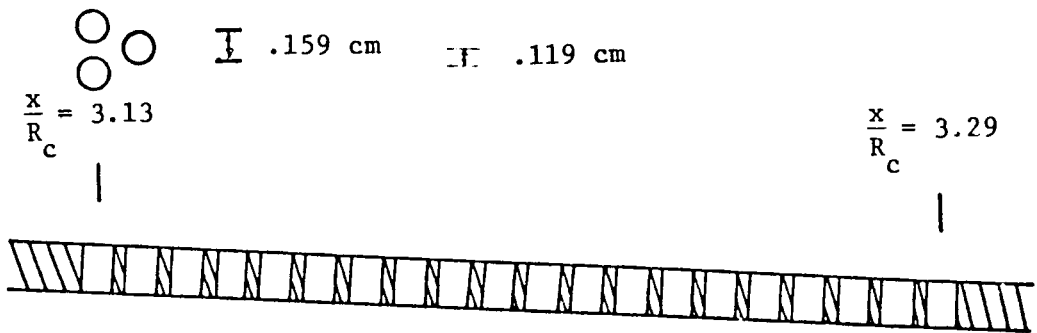
Figure 2.8b Cowl Bleed Region (Small Normal Holes)

.318 cm   .238 cm

$\dfrac{x}{R_c} = 3.05$ $\dfrac{x}{R_c} = 3.29$

Figure 2.8c Cowl Bleed Region (Slanted Holes)
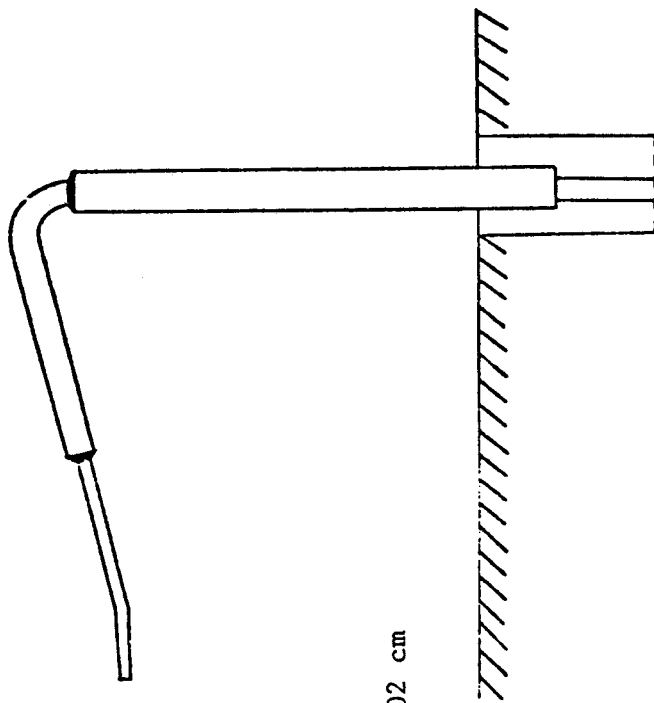
Figure 2.9 Schematic of Traversing Total Pressure Probe

.0102 cm

.096 cm

.0203 cm

37
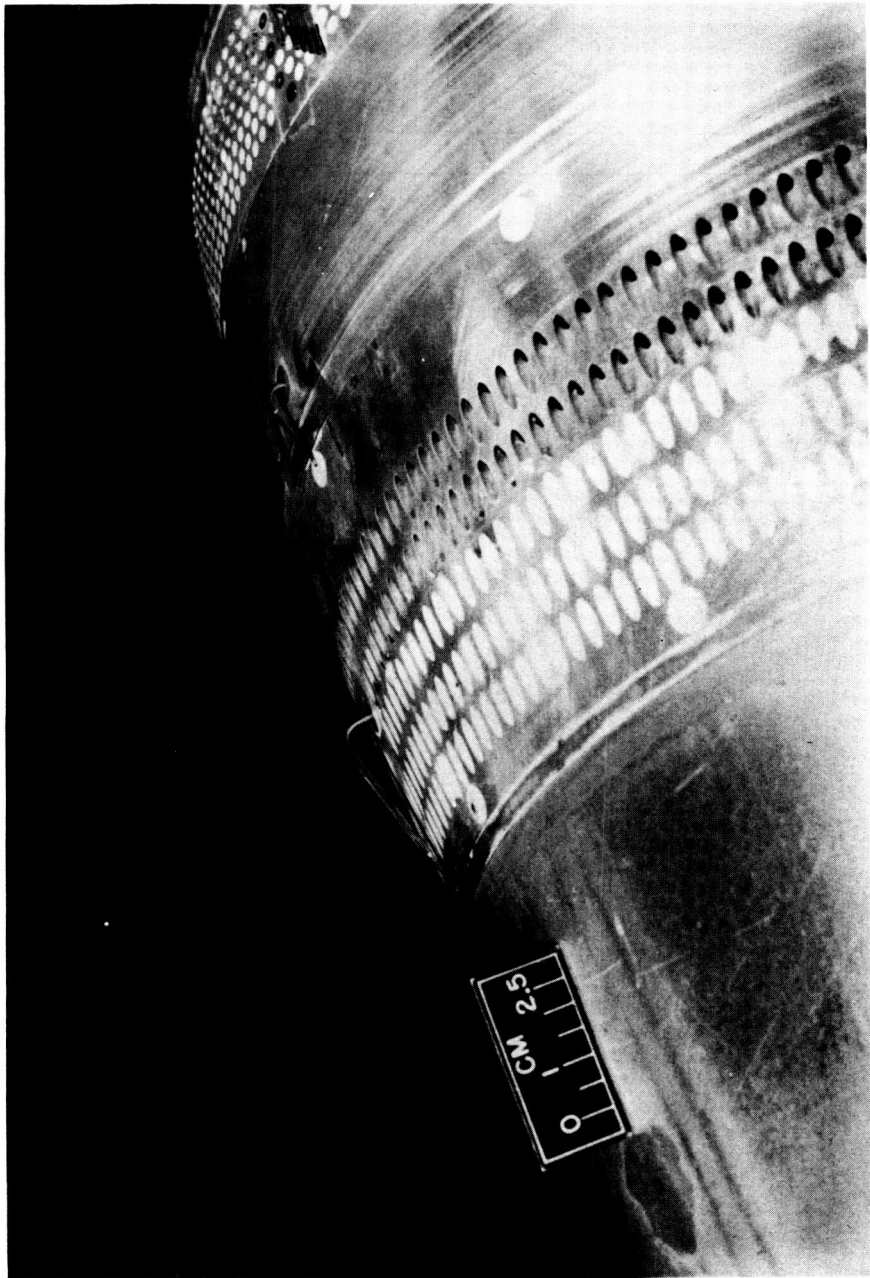
Figure 2.10 Photograph of Probes 1 and 2

CHAPTER III

RESULTS AND DISCUSSION

The results of the experiment are presented in three sections; the centerbody and cowl shock boundary layer interactions and compressor fact total pressure information. The shock-boundary layer data consists of boundary layer integral parameters, edge Mach numbers, bleed mass flow rates and total and wall temperatures before and after each of the interaction regions. Representative sets of boundary layer velocity profiles have also been included.
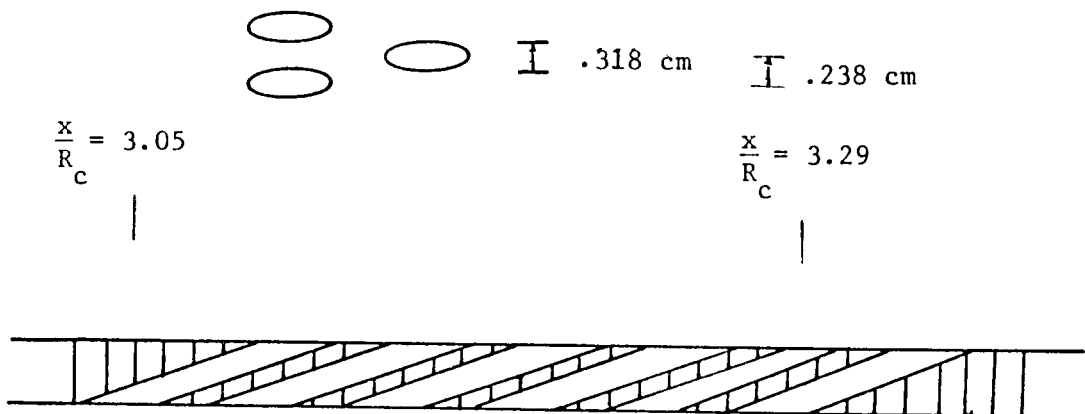
Section 3.1 Centerbody Shock-Boundary Layer Interactions

Inlet operation in the supercritical mode involved several shock-boundary layer interactions but only the first and second interactions on the centerbody, namely those upstream of the geometric throat, were investigated. The boundary layer on the centerbody was surveyed before and after each of the two interactions by Probes 1 to 4 at respective $\frac{x}{R_c}$ locations of 2.685, 3.039, 3.303 and 3.557. The shock impingement locations as calculated by the method of Reference 12 were respectively at $\frac{x}{R_c}$ values of 2.88 and 3.48 for the first two interactions.

One of the features of a shock-boundary layer interaction is the spreading of the pressure rise, due to the shockwaves, upstream and

downstream for several boundary layer thicknesses. This propagation of higher pressure upstream is accomplished primarily in the subsonic portion of the boundary layer. This is a complex phenomenon and very little analytical work has been done in this area particularly where effects of bleed are considered.

It was found that the placement of the bleed region relative to the shock-induced pressure distribution had a significant effect on the state of the boundary layer downstream of the interaction region. The centerbody static pressure distributions for Runs 2 to 6 and Run 10, presented in Figures 3.1 to 3.6 respectively, show the characteristic spreading of the shock-wave pressure rise. Also indicated on the figures is the length and location of the forward and aft centerbody bleed regions as measured from the leading edge of the first row of holes to the trailing edge of the last open row of holes. The aft centerbody bleed section was not changed during the experiment while the forward centerbody bleed configuration was varied. The lengths of bleed regions are summarized in Table 3-I. The bleed hole configurations for the forward centerbody bleed region are presented graphically in Figure 3.7. There were several different downstream (DS) bleed configurations used in the forward centerbody and these were labelled DS A, DS B and DS C in Runs 2,3, and 5 respectively.

A comparison of the static pressure distribution of Run 2, bleed configuration DS A, with that predicted by the method of characteristics solution of Reference 12 is shown in Figure 3.8. Also included in the figure are the shock impingement points cal-

culated by the δ* added method previously mentioned. The only bleed configuration that seemed to minimize the extent of spreading of the shock induced pressure rise was the scoop bleed configuration. The scoop bleed removed a significant portion of the boundary layer at one location and the resulting new boundary layer minimized the thickness of any subsonic region through which an upstream influence could propagate.

Section 3.1.1 <u>First Interaction Region</u>

Only the data for the smaller slanted hole bleed series, 0.159 cm minor axis, and the scoop bleed configuration in the first interaction are presented due to a change in the Probe 1 boundary layer for the larger slanted hole bleed series (0.318 cm minor axis). In the smaller slanted hole bleed series, several of the DS bleed configurations were used, DS A, DS B, and DS C in Runs 2,3 and 5 respectively, while only single across-shock (AS) and upstream (US) bleed configurations, Runs 4 and 6 respectively, were tested.

The velocity profile at Probe 1, at an $\frac{x}{R_c}$ location of 2.685, which was upstream of the first centerbody interaction region, is shown in Figure 3.9. The edge Mach number was 2.09 and the transformed form factor, H_{tr}, was 1.26. The compressible displacement and momentum thicknesses, δ* and θ, were 0.096 cm and 0.030 cm respectively. The wall temperature of 297°K was very close to the adiabatic wall temperature. In comparison, calculations by the method of Reference 9 yield an H_{tr}, δ* and θ of 1.30, 0.134 cm and

41

0.0381 cm respectively.

The data at Probe 1 showed slight variations in H_{tr}, $\delta*$ and θ for the different bleed configurations and for different mass flow rates. For a given bleed configuration, increasing the bleed mass flow in the forward centerbody bleed region had the tendency to slightly decreast H_{tr}, $\delta*$ and θ at Probe 1. For example, in Run 5, $\delta*$, θ and H_{tr} were .095 cm, .030 cm and 1.26 respectively at a bleed rate of 41% of $\dot{M}_{BL_1}$ while at a bleed rate of 11.3% of $\dot{M}_{BL_1}$, $\delta*$, θ and H_{tr} were .100 cm, .032 cm and 1.27 respectively.

The variation of the transformed form factor, H_{tr}, with bleed mass flow at Probe 2 is shown in Figure 3.10. Also shown in Figure 3.10 is the theory of References 9 and 10. The scoop bleed model was used in the interaction for all bleed regions. Verification that the scoop bleed model may be used for all bleed regions can be found in Reference 24. Probe 2 was downstream of the first interaction region at an $\frac{x}{R_c}$ location of 3.04. The bleed mass flow, $\dot{M}_{BLEED}$, has been non-dimensionalized by the boundary layer mass flow at Probe 1, $\dot{M}_{BL_1}$. The boundary layer mass flow at Probe 1 was 0.242 kg/sec which corresponded to 1.87% of the capture mass flow. The equation used to calculate the boundary layer mass flow is shown below.

$$\dot{M}_{BL} \approx 2\pi R \int_o^\delta \rho u dy = 2\pi R \, \rho_e U_e \, (\delta - \delta*) \tag{3.1}$$

42

This equation is valid when the boundary layer thickness, δ, is much smaller than the local centerbody radius, R. Also in equation (3.1) ρ_e and U_e refer to the density and velocity respectively at the edge of the boundary layer and δ* is the compressible displacement thickness.

The transformed form factor, H_{tr}, at Probe 2 varied smoothly for all bleed configurations tested and in most cases asymptotically reached a minimum value. This plateau was generally reached at a bleed mass flow of 30% to 40% of the Probe 1 boundary layer mass flow but the values of the plateau form factors were not necessarily the same for the different bleed configurations. The position representing 30% of the boundary layer mass flow is shown on the Probe 1 boundary layer velocity profile, Figure 3.9. Very little change in the transformed form factors at Probe 2 were obtained for bleed mass flows larger than those needed to reach the plateau.

The effect of bleed in the first centerbody interaction region on the velocity profiles of the Probe 2 boundary layer is illustrated in Figures 3-11 a-h. The data are that of Run 2, the DS A bleed configuration, with a bleed mass flow ranging from 2.5% to 60% of the boundary layer mass flow at Probe 1. With bleed rates greater than 30% of the $\dot{M}_{BL_1}$, the velocity profiles showed little change in shape but the thicknesses became progressively smaller, while for lesser bleed rates the velocity profiles were also less full. This trend was reflected in the transformed form factors as the H_{tr} for

a bleed mass flow at 60% was 1.32 while the H_{tr} for a bleed mass flow of 2.5% was 1.43.

This points out that the removal of more than the low momentum portion of the boundary layer by bleeding is unnecessary as further bleed gave little or no further decrease in the transformed form factor. In general, removal of more than approximately 35% of the Probe 1 boundary layer mass flow or 0.6% of the capture mass flow could be considered as overbleeding.

To be noted also in Figure 3.10, is that the consistently largest form factors for a given bleed rate were obtained by using the AS bleed configuration of Run 4. The centerbody static pressure distribution for Run 4, Figure 3.3, showed that the bleed region spanned the entire shock induced pressure rise thus some amount of recirculation from the high pressure side to low pressure side of the bleed region may have been present. The recirculation would have increased the form factors and other integral parameters and decreased the effectiveness of the bleed. In general, the DS bleed configurations of Runs 2, 3 and 5 provided the lowest form factors for a given bleed rate with the US bleed configuration of Run 6 and the AS bleed configuration of Run 4 respectively higher. A seeming anomaly occurred between Run 4, AS, and Run 5, DS C with six rows of holes open, as the location of the bleed regions was almost identical. However, an inspection of the static pressure distributions revealed that a much more severe adverse pressure

rise occurred in Run 4 than in Run 5. The static pressure ratio

across the bleed region was 2.4 for Run 4 compared to 1.4 in Run 5.

These data point out that the location of the bleed region relative

to the shock-induced pressure distribution and the magnitude of

that local pressure gradient are very important in determining the

characteristics of the boundary layer downstream of the interaction

region.

In Runs 2 and 3 DS A and DS B respectively, the bleed regions

were placed downstream of the major portion of the shock-induced

pressure rise. For Run 2, the last four rows of holes were open,

while for Run 3, the last two of these rows were closed and only the

prior two rows of holes were open (see figure 3.7). The data for

these bleed regions were almost identical but with more bleed capa-

bility in Run 2. The plateau transformed form factors for both Runs

2 and 3 were approximately 1.30 - 1.33. The data for Run 5, DS C

with the last six rows of holes open show the same behavior as the

other two DS bleed configurations. Evidently, the two rows of

open holes in Run 3, DS B, are sufficient for achieving the plateau

in H_{tr}.

The US bleed configuration was used in Run 6 and the static

pressure distribution, Figure 3.5, shows a very slight adverse

pressure gradient along the bleed region. The data again show a

smooth variation of H_{tr} with bleed mass flow until at $\dot{M}_{BLEED}/\dot{M}_{BL_1}$

of approximately 0.25, the transformed form factor reaches a plateau

value of approximately 1.37.

The scoop bleed configuration of Run 10 showed almost no change in transformed form factor with bleed however only a small range of bleed mass flows, $\dot{M}_{BLEED}/\dot{M}_{BL_1}$ from 0.07 to 0.22, were obtained. The static pressure distribution for the scoop bleed, Figure 3.6, showed the almost 'inviscid' static pressure distribution in the interaction region as discussed previously. The scoop was placed at $\frac{x}{R_c} = 2.84$, which is in the middle of the shock interaction region, and seemed to minimize the upstream effects of the pressure rise across the shock wave. The reduced upstream effect indicates that the scoop type bleed may be very effective in stronger shock-interaction regions because of the reduced possibility of separation upstream of the 'impingement' point due to upstream pressure propagation.

A tabulation of bleed mass flows, H_{tr}, δ^*, θ and other relevant parameters for Probe 2 is presented in Table 3-II.

An extrapolation of the data to zero bleed showed that the different bleed configurations had unequal transformed form factors, displacement and momentum thicknesses at Probe 2. This was probably due to the location of the bleed region relative to the interaction. Also because of the bleed holes there are possible effects of roughness and flow recirculation via the bleed plenum between Probes 1 and 2. In a previous investigation[23] using the same inlet and test conditions except that a solid wall was present

between Probes 1 and 2 the transformed form factors were 1.28 at Probe 1 and 1.48 at Probe 2. In this investigation, the extrapolated zero bleed form factors at Probe 2 for the DS, US and AS bleed configurations were approximately 1.43, 1.50 and 1.55 respectively.

The variation of $\delta*$ and θ with bleed at Probe 2 are presented in Figures 3.12 and 3.13 respectively and in Table 3-II. Also included is the theory of References 9 and 10. These data show the same trends as the form factor data in that the AS and US bleed configurations had the largest values and the three DS configurations were grouped at lower values. The data show that $\delta*$ and θ were still decreasing at the larger bleed mass flow rates as mass was still being removed from the boundary layer, however the ratio of these parameters, the compressible form factor, remained constant. The ranges of $\delta*$ and θ obtained were .17 cm to .04 cm and .065 cm to .018 cm respectively for bleed mass flows from 0.2% to 65% of $\dot{M}_{BL_1}$. At bleed rate of 30% of $\dot{M}_{BL_1}$ for Run 3, DS B, $\delta*$ was .089 cm and θ was .036 cm which were approximately the same as those obtained at Probe 1.

The $\delta*$ and θ data for the US bleed configuration, Run 6, lie above the data for all DS bleed configurations although the plateau H_{tr}'s were similar at large bleed rates. Also, at large bleed rates the US bleed configuration data lie slightly above the AS bleed configuration data.

The three DS bleed configurations show almost the same

behavior at bleed rates below 25% of M_{BL_1} and only at larger bleed
rates do the differences manifest themselves. However, the data for
large bleed rates are quite sketchy and nothing concrete may be said
about the differences due to different DS bleed regions.

The scoop model of Seebaugh, Paynter and Childs[10] was used to
calculate the change of the boundary layer parameters across the
shock-boundary layer interaction region with and without bleed.
It has been shown by Hingst and Towne[24] that the scoop bleed
model can be used for all types of bleed regions in the interaction
region. Boundary layer calculations before and after the interaction
region were made with the Sasman Cresci[9] integral model. A comparison
of the calculation with the experimental data show good agreement in
H_{tr} but the theory predicts larger $\delta*$'s and θ's than were actually
obtained. The shapes of all of the calculated curves are quite
similar to the data and quite reliably followed the trends observed.
A very interesting thing to note is that the theoretical model pre-
dicts a very slight rise in H_{tr} at bleed rates greater than 40% of
$\dot{M}_{BL_1}$. The data of Run 2, DS A, show the same behavior at large
bleed rates and this may be taken as another argument against over-
bleeding. It must be remembered that the Seebaugh-Paynter-Childs[10]
interaction model cannot distinguish between the US, AS, DS and
scoop bleed configurations.

The results at Probe 2 indicate that the DS bleed configurations
gave the lowest H_{tr}'s, $\delta*$'s and θ's of all the bleed regions over

almost the entire range of bleed mass flows obtained. However the data at Probe 2 were influenced by the location and strength of the shock induced pressure rise as well as the position of the bleed region relative to the pressure rise and to the measurement point. In other words, the data at Probe 2 may have been affected by its closeness to the different bleed regions. In order to examine this point more closely, the data at Probe 3 have been analyzed to see it the effects observed at Probe 2 persist downstream. These results will be presented in the next section.

Section 3.1.2 Second Centerbody Interaction Region

This interaction region occurred near the geometric throat on the centerbody and oblique shock waves were present instead of a normal shock due to supercritical inlet operation. A single bleed pattern, five rows of 0.318 cm diameter normal holes, was used slightly upstream of the interaction region. This bleed region was primarily for preventing boundary layer separation and inlet unstart when the inlet was operated in the critical mode.

The data of Run 3 at Probe 3 are not presented because a strong shock was present ahead of or near Probe 3 which caused the edge Mach number at Probe 3 to be drastically different from all other data presented. The static pressure distribution for Run 3, Figure 3.2, shows the change in static pressure distribution very clearly.

The boundary layer was measured by total pressure probes, 3 and 4, before and after the interaction region at $\frac{x}{R_c}$ = 3.303 and 3.557

49

respectively. The Probe 3 data also gave information on the boundary layer development subsequent to the first interaction region as mentioned previously.

The variations of H_{tr}, δ^* and θ at Probe 3 with $\dot{M}_{BLEED}/\dot{M}_{BL_1}$ are presented in Table 3-III and Figures 3.14 to 3.16 respectively. Note that the bleed mass flow is still non-dimensionalized by the Probe 1 boundary layer mass flow.

The form factors in all cases presented were lower at Probe 3 than at Probe 2 for the same bleed mass flow rate. This seemed to be caused by two effects. The primary effect seemed to be the 'recovery' of the boundary layer after the shock interaction region. In the interation region the boundary layer is subjected to a severe adverse pressure gradient and growth is correspondingly rapid. Once out of the interaction region, the rapid growth cannot be sustained due to a much milder pressure gradient. This has a tendency to decrease H_{tr}. The secondary cause was the existence of a slightly favorable pressure gradient ahead of Probe 3 which would decrease the rate of boundary layer growth. These effects are illustrated in Figure 3.17 where the transformed form factor as calculated by the methods of References 9 and 10 vs. $\frac{x}{R_c}$ is shown with no bleed in the interaction region.

The data on the transformed form factors, Figure 3.14, show that the US and DS C bleed configurations. Runs 6 and 5 respectively, now have the lowest form factors. There was also much less variation

50

of H_{tr} bleen at Probe 3 as compared with that at Probe 2. This
indicates that the data obtained at Probe 2 exhibited the local
effect of bleed in the interaction region and a physical smoothing
out process occurs further downstream that decreases the sensitivity
to the local bleed geometry in the first interaction region. The
US bleed configurations, Run 6, seemed relatively insensitive to
the bleed rate in the first interaction region as H_{tr} at a bleed
rate of 0.43 was 1.23 while at a bleed rate 0.02, H_{tr} was 1.28.
All other bleed configurations showed the same behavior in that
the variation of H_{tr} with $\dot{M}_{BLEED}/\dot{M}_{BL_1}$ decreased.

The change in δ^* and θ at Probe 3 with the bleed mass flow
in the first interaction region is presented in Figures 3.15 and
3.16 respectively and in Table 3-III. Again the effects of bleed
geometry are seen to have been reduced and it seems that δ^* and θ
at Probe 3 were dependent only on the bleed mass flow rates in the
first interaction region with only slight differences ascribable
to effects of bleed geometry. Most of the data on δ^* and θ at
Probe 3 fall on a single curve except for the US bleed configuration
of Run 6 which showed larger values of these thicknesses at bleed
rates greater than 40% of $\dot{M}_{BL_1}$.

The comparison between the experimental data and the theory of
references 9 and 10 again show similar behavior although the cal-
culated thicknesses were larger than experimentally observed.

An examination of the centerbody static pressure measurements reveals that the second centerbody interactions occurred further downstream in Runs 5 and 6 than in Runs 2, 4 and 10. This was probably due to the large amount of bleed used on the cowl for these runs. The slanted hole bleed region was used on the cowl in Runs 5 and 6 and large bleed mass flows were obtained, approximately 4% of the inlet capture mass flow. This may have caused the second centerbody shock to move downstream slightly because of the decreased boundary layer thickness on the cowl. In both Runs 5 and 6, the downstream movement of the shock wave caused the local pressure rise around Probe 3 to be extended further downstream. When normal holes were used on the cowl as in Runs 2 and 4, larger pressures obtained behind the shock in the second centerbody interaction region seemed to have affected the static pressures at Probe 3 in that the edge Mach numbers were in the 1.45 to 1.47 range while for the slant holes on the cowl , they were in the 1.51 to 1.54 range.

At Probe 3, H_{tr}'s of 1.23-1.35 were obtained for bleed rates in the first interaction region of 0-60% of $\dot{M}_{BL_1}$. This range of transformed form factor would be adequate for entering the second centerbody interaction. In view of the general smoothing effect on the boundary layer after the first interaction region and because of the low values of H_{tr} obtained at Probe 3 for bleed rates less than 35% of $\dot{M}_{BL_1}$ in the first interaction region, large amounts of bleed are probably not needed in the second centerbody interaction region.

A significant amount of bleeding, 0.8% to 2.3% of the inlet capture mass, took place in the second centerbody interaction region. This range represents 40% to 120% of the boundary layer mass flow at Probe 1. As a result of bleeding in two different regions and the variable nature of the boundary layer at Probe 3, the data are presented as a function of the bleed ratio $\dot{M}_{TOTAL}/\dot{M}_C$. The total bleed mass flow, $\dot{M}_{TOTAL}$, is defined as the total bleed mass flow from both centerbody interaction regions and non-dimensionalized by the inlet capture mass flow, $\dot{M}_C$. ($\dot{M}_{BL_1}$ is approximately 1.8% of $\dot{M}_C$.)

A compilation of the bleed mass flow rates and the boundary layer parameters at Probe 4, $\frac{x}{R_c} = 3.557$, is presented in Table 3-IV. Probe 4 was downstream of the second interation region.

The variation of H_{tr} with bleed at Probe 4 is presented in Figure 3.18. This figure shows a cluster of points in the bleed mass flow ration of 2% to 2.5% where the transformed form facturs varied from 1.33 to 1.43.

For lower total bleed rates, the data of Run 5, DS C in the first interaction region, show a slight increase in H_{tr} for decreasing total bleed. The transformed form facturs for Run 5 ran from 1.4 at a bleed rate of 2.17% of $\dot{M}_C$ to 1.45 at a bleed rate of 1.25% of $\dot{M}_C$. A plateau in H_{tr} is seemingly reached for $\dot{M}_{TOTAL}/\dot{M}_C$ of 1.7%.

The variations of δ* and θ at Probe 4 are presented in Figures 3.19 and 3.20 respectively and expectedly show a decrease with

increasing bleed. Again this shows that decreasing $\delta*$ and θ by

bleeding does not decrease H_{tr} below the plateau value.

In view of the sketchiness of the Probe 4 data and their in-

applicability to critical operation, they do not warrant further

discussion.

Section 3.2 Cowl Shock-Boundary Layer Interaction

Supercritical operation again presented several shock-boundary

layer interactions on the cowl for investigation but only the first

interaction region was studied. The first shock-boundary layer

interaction on the cowl would not have been changed by critical

rather than supercritical operation of the inlet. The cowl boundary

layer was surveyed before the interaction by Probe 5, at $\frac{x}{R_c}$ = 3.006,

and after the interaction by Probes 6 and 7, at $\frac{x}{R_c}$ = 3.394 and 3.555

respectively. The shock impingement point calculated by the method

of Reference 12 was at $\frac{x}{R_c}$ = 3.25 while the $\delta*$ added method predicted

a shock impingement point at $\frac{x}{R_c}$ = 3.20.

The boundary layer at Probe 5, before the interaction region,

varied slightly for the different bleed configurations and to different

mass flow rates. The average values of $\delta*$, θ and H_{tr} at Probe 5 were

0.061 cm, 0.023 cm and 1.34 cm respectively. The edge Mach number

was 1.66 and the wall temperature of 307°K was very close to the

adiabatic wall temperature. The boundary layer mass flow as defined

by equation 3.1, was 0.486 kg/sec which corresponded to 3.6% of the

inlet's capture mass flow. The boundary layer velocity profile at

54

Probe 5 is presented in Figure 3.21.

The data for the cowl shock-boundary layer interaction will also be presented in terms of the nondimensional bleed mass flow $\dot{M}_{BLEED}/ \dot{M}_{BL_5}$ where $\dot{M}_{BLEED}$ represents the bleed mass flow in the cowl inter-action region and here $\dot{M}_{BL_5}$ now represents the boundary layer mass flow at Probe 5. Also, the data taken for Run 3 will not be presented since the stronger shock experienced in this case did not allow for adequate comparison with other data.

The three types of bleed regions used on the cowl were: (1) 10 rows of 0.318 cm diameter normal holes, (2) 20 rows of 0.159 cm diameter normal holes and (3) 6 rows of 0.318 cm minor axis holes at 20° to the surface tangent. The three bleed sections were designated LN, SN and Slant respectively. The lengths of the various bleed regions are presented in Table 3-V.

The location of the bleed region relative to the shock-induced pressure rise played an even more important role in the cowl inter-action than it did on the centerbody. Slight changes in the shock-induced pressure gradients caused noticeable differences in the data and this was found by an examination of the cowl static pressure distributions. The probable cause of the movement of the shock-indiced pressure gradient was the variation of boundary layer growth on the centerbody. The testing procedure was to hold the cowl bleed pipe exit plugs at the full open position and to vary the centerbody bleed mass flow and then for the centerbody bleed pipe exit plugs

at the full open position, to vary the cowl bleed. The variation in size of the centerbody boundary layer caused by centerbody bleeding apparently caused a movement of the cowl shock impingement point. This in turn caused a change, in some cases, of the position of the bleed region relative to the shock-induced pressure distribution. These changes were apparent in the data when shock movement caused a bleed region to go from a US configuration to an AS configuration. Shock movement was also present in the second centerbody interaction but the aft centerbody bleed region was placed far enough upstream of the interation so that no change to an AS or DS bleed configuration was experienced.

The static pressure distributions for Run 2 and Runs 4 through 10 are presented in Figures 3.22 through 3.29 respectively and these show a region of high pressure around Probe 6, which was downstream of the interaction region. The actual shock impingement point occurred downstream of the bleed region. The shock wave was also stronger than expected as the actual Mach numbers in the region near Probe 6 were very close to one while the calculated theoretical Mach number was 1.20. A comparison of the static pressure distribution of Run 4 with that predicted by the method of characteristics solution of Reference 12 is presented in Figure 3.30. Also included in this figure is the shock impingement point predicted by the δ^* added method. The differences between both predicted shock impingement points and the actual impingement point is apparent from this figure. The

shock-induced pressure distributions on the cowl in the interaction region are readily seen in Figures 3.22 to 3.29. The cowl static pressure distributions show a larger pressure rise across the interaction region than the first centerbody interaction region. For this reason, unstart due to boundary layer separation became a prominent danger at the lowest bleed mass flow rates. Unstart was obtained at the lowest bleed mass flow rates for several of the bleed configurations pointing out the necessity for careful analysis before the actual design of the inlet.

Most of the bleed regions tested were upstream of the shock-impingement point as indicated by the static pressure distributions. Thus there was little variation in the data for most cases. The different US bleed configurations were designated US 1 through US 6 corresponding to Runs 4,5,7,8,9 and 10. In Runs 2 and 6, the bleed regions appeared to be across the shock and are hence designated AS1 and AS 2 respectively. A schematic representation of the bleed configurations is shown in Figure 3.31.

The variation of H_{tr} with bleed at Probe 6 for the normal bleed configurations only is presented in Figure 3.32 and in Table 3-VI . The immediate difference noted as that the data for Run 2, AS 1, lie well above all data at low bleed rates. An examination of the Run 2 static pressure distribution, Figure 3.22, shows that the aft part of the bleed lies in a region of an extremely large pressure gradient and some recirculation may have occurred at the lower bleed

rates. Thus the AS bleed configuration, when placed in a strong adverse pressure gradient, gave rise to larger transformed form factors in both cowl and first centerbody interaction regions.

At the very low bleed rates, the AS 1 bleed configuration of Run 2 gave very large transformed form factors and no bleed data were obtained below bleed rates at 6.6% of $\dot{M}_{BL_5}$ due to inlet unstart. The large transformed form factors obtained at low bleed rates and the subsequent unstart imply that improper placement of the bleed region relative to the shock-induced pressure rise may lead to very undesirable inlet performance.

The bleed regions of Runs 2 and 4 were comprised of rows of 0.3175 cm diameter normal holes, LN, while the 0.1588 cm diameter normal rows, SN, were used in Runs 8-10. Since Run 4 and Runs 8-10 were all in the US bleed configuration, the effects of hole size can be determined by comparison of the data for these different Runs. The H_{tr} data, Figure 3.32, show that there was very little difference in the transformed form factors for the different size holes. A comparison of the static pressure distributions of Run 4 and Run 10, Figure 3.23 and 3.29 respectively, show that they were both in approximately the same position with respect to the shock-induced pressure gradient although the Run 4 bleed region extended upstream a little further than that of Run 10. A comparison of the data for these two bleed configurations showed that the data of Run 4 lay slightly above that of Run 10. But because the data of Runs 8 and 9 were very similar to that of Run 4, the differences between that 0.3175 cm

diameter holes and 0.1588 cm diameter holes cannot be taken as significant.

The H_{tr} data for Run 4 and Runs 8 through 10 again showed the existence of a plateau form factor of approximately 1.52. A continuous decrease in H_{tr} was observed for bleed mass flows below 0.3 and this gave further evidence that large amounts of bleed are not really helpful. A non-dimensional bleed mass flow of 0.3 is equivalent to approximately 1% of the inlet's capture mass flow. The 30% level of $\dot{M}_{BL_5}$ is shown in Figure 3.21, the Probe 5 velocity profile.

An interesting result obtained was the inability to maintain the same static pressure distributions for slightly different bleed con-figurations. This is illustrated in Figure 3.33 where the pressure ratios in the vicinity of the shock reflection for Run 2, AS 1, and Run 9, US 5, have been plotted. The pressure data were taken to a bleed mass flow rate of 0.177 and represent the true AS bleed con-figuration for Run 2. The bleed regions were from $\frac{x}{R_c}$ locations of 3.22 to 3.25 for Run 2 and 3.17 to 3.24 for Run 9 and these are shown on the figure. The moderate pressure gradient along the bleed region in Run 9 was contrasted with the severe pressure gradient at the aft portion of the bleed region in Run 2. As a result of the differences in placement of bleed region to shock-induced pressure rise, the transformed form factors obtained in Run 2 were larger than those of Run 9. Since the static pressure distribution in a bleed region cannot be predicted with any certainty, it is felt that tolerances should be allowed in the placement of a bleed region relative to the

shock-induced pressure rise.

The variation of δ^* and θ with bleed, for the normal hole bleed configurations at Probe 6 are presented in Figures 3.34 and 3.35 respectively and in Table 3-VI. Since most of the bleed configurations were in the US mode, the values of δ^* and θ show very little difference between the various US configurations with the exception of Run 2, the AS 1 bleed configuration. A comparison of δ^* and θ for Run 4, US 1 LN, and Run 10 US 6 SN, shows that hole size had little or no effect on the data. The δ^* and θ data again show decreasing height with increasing bleed and continue to decrease even after a plateau in H_{tr} was attained. These were the same trends noted on the centerbody at Probe 2. The US bleed configurations on centerbody and cowl showed similar trends for the δ^* and θ data taken directly behind the bleed regions.

It should be mentioned at this point that the calculations by the method of Seebaugh, Paynter and Childs[10] across the interaction region indicated separation of the boundary layer even beyond bleed mass flows of 2 % of $\dot{M}_{BL_5}$. Thus no theoretical curves have been shown for the cowl interaction region.

The data for Probe 7, $\frac{x}{R_c} = 3.555$, for the normal hole bleed configurations are presented in Figures 3.36 to 3.38 and in Table 3-VII. Probe 7 was slightly downstream of the geometric throat and because of supercritical operation the Mach numbers were greater than one. The Probe 7 data compared to those at Probe 6 showed the same trends observed on the centerbody in going from Probe 2 to

Probe 3; namely, that there was an observed decrease in H_{tr}, δ^* and θ when compared to data directly behind the interaction region. Again the boundary layer growth caused by the shock-induced pressure gradient could not be sustained. As a result of this and the favorable pressure gradient between Probes 6 and 7, H_{tr}, δ^* and θ decrease behind the interaction region. The transformed form factor data, Figure 3.36, shows that the plateau H_{tr} was approximately 1.27 as compared to 1.52 at Probe 6. The transformed form factors, displacement and momentum thicknesses obtained with AS 1 bleed configuration of Run 2 were still persistently larger than those for other bleed configurations. Again the effects of hole size were slight with the larger normal holes having slightly larger H_{tr}'s, δ^*'s and θ's than the smaller normal holes.

The data taken at Probe 7 again indicate that measurements taken directly behind a shock-boundary layer interaction region, Probe 2 on the centerbody and Probe 6 on the cowl, are directly influenced by the 'recovery' of the boundary layer. So care must be used in examining and evaluating data from shock-boundary layer interactions.

The data at Probe 6 for the slanted bleed hole series, Runs 5 to 7, are presented in Figures 3.39 to 3.41 and in Table 3-VI. Much larger bleed mass flow rates were obtained with these bleed configurations. As a result, the data obtained were rather sketchy in the bleed range from 0 to 30% of $\dot{M}_{BL_5}$. However a vague plateau with transformed form factors of approximately 1.4 were obtained at

61

Probe 6 as compared to 1.52 at Probe 6 for the normal hole bleed

series. In general, the plateau transformed form factors for the

slanted hole bleed series were obtained at bleed mass flow rates

greater than 0.5, which corresponded to 1.8% of the inlet's capture

mass flow. However at a bleed rate of 30% of $\dot{M}_{BL_5}$, the amount of

bleed needed at attain the plateau H_{tr} of 1.52 with normal hole bleed,

the plateau transformed form factors for the slanted hole bleed

regions were below 1.40 for most cases.

The differences between the normal hole and slanted hole bleed

regions is magnified when comparing the $\delta*$ and θ data at Probe 6.

The slanted hole bleed regions provided smaller displacement and

momentum thicknesses when compared to the normal hole bleed at

larger bleed rates. Thus these data indicate that bleeding with

rows of slanted holes provides lower H_{tr}'s and θ's and approxi-

mately equal $\delta*$'s at the larger bleed mass flows. For bleed mass

flows below 0.3, the data for slanted hole bleed are sketchy and no

fair comparison can be made.

A comparison of transformed form factor versus bleed rate at

Probe 6 between Runs 6 and 7, AS 2 and US 3 Slant respectively and

Run 8, US 4 SN, is presented in Figure 3.42. The plateau H_{tr}'s

for Runs 6 and 8, slanted hole bleed regions, are obviously much

less than that for Run 8, normal hole bleed. As was previously

mentioned, the Run 8 plateau H_{tr}, 1.51, was obtained at an approxi-

mate bleed mass flow rate of 0.3 while the plateau H_{tr} for the slanted

hole bleed regions, approximately 1.4, were obtained at an approximate bleed mass flow rate of 0.45. From this direct comparison, it is obvious that at Probe 6, the slanted hole bleed regions provided smaller plateau transformed form factors than the normal hole bleed region although a larger mass flow was needed to attain the plateau when the slanted hole bleed was used.

Slight movements of the shock induced pressure rise caused some fluctuation in the data. The static pressure distributions for Runs 5 and 7, Figures 3.24 and 3.26 respectively, indicate that both bleed regions are in the US bleed configuration. The extreme aft portion of the bleed region for Run 7 appears to be in a slight adverse gradient but it was still classified as a US bleed configuration. During Run 7 at low bleed mass flows, less than 0.15 of $\dot{M}_{BL_5}$, the shock-induced pressure gradient shifted forward slightly as the bleed mass flow was reduced. This caused the bleed configuration to change from US to AS and a large H_{tr} was recorded. These data were eliminated because of the change in bleed configuration due to shock movement. The pressure distribution-data of Run 6 showed that the bleed region was in the AS bleed configuration.

The slanted hole bleed data at Probe 6 presented an anomaly in that the transformed form factors obtained using the AS 2 configuration of Run 6 were less than or equal to the transformed form factors obtained using the US bleed configurations of Runs 5 and 7. The static pressure distribution for Run 6, Figure 3.25,

showed that the pressure gradient across the bleed region was very mild. In other AS bleed configurations considered, the pressure rise across the bleed region has been a major portion of the entire pressure rise across the shock waves so that a much milder pressure rise across the bleed region may have changed the effect of the bleed on the boundary layer.

The data for the slanted hole bleed series at Probe 7 are presented in Figures 3.43 through 3.45 and in Table 3-VII. Although the data were quite limited, a comparison of the transformed form factors, Figure 3.44, showed that the data seemed to lie on a single curve with a plateau H_{tr} of approximately 1.3. So again the effect of bleed configuration, in terms of H_{tr}, has been reduced considerably at Probe 7. The differences in bleed configuration manifest themselves in the δ^* and θ data, Figures 3.44 and 3.45 respectively, at low bleed rates. For bleed rates greater than 25% of $\dot{M}_{BL_5}$ the differences in the data for the various bleed configurations is not significant while for lower bleed rates the data of Run 5, US 2, lie above that of Run 6, AS 2.

It must be emphasized again that the data previously presented were for supercritical mode inlet operation where the terminal shock stood downstream of the geometric throat. The normal cruise condition would be critical mode operation where the terminal shock stands just behind the geometric throat. Relatively large transformed form factors after the first cowl interaction region may mean

64

separation of the boundary layer in the throat interaction region
for critical operation.

Section 3.3 Pressure Recovery Results

3.3.1 Supercritical Operation

Supercritical inlet operation forced the total pressure
recoveries at the compressor face to be in the 77% - 79% range with
the terminal shock being held at an approximate $\frac{x}{R_c}$ location of 4.5.
The terminal shock position was far into the subsonic diffuser
section and even downstream of the vortex generators, positioned at
$\frac{x}{R_c}$ = 4.15. As a result, the compressor face pressure recoveries
were very low and the compressor face Mach numbers were approximately
0.5 rather than 0.4 in critical operation.

The data for compressor face total pressure recovery, p_{oc}/p_o
show a slight increase in pressure recovery with decreasing bleed
mass flow. There was also an unusual 1% drop in pressure recovery for
bleed mass flows greater than 5% of capture. However, conclusions
about inlet performance cannot be made from these data because of
the supercritical operation of the inlet.

It should be noted that the bleed mass flow rates used were
not very large in comparison with prior experiments on the same
inlet. This was also true for the few critical mode measurements
taken.

Section 3.2 Critical Mode Operation

A few data points were taken in critical mode operation and compressor face stagnation pressure recoveries between 89.2% and 89.9% were recorded. These data are presented in Table 3-VIII with bleed mass flow rates and compressor face distortion measurements. Since no attempt was made to use post-terminal shock bleed or bypass bleed the compressor recoveries were quite adequate. Also, no effort was made to optimize the effect of the bleed configurations that were used for maximum compressor face total pressure recoveries.

The largest compressor face total pressure recovery obtained was 89.94% with a distortion level of 10.3% at a bleed mass flow rate of 4.71% of the capture mass flow. The lowest compressor face total pressure recovery obtained was 89.16% with distortion of 11.1% at a bleed rate of 4.34% of capture. A very interesting result was that a compressor face total pressure recovery of 89.21% was obtained with distortion of 11.1% with the bleed mass flow rate being only 3.07% of the inlet's capture mass flow. The latter results seems very promising since no attempt was made to optimize the bleed configuration for pressure recovery.

The boundary layer contains a range of stagnation pressures varying from the external static pressure at the wall, assuming $\frac{\partial p}{\partial y} \approx 0$, to the external stagnation pressure at the edge of the boundary layer. This stagnation pressure gradient is a cause for the compressor face radial distortion and some of the stagnation pressure loss at the compressor face. Removal of the cowl boundary layer

66

helps to increase the total pressure recovery and decrease the distortion at the compressor face. Bleed flows that remove more than the boundary layer mass flow actually remove higher pressure flow in the freestream and would not, from this point of view, increase the compressor face stagnation pressure. As most of the boundary layer mass flow is away from the wall and this would be the large stagnation pressure region, removal of only the low stagnation pressure region close to the wall would seem to be more useful for the overall inlet performance.

It has been shown by Cubbison et al[21], and Choby[22] that removal of the cowl boundary layer by use of a bypass system near the compressor face increases the compressor face stagnation pressure recovery and decreases the distortion. In addition, bleeding behind the terminal shock in critical operation again increases the compressor face total pressure recovery and decreases the distortion. The data showed that for this inlet, pressure recoveries of 92% were obtained with no bypass and with bleed mass flows of 10% of the inlet's capture mass flow. Compressor face total pressure recoveries of 95% were obtained with both bleed, 8% of $\dot{M}_c$, and bypass, 8% of $\dot{M}_c$, utilized. These data indicate that significantly higher compressor face total pressure recoveries might have been obtained in the present tests and bypass bleed and bleed downstream of the geometric throat been used.

TABLE 3-I

LOCATION OF CENTERBODY BLEED REGIONS

			From $\dfrac{x}{R}_c$	To $\dfrac{x}{R}_c$
Run 2	DS	A	2.853	2.943
Run 3	DS	B	2.853	2.895
Run 4	AS		2.780	2.871
Run 5	DS	C	2.804	2.943
Run 6	US		2.706	2.846
Run 10	Scoop		2.840	

The distances are given from the leading edge of the first open row of holes to the trailing edge of the last row of open holes.

TABLE 3-II

PROBE 2 BOUNDARY LAYER PARAMETERS

Run Number	$\dot{M}_{BLEED}/\dot{M}_{BL_1}$ (%)	M_e	T_w (°K)	H_{tr}	δ^* (cm)	θ (cm)
2	64.6	1.63	307.0	1.328	.0428	.0172
DS A	63.4	1.63	306.6	1.325	.0432	.0173
	61.7	1.62	307.1	1.324	.0438	.0176
	60.5	1.62	307.6	1.326	.0443	.0178
	59.9	1.62	307.6	1.323	.0450	.0181
	57.3	1.62	307.4	1.319	.0470	.0190
	51.9	1.62	306.3	1.316	.0501	.0204
	45.2	1.63	305.6	1.302	.0597	.0243
	36.9	1.63	304.7	1.299	.0676	.0276
	31.4	1.62	308.1	1.316	.0766	.0312
	17.0	1.63	301.5	1.354	.1045	.0421
	2.6	1.60	300.4	1.429	.1433	.0560
3	29.7	1.62	299.1	1.329	.0894	.0362
DS B	26.6	1.63	299.1	1.330	.0918	.0371
	25.8	1.62	299.1	1.333	.0922	.0373
	25.1	1.62	299.2	1.329	.0923	.0374
	22.8	1.62	299.4	1.336	.0952	.0385
	18.9	1.61	298.7	1.341	.1003	.0405
	13.3	1.61	298.0	1.357	.1085	.0436
	7.5	1.60	297.6	1.384	.1219	.0485
	1.2	1.58	296.7	1.447	.1464	.0571
4	19.6	1.61	296.1	1.427	.1273	.0495
AS	18.0	1.61	296.4	1.439	.1306	.0504
	10.3	1.61	296.6	1.461	.1428	.0543
	5.6	1.60	295.6	1.501	.1568	.0588
	2.9	1.60	295.9	1.534	.1708	.0632
5	33.9	1.65	301.2	1.317	.0586	.0234
DS C	25.3	1.65	300.3	1.325	.0758	.0302
	20.7	1.66	299.5	1.329	.0877	.0348
	14.8	1.65	298.6	1.354	.0997	.0395
	11.7	1.65	298.2	1.377	.1115	.0436

Table 3-II, Cont'd.

Run Number	$\dot{M}_{BLEED}/\dot{M}_{BL_1}$ (%)	M_e	T_w (°K)	H_{tr}	δ^* (cm)	θ (cm)
6	42.9	1.65	299.5	1.361	.1332	.0522
US	40.0	1.66	300.0	1.366	.1349	.0526
	22.7	1.65	300.3	1.377	.1364	.0533
	12.4	1.63	297.1	1.429	.1495	.0575
	9.6	1.62	298.9	1.442	.1514	.0578
	5.8	1.62	297.4	1.454	.1550	.0591
	0.2	1.62	295.9	1.502	.1695	.0632
10	22.5	1.64	301.6	1.359	.0923	.0362
Scoop	21.6	1.64	301.9	1.355	.0924	.0363
	21.2	1.64	301.3	1.360	.0931	.0362
	21.0	1.64	301.4	1.358	.0923	.0362
	19.6	1.64	301.5	1.357	.0933	.0366
	8.4	1.64	299.1	1.359	.0948	.0375

TABLE 3-III

PROBE 3 BOUNDARY LAYER PARAMETERS

Run Number	$\dot{M}_{BLEED}/\dot{M}_{BL_1}$ (%)	M_e	T_w (°K)	$\dot{H}_{tr}$	δ^* (cm)	θ (cm)
2	64.6	1.45	310.7	1.300	.0640	.0287
DS A	63.4	1.45	310.1	1.336	.0653	.0287
	61.7	1.45	310.8	1.320	.0664	.0294
	60.5	1.46	311.4	1.333	.0682	.0299
	59.9	1.46	311.1	1.324	.0691	.0305
	57.3	1.46	311.1	1.330	.0711	.0312
	51.9	1.46	311.1	1.331	.0746	.0327
	45.2	1.46	309.5	1.312	.0796	.0354
	36.9	1.46	309.5	1.298	.0879	.0395
	31.4	1.46	306.4	1.302	.0997	.0446
	17.0	1.46	305.6	1.310	.1232	.0552
	2.6	1.43	304.7	1.353	.1532	.0683
4	19.6	1.47	302.2	1.303	.1135	.0507
AS	18.0	1.47	302.5	1.292	.1128	.0507
	10.3	1.47	302.3	1.289	.1224	.0552
	5.6	1.47	304.5	1.311	.1344	.0600
	2.9	1.46	304.5	1.321	.1440	.0642
5	33.9	1.54	304.4	1.223	.0869	.0391
DS C	25.3	1.54	303.9	1.251	.0966	.0429
	20.7	1.54	303.6	1.260	.1028	.0454
	14.8	1.53	302.8	1.264	.1090	.0483
	11.7	1.50	302.5	1.296	.1304	.0575
6	42.9	1.54	303.6	1.233	.1005	.0451
US	40.0	1.54	304.2	1.230	.0997	.0448
	22.7	1.53	304.7	1.239	.1053	.0472
	12.4	1.52	301.0	1.247	.1212	.0550
	9.6	1.51	303.4	1.260	.1251	.0561
	5.8	1.52	301.4	1.261	.1372	.0615
	0.2	1.52	299.8	1.282	.1506	.0667
10	22.5	1.52	304.3	1.320	.1196	.0511
Scoop	21.6	1.52	303.7	1.304	.1160	.0500
	21.2	1.52	303.7	1.310	.1240	.0535
	21.0	1.52	302.9	1.303	.1168	.0505
	18.6	1.51	302.8	1.309	.1278	.0554
	8.4	1.52	302.6	1.306	.1346	.0585

TABLE 3-IV

PROBE 4 BOUNDARY LAYER PARAMETERS

Run Number	$\dot{M}_{FORWARD}/\dot{M}_c$ (%)	$\dot{M}_{TOTAL}/\dot{M}_c$ (%)	M_e	T_w ($^\circ$K)	H_{tr}	δ^* (cm)	θ (cm)
2	1.04	2.85	1.15	313.9	1.409	.0356	.0176
DS A	1.07	2.78	1.16	313.6	1.424	.0350	.0171
	1.17	2.77	1.16	313.3	1.401	.0355	.0176
	1.09	2.75	1.16	314.0	1.411	.0353	.0174
	1.13	2.72	1.16	312.7	1.399	.0356	.0176
	0.83	2.45	1.15	312.3	1.363	.0476	.0242
	0.73	2.36	1.15	311.8	1.354	.0523	.0269
	0.59	2.26	1.15	309.8	1.364	.0610	.0312
	0.32	2.08	1.11	309.5	1.368	.0807	.0421
4	0.84	2.75	1.06	306.9	1.370	.0612	.0326
AS	0.21	2.52	1.03	305.6	1.403	.0530	.0282
	0.29	2.31	1.08	306.9	1.360	.0514	.0273
	0.31	2.31	1.08	306.7	1.356	.0522	.0278
	0.36	2.26	1.06	306.2	1.353	.0582	.0314
	0.33	2.26	1.07	306.6	1.363	.0555	.0296
	0.34	2.24	1.07	306.4	1.359	.0616	.0330
	0.37	2.20	1.06	307.0	1.405	.0640	.0335
	0.19	2.13	1.07	306.7	1.347	.0584	.0315
	0.10	2.11	1.08	305.7	1.334	.0626	.0339
	0.05	2.10	1.08	306.2	1.332	.0670	.0366
5	0.22	2.17	1.04	307.6	1.402	.0815	.0431
DS C	0.74	1.72	1.10	308.0	1.402	.0820	.0421
	0.80	1.66	1.09	307.4	1.403	.1283	.0661
	0.61	1.44	1.10	307.4	1.430	.1242	.0628
	0.46	1.30	1.10	307.5	1.448	.1267	.0633
	0.39	1.25	1.10	307.4	1.450	.1294	.0643
	0.28	1.20	1.11	307.0	1.453	.1312	.0651
10	0.30	2.22	1.06	307.3	1.395	.0528	.0278
Scoop	0.33	2.18	1.07	307.3	1.358	.0481	.0256
	0.37	2.12	1.12	307.6	1.370	.0460	.0238
	0.39	2.03	1.13	307.3	1.363	.0514	.0265
	0.42	1.97	1.13	307.9	1.358	.0531	.0276

TABLE 3-V

LOCATION OF COWL BLEED REGIONS

			From $\frac{x}{R_c}$	To $\frac{x}{R_c}$
Run 2	AS 1	(LN)	3.223	3.254
Run 4	US 1	(LN)	3.118	3.201
Run 5	US 2	(Slant)	3.048	3.161
Run 6	AS 2	(Slant)	3.228	3.306
Run 7	US 3	(Slant)	3.132	3.258
Run 8	US 4	(SN)	3.209	3.277
Run 9	US 5	(SN)	3.168	3.242
Run 10	US 6	(SN)	3.121	3.198

The distances are given from the leading edge of the first open row of holes to the trailing edge of the last open row of holes.

TABLE 3-VI

PROBE 6 BOUNDARY LAYER PARAMETERS

Run Number	$\dot{M}_{BLEED}/\dot{M}_{BL_\delta}$ (%)	M_e	T_w (°K)	H_{tr}	δ^* (cm)	θ (cm)
2	21.4	1.08	310.4	1.687	.1479	.0652
	18.5	1.08	310.3	1.692	.1486	.0654
	14.8	1.08	309.9	1.690	.1511	.0667
	11.8	1.08	310.2	1.690	.1525	.0672
	7.8	1.10	309.6	1.728	.1744	.0747
	6.6	1.11	308.8	1.785	.1880	.0780
4	43.6	1.04	313.4	1.509	.0945	.0458
	42.0	1.04	313.0	1.519	.0956	.0462
	37.4	1.04	312.8	1.530	.0981	.0471
	29.9	1.04	311.1	1.522	.1002	.0485
	26.1	1.05	310.6	1.518	.1049	.0505
5	100.7	1.00	306.6	1.411	.0358	.0194
	46.1	1.07	306.8	1.525	.0947	.0460
	28.9	1.09	304.1	1.469	.1229	.0613
	18.8	1.10	304.2	1.572	.1566	.0732
6	92.3	1.01	304.8	1.571	.0131	.0064
	59.3	0.98	309.3	1.435	.0207	.0111
	43.0	1.03	308.3	1.322	.0385	.0216
	28.1	1.05	308.4	1.389	.0611	.0325
	9.3	1.09	306.8	1.474	.1022	.0508
7	114.4	.97	303.7	1.545	.0194	.0099
	110.3	.98	304.6	1.513	.0235	.0121
	68.7	1.01	305.8	1.419	.0304	.0162
	50.9	1.03	304.8	1.364	.0427	.0235
	43.8	1.04	304.9	1.383	.0574	.0310
	33.2	1.05	303.8	1.342	.0629	.0348
8	51.8	1.02	305.4	1.446	.0637	.0332
	44.4	1.01	305.6	1.519	.0684	.0343
	35.2	1.04	306.0	1.506	.0860	.0428
	31.0	1.04	305.1	1.497	.0877	.0438
	16.1	1.05	304.9	1.503	.1026	.0509
	6.5	1.07	304.6	1.559	.1231	.0588
	1.6	1.09	305.6	1.635	.1441	.0654

Table 3-VI, Cont.

Run Number	$\dot{M}_{BLEED}/\dot{M}_{BL_5}$ (%)	M_e	T_w (°K)	H_{tr}	δ^* (cm)	θ (cm)
9	58.7	1.03	306.1	1.513	.0677	.0336
	58.5	1.03	306.1	1.497	.0651	.0326
	54.1	1.04	306.9	1.519	.0703	.0348
	53.4	1.04	305.9	1.538	.07404	.0362
	44.1	1.04	305.9	1.538	.0796	.0388
	36.0	1.05	306.1	1.545	.0868	.0421
	26.2	1.05	305.7	1.549	.0945	.0457
	18.1	1.05	305.6	1.549	.1007	.0487
	7.8	1.08	305.2	1.598	.1261	.0586
	2.1	1.09	304.7	1.637	.1368	.0621
10	47.2	1.06	306.2	1.459	.0835	.0424
	39.6	1.06	305.5	1.437	.0888	.0447
	31.2	1.06	305.1	1.489	.0957	.0476
	20.7	1.06	304.3	1.480	.0996	.0500
	14.7	1.06	304.4	1.469	.1023	.0518

TABLE 3-VII

PROBE 7 BOUNDARY LAYER PARAMETERS

Run Number	$\dot{M}_{BLEED}/\dot{M}_{BL_5}$ (%)	M_e	T_w ($^\circ$K)	H_{tr}	δ^* (cm)	θ (cm)
2	21.4	1.24	305.1	1.300	.1071	.0553
	18.5	1.23	304.7	1.301	.1076	.0557
	14.8	1.23	303.8	1.312	.1098	.0569
	11.8	1.22	303.8	1.322	.1124	.0581
	7.8	1.20	303.6	1.350	.1320	.0681
	6.6	1.20	303.5	1.338	.1341	.0692
4	43.6	1.20	306.7	1.281	.0855	.0448
	42.0	1.19	306.6	1.283	.0850	.0446
	37.4	1.20	306.1	1.282	.0863	.0452
	29.9	1.21	304.7	1.278	.0871	.0457
	26.1	1.21	304.2	1.279	.0870	.0458
5	100.7	1.19	299.3	1.292	.0330	.0177
	46.1	1.21	299.4	1.280	.0682	.0364
	28.9	1.19	300.0	1.283	.1308	.0706
	18.8	1.15	299.9	1.303	.1465	.0801
6	92.3	1.18	299.5	1.335	.0280	.0146
	59.3	1.18	307.9	1.301	.0371	.0198
	43.0	1.22	301.5	1.271	.0516	.0276
	28.1	1.22	301.6	1.257	.0639	.0343
	9.3	1.09	301.4	1.403	.1153	.0609
7	114.4	1.17	299.1	1.369	.0239	.0123
	110.3	1.16	299.3	1.367	.0244	.0126
	68.7	1.17	299.5	1.309	.0395	.0211
	50.9	1.19	299.8	1.316	.0377	.0200
	43.8	1.18	299.5	1.248	.0523	.0290
	33.2	1.23	299.8	1.234	.1297	.0706
8	51.8	1.25	299.1	1.256	.0575	.0303
	44.4	1.24	299.3	1.261	.0632	.0334
	35.2	1.25	299.2	1.267	.0703	.0369
	31.0	1.26	299.1	1.269	.0717	.0376
	16.1	1.26	299.2	1.266	.0816	.0426
	6.5	1.27	299.5	1.273	.0942	.0489
	1.6	1.23	299.1	1.311	.1080	.0563

Table 3-VII, cont'd.

Run Number	$\dot{M}_{BLEED}/\dot{M}_{BL_5}$ (%)	M_e	T_w (°K)	H_{tr}	$\delta *$ (cm)	θ (cm)
9	58.8	1.26	298.8	1.269	.0617	.0322
	58.5	1.27	298.8	1.273	.0593	.0308
	54.1	1.26	299.3	1.270	.0629	.0329
	53.4	1.26	298.8	1.272	.0642	.0335
	44.1	1.26	299.1	1.272	.0686	.0357
	36.0	1.26	299.3	1.274	.0728	.0378
	26.2	1.26	299.8	1.275	.0781	.0405
	18.1	1.27	299.9	1.272	.0840	.0435
	7.8	1.26	300.0	1.294	.1001	.0514
	2.1	1.20	300.0	1.352	.1218	.0623
10	47.2	1.28	299.5	1.251	.0652	.0340
	39.6	1.24	299.3	1.278	.0698	.0367
	31.2	1.20	299.1	1.300	.0766	.0406
	20.7	1.23	298.9	1.272	.0817	.0436
	14.7	1.24	299.1	1.269	.0873	.0461

TABLE 3-VIII

COMPRESSOR FACE AND BLEED PARAMETERS FOR CRITICAL OPERATION

Run Number	6	8	8	9	9	10	10
P_{oc}/P_o (%)	89.2	89.8	89.2	89.3	89.9	89.8	89.2
Distortion (%)	9.9	11.1	11.1	11.3	10.3	11.1	11.5
$\dot{M}_{COWL}/\dot{M}_c$ (%)	3.38	2.20	2.16	2.15	2.25	2.20	1.02
$\dot{M}_{FCB}/\dot{M}_c$ (%)	0	0.90	0.89	1.02	0.74	0.90	0
$\dot{M}_{CB}/\dot{M}_c$ (%)	1.94	2.55	1.29	1.26	1.72	1.65	2.05
$\dot{M}_{TB}/\dot{M}_c$	5.32	4.75	4.34	4.43	4.71	4.75	3.07
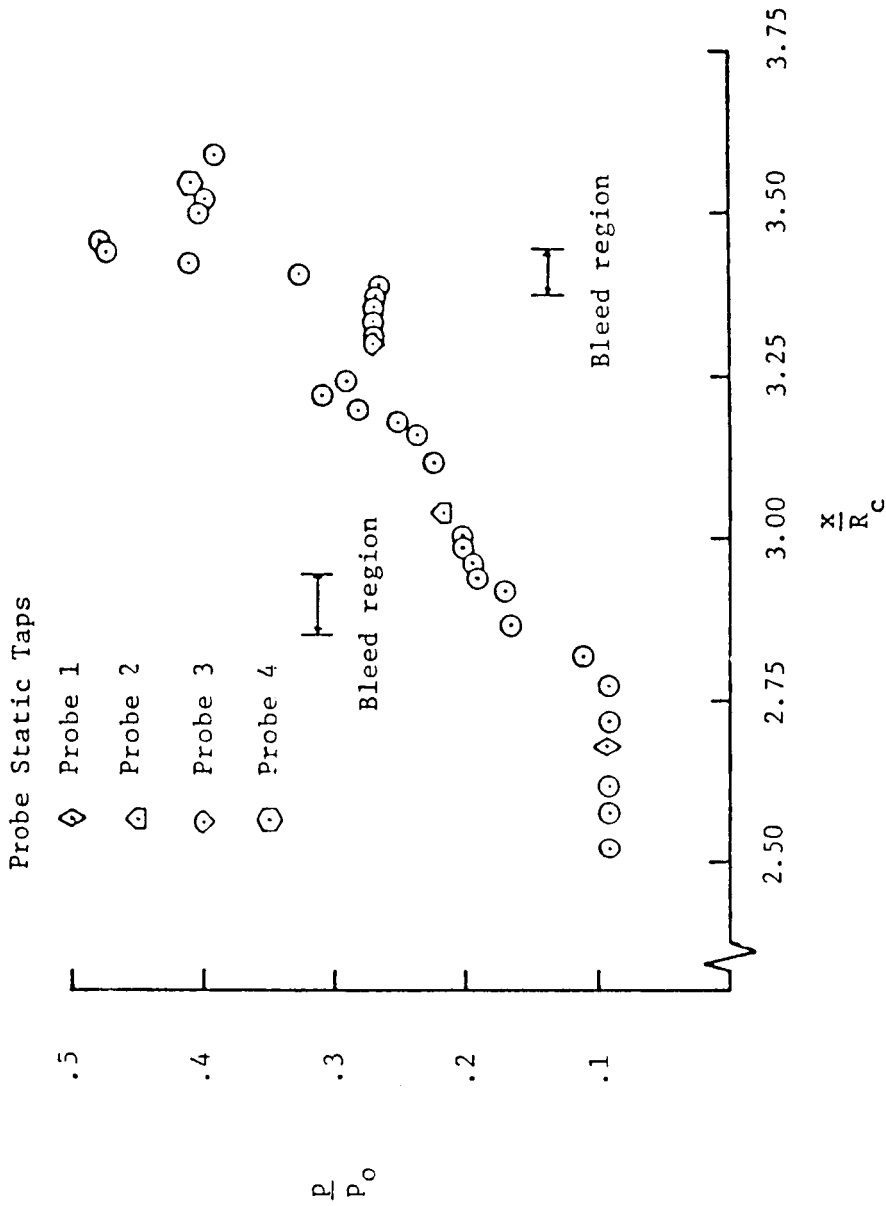
Figure 3.1   Run 2 Centerbody Static Pressure Distribution
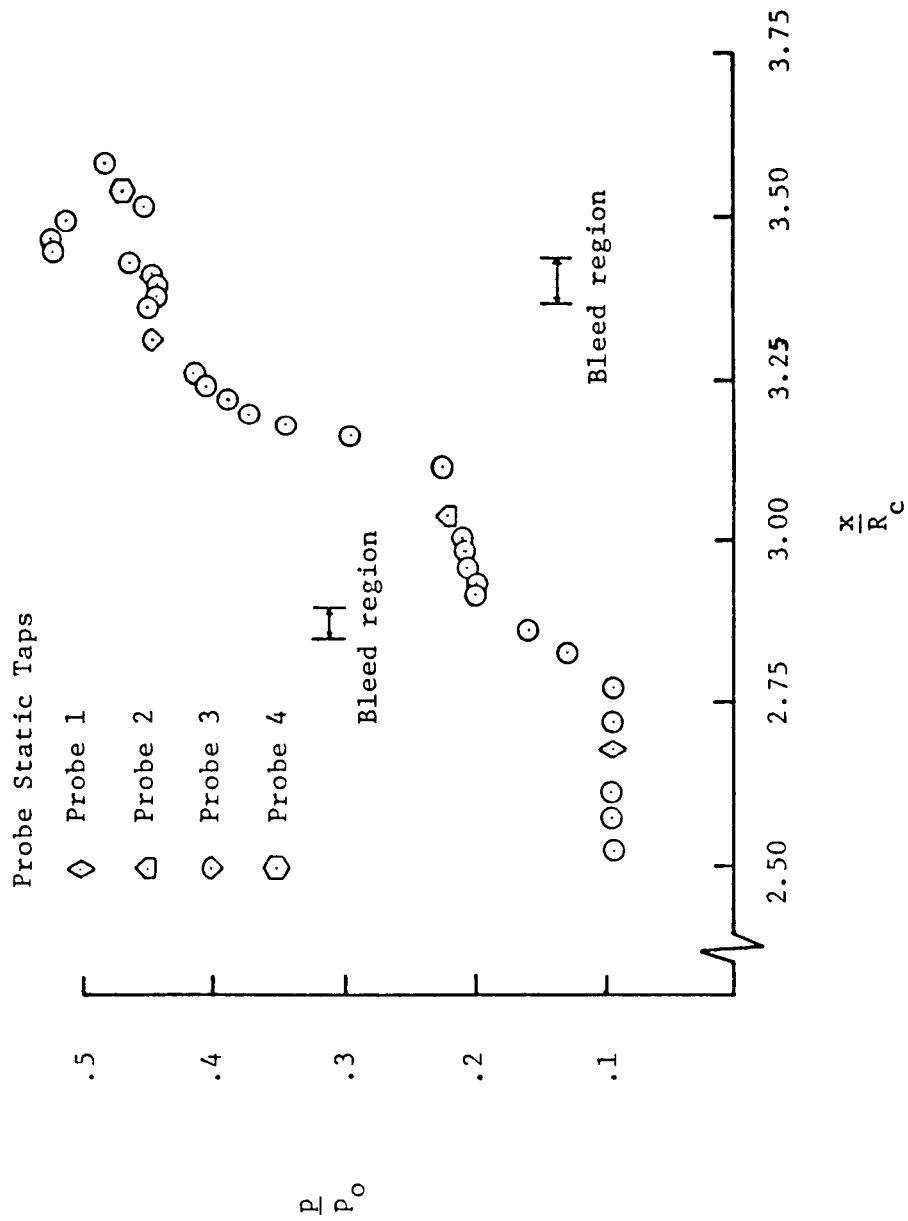
Figure 3.2 Run 3 Centerbody Static Pressure Distribution
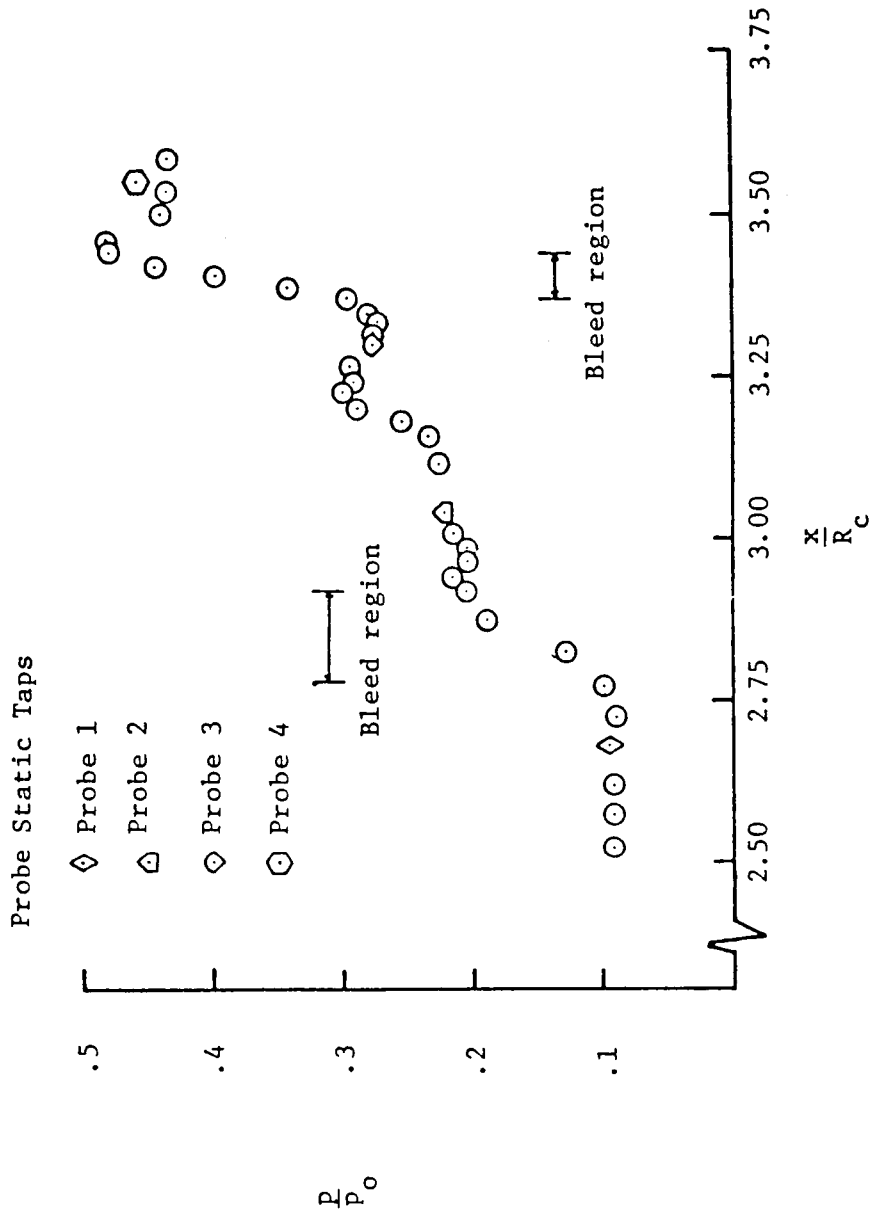
Figure 3.3   Run 4 Centerbody Static Pressure Distribution

81
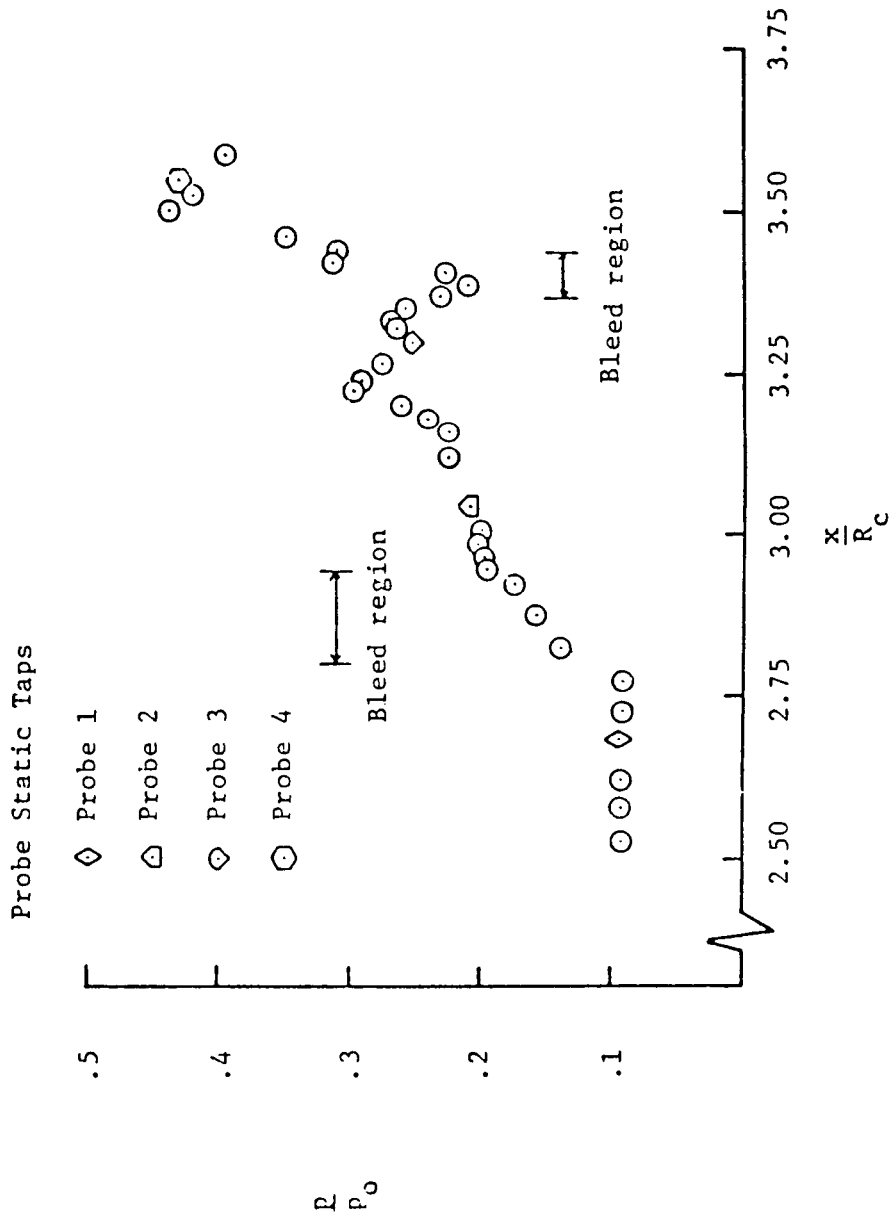
Figure 3.4 Run 5 Centerbody Static Pressure Distribution

82
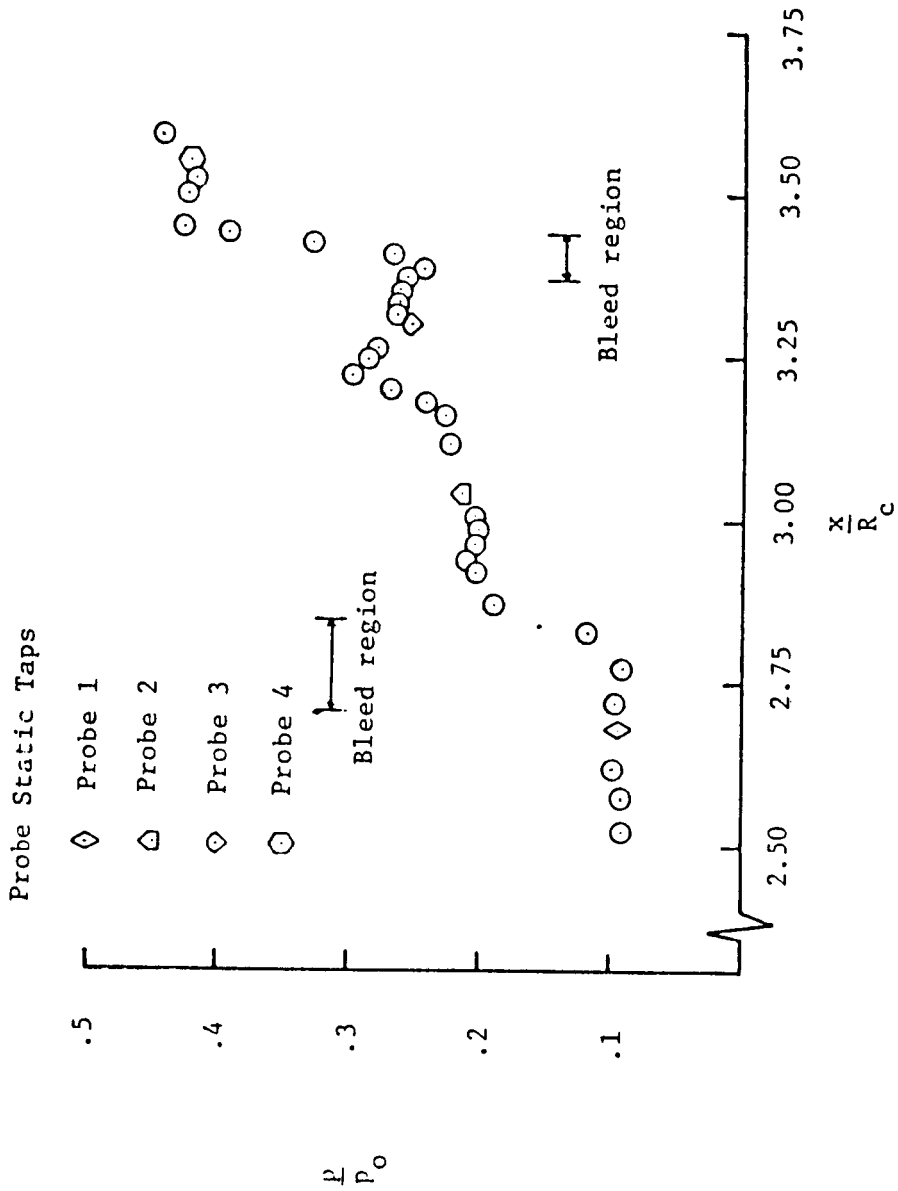
Figure 3.5 Run 6 Centerbody Static Pressure Distribution
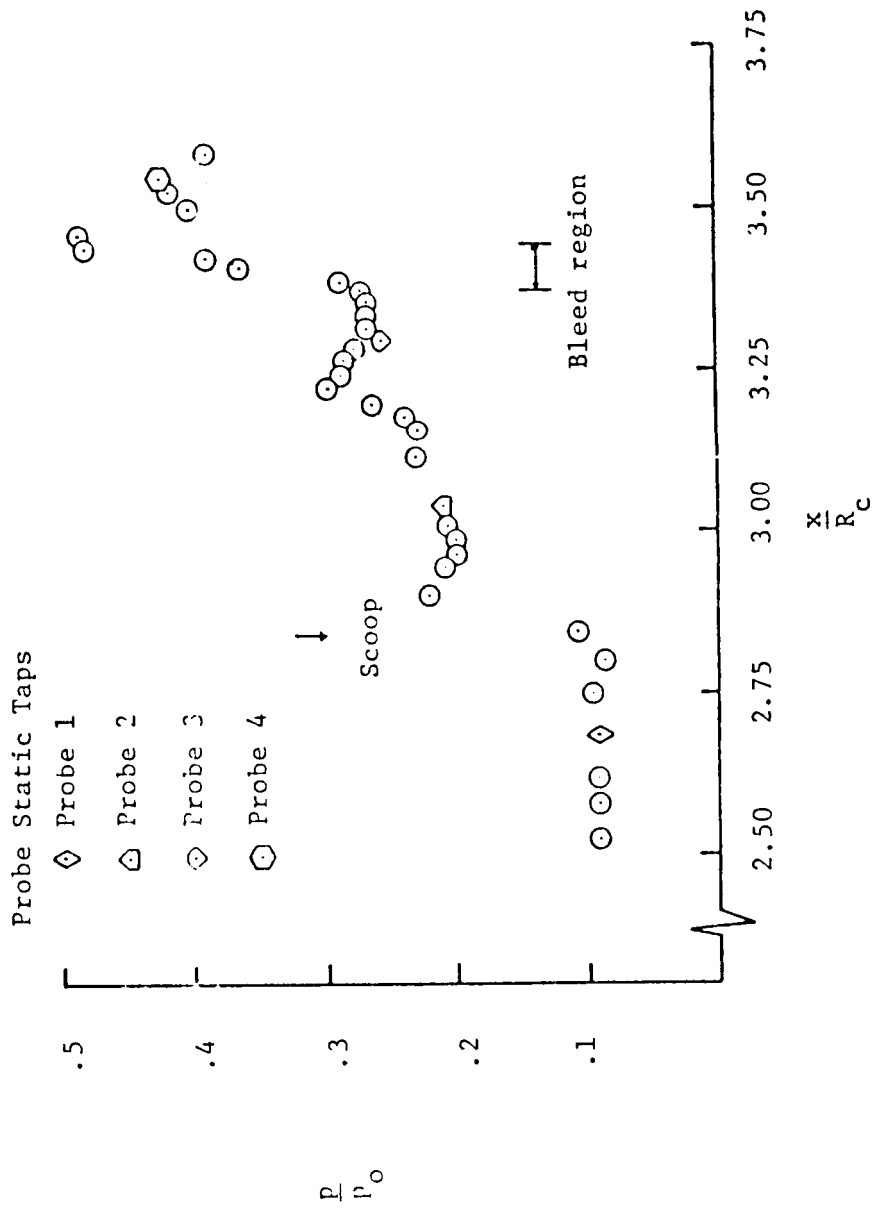
Figure 3.6 Run 10 Centerbody Static Pressure Distribution

Figure 3.7   Schematic of Centerbody Bleed Regions
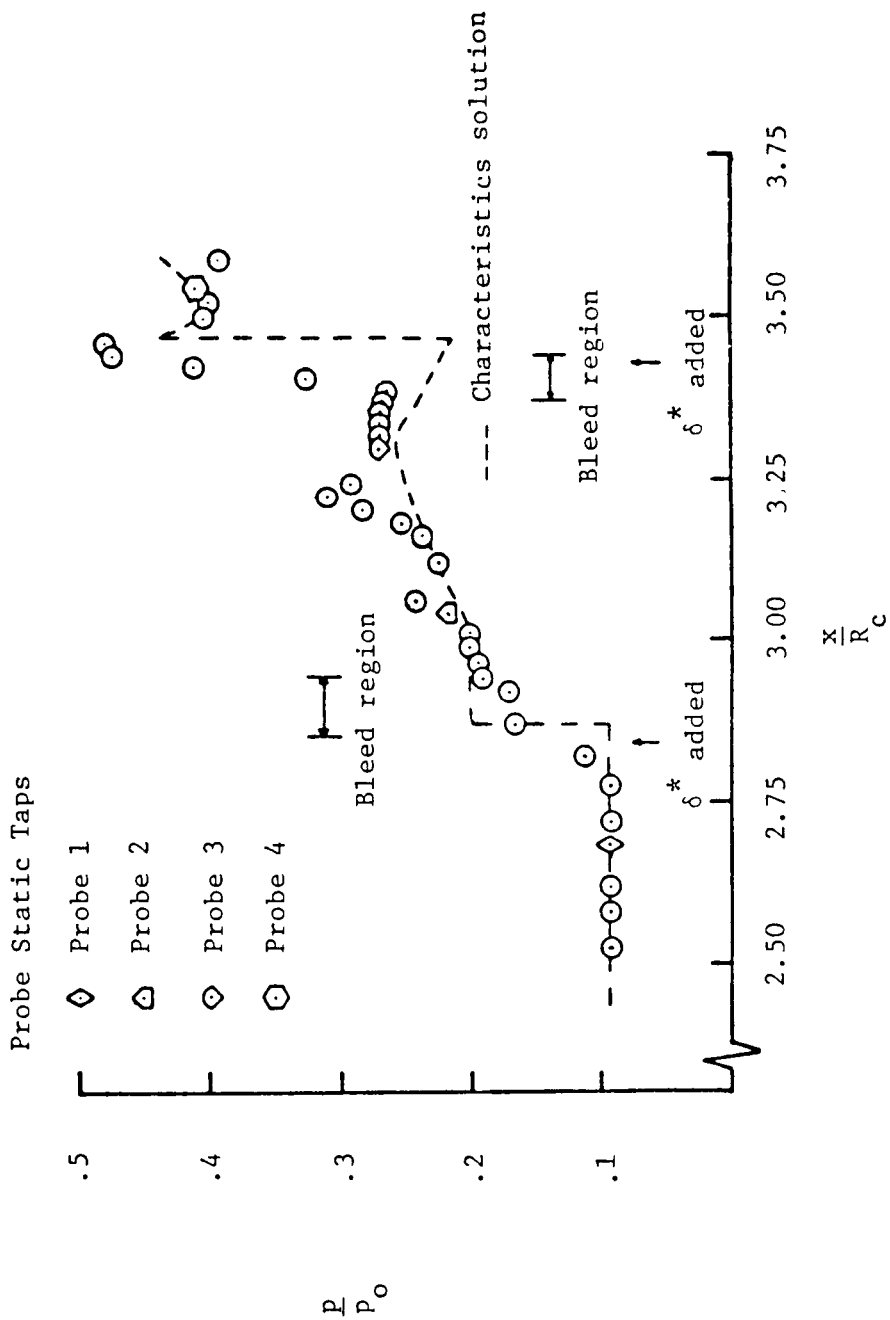
Figure 3.8 Comparison of Run 2 Centerbody Static Pressure Distribution with the Method of Characteristics Solution
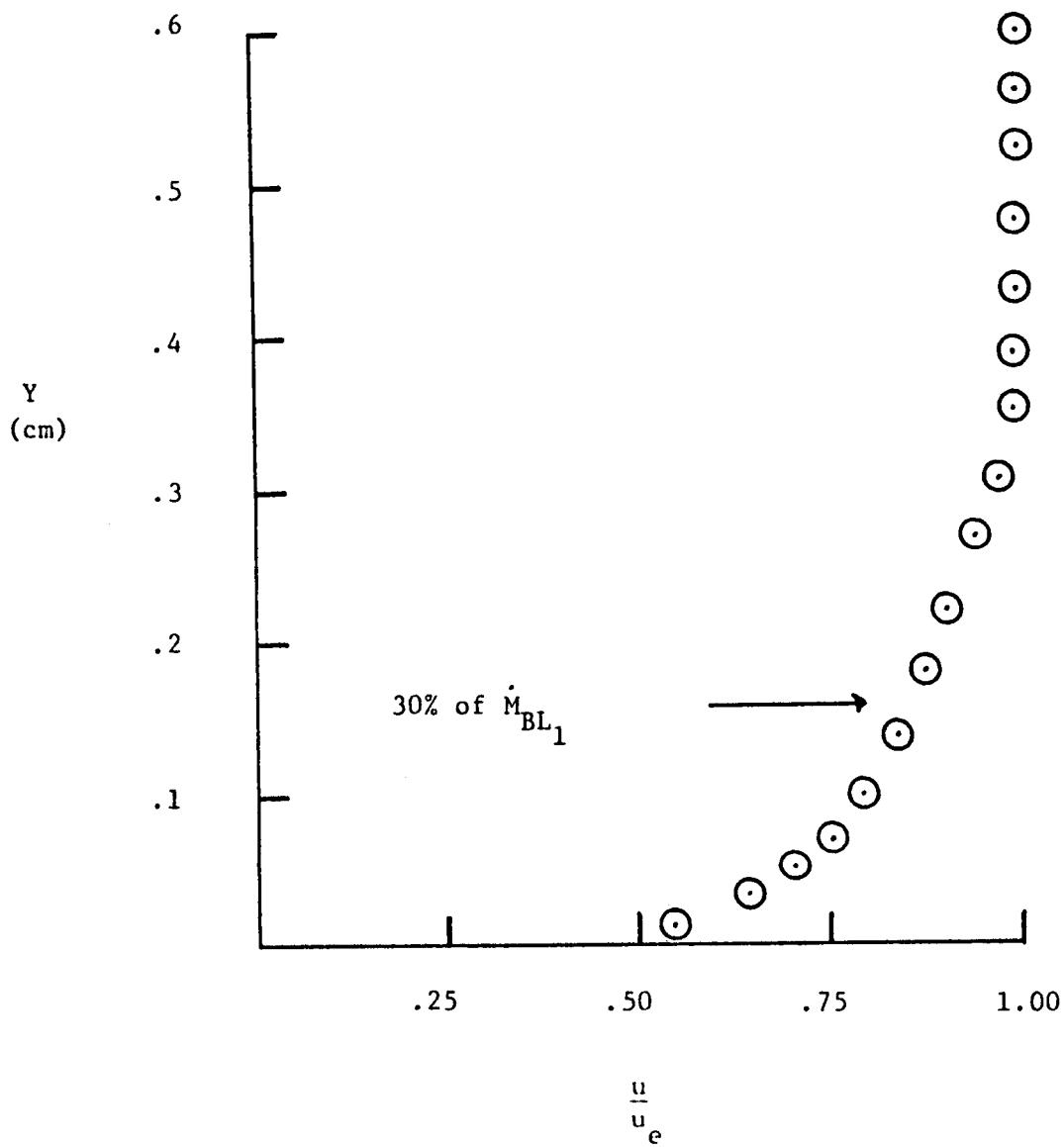
Figure 3.9 Probe 1 Boundary Layer Velocity Profile
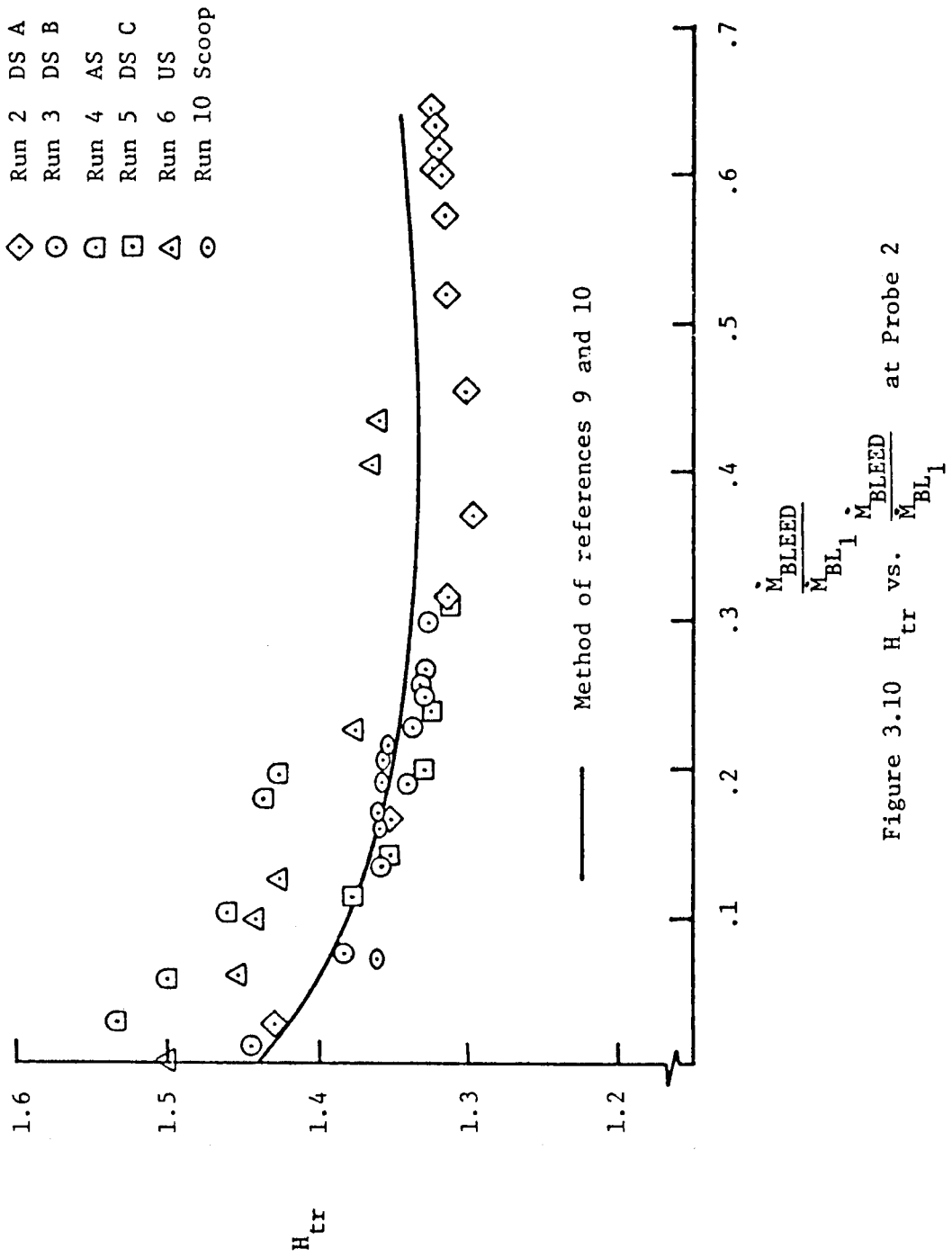
Figure 3.10 H_{tr} vs. $\dfrac{\dot{M}_{BLEED}}{\dot{M}_{BL_1}}$ at Probe 2
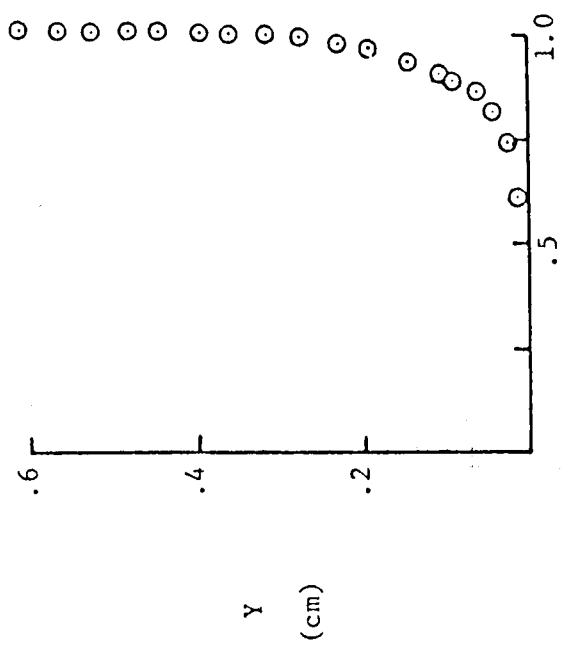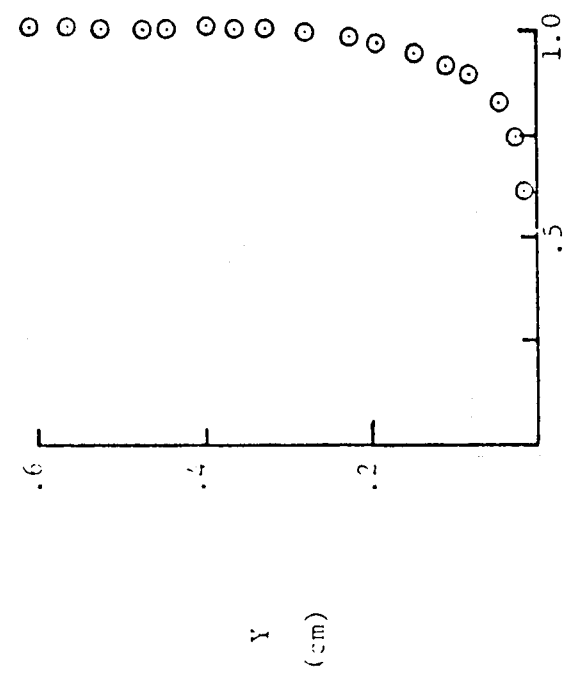
Figures 3.11 a and b Probe 2 Boundary Layer Velocity Profiles
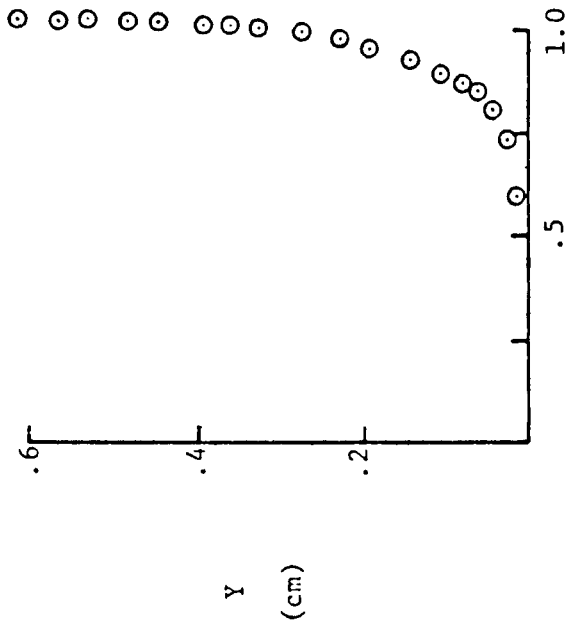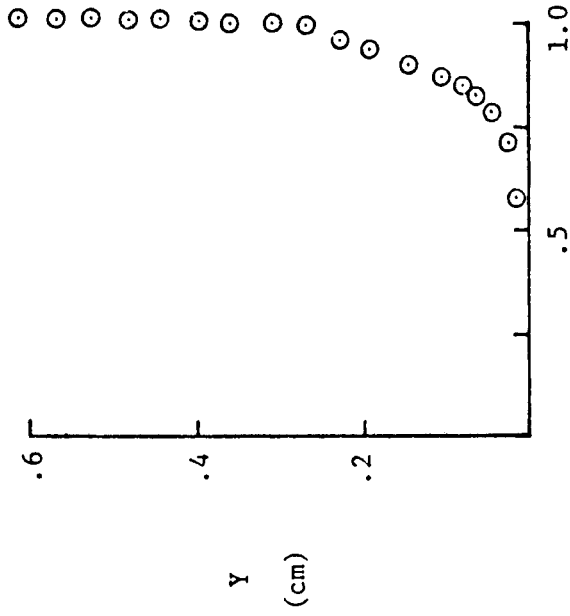
Figures 3.11 c and d Probe 2 Boundary Layer Velocity Profiles

90
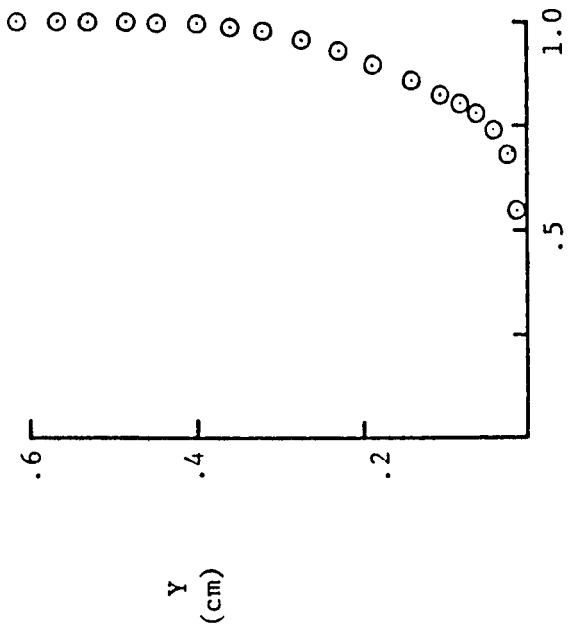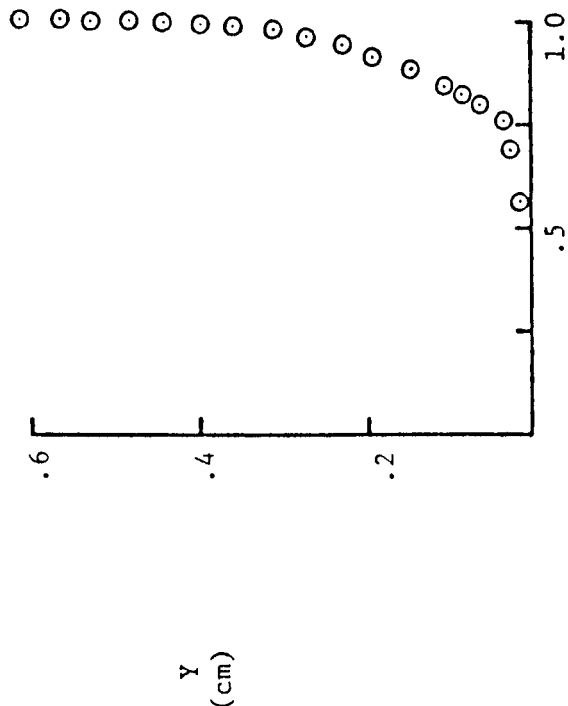
Figures 3.11 e and f   Probe 2 Boundary Layer Velocity Profiles
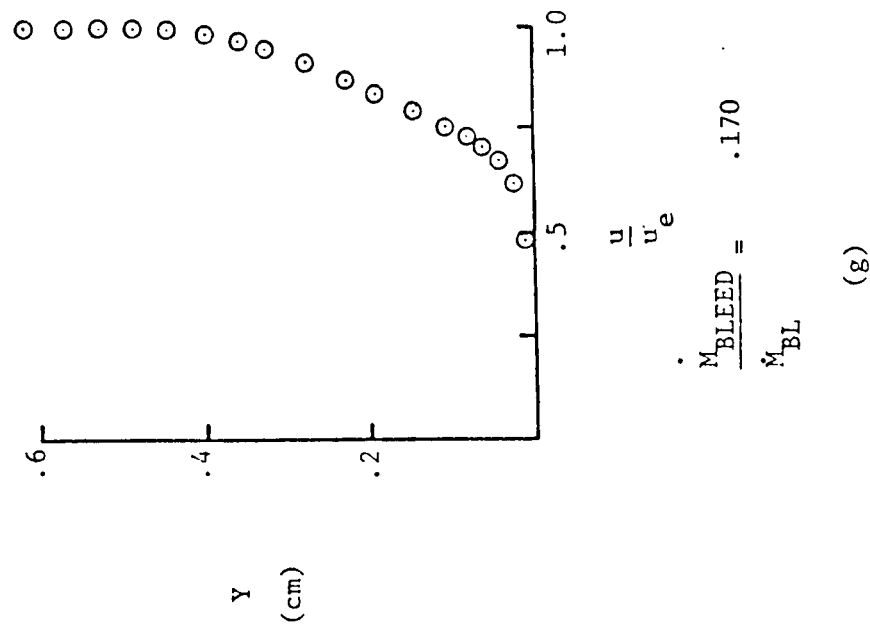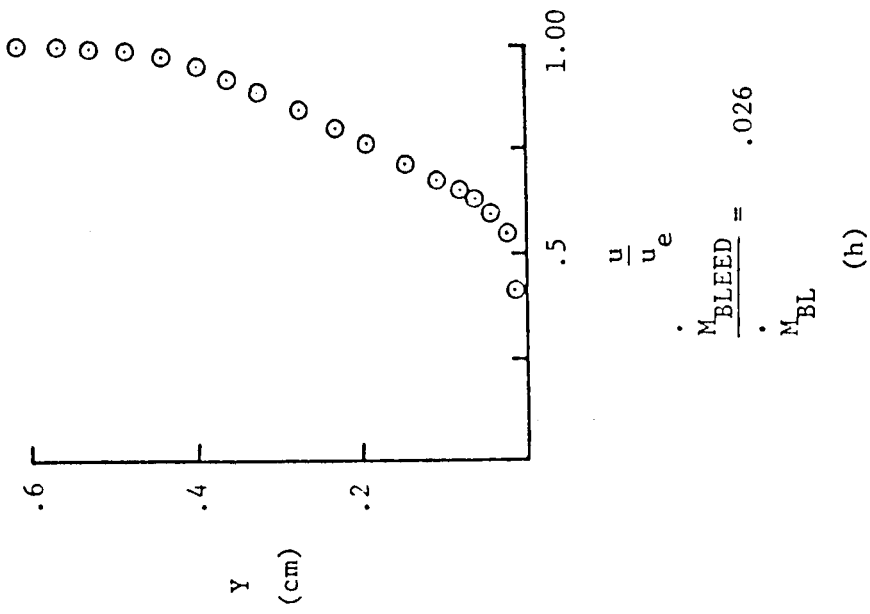
Figures 3.11 g and h Probe 2 Boundary Layer Velocity Profiles
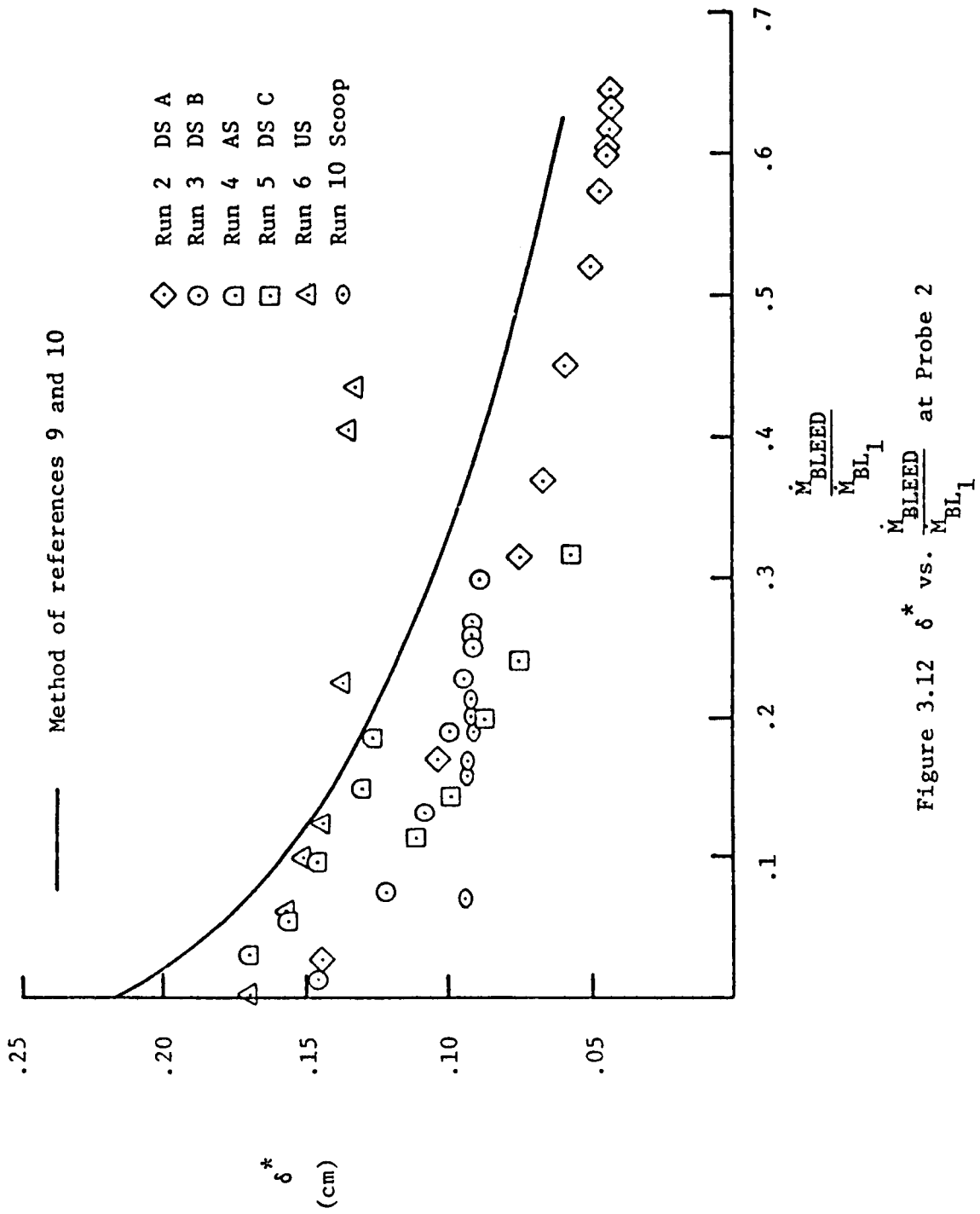
Figure 3.12 δ^* vs. $\dfrac{\dot{M}_{BLEED}}{\dot{M}_{BL_1}}$ at Probe 2

Figure 3.13 θ vs. $\dfrac{\dot{M}_{BLEED}}{\dot{M}_{BL_1}}$ at Probe 2

94
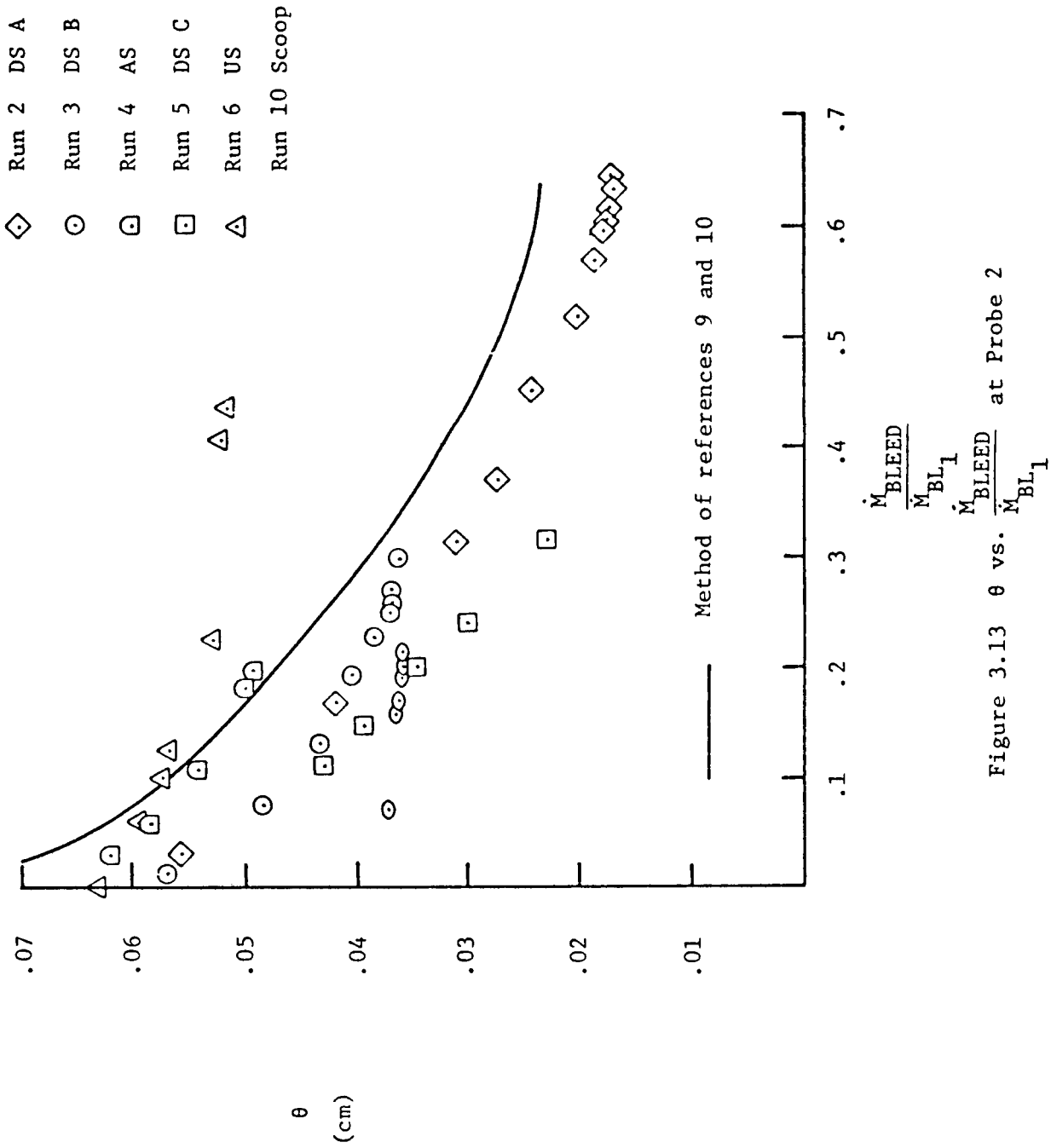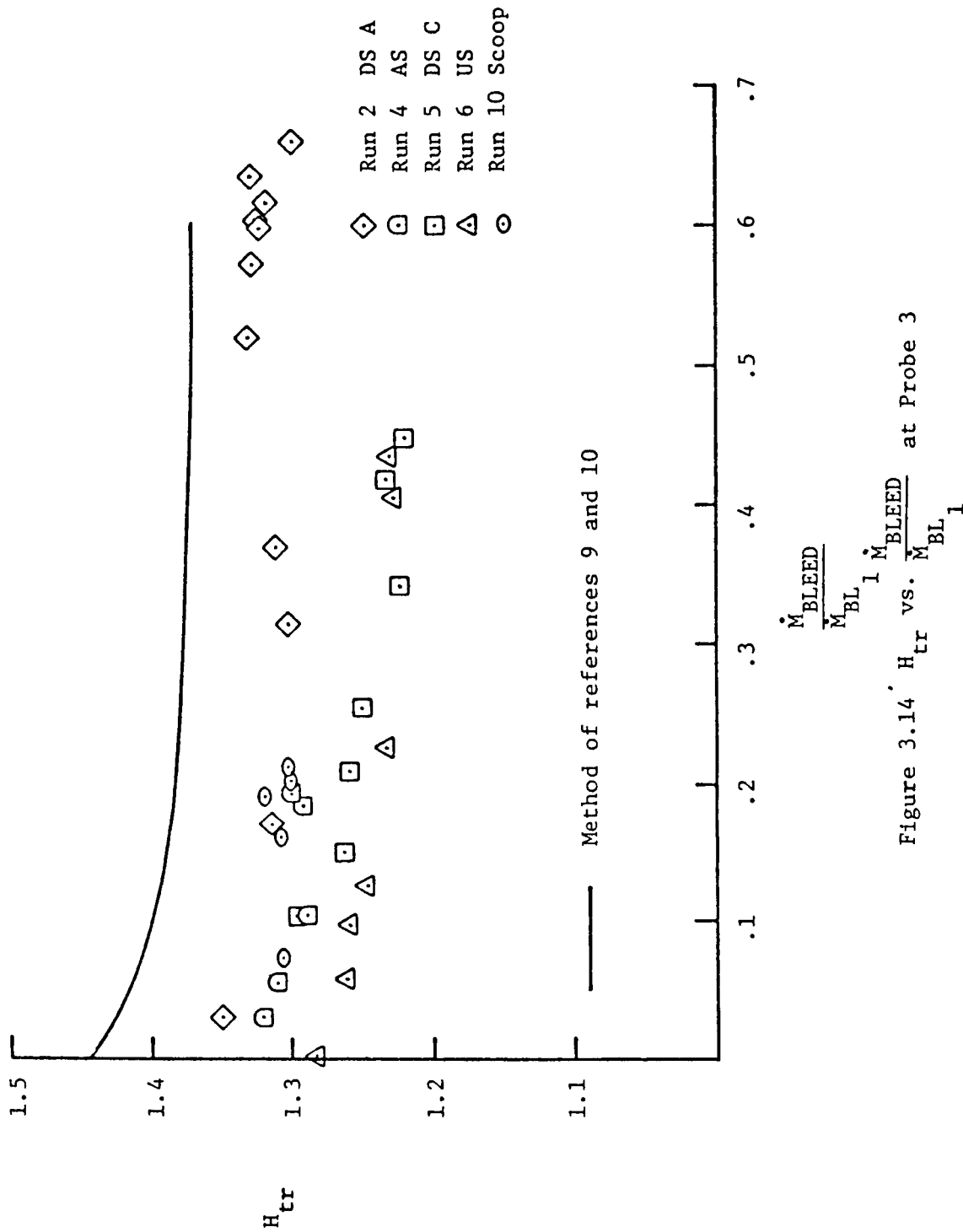
Figure 3.14. H_{tr} vs. $\frac{\dot{M}_{BLEED}}{\dot{M}_{BL_1}}$ at Probe 3
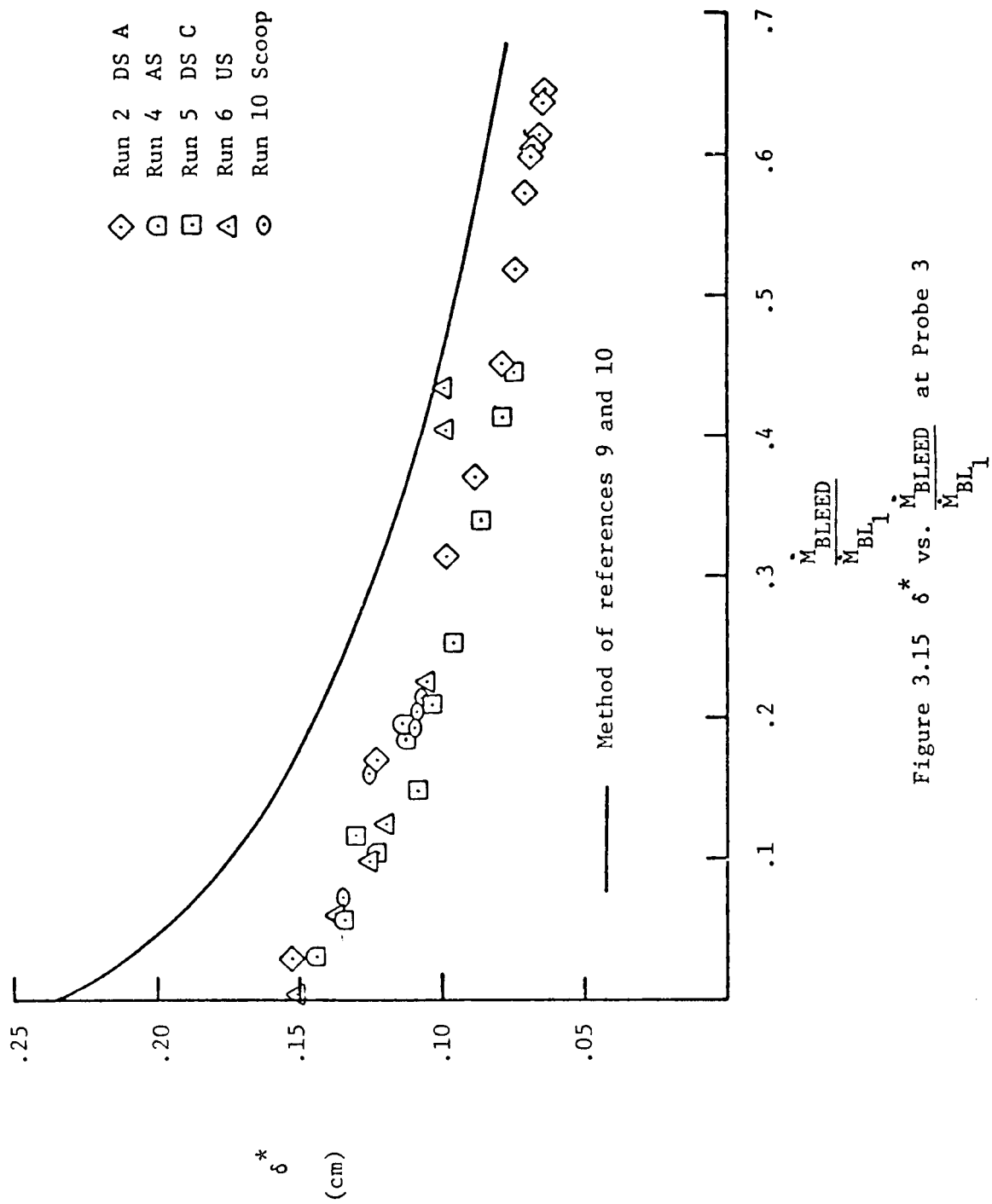
Figure 3.15 δ^* vs. $\dfrac{\dot{M}_{BLEED}}{\dot{M}_{BL_1}}$ at Probe 3
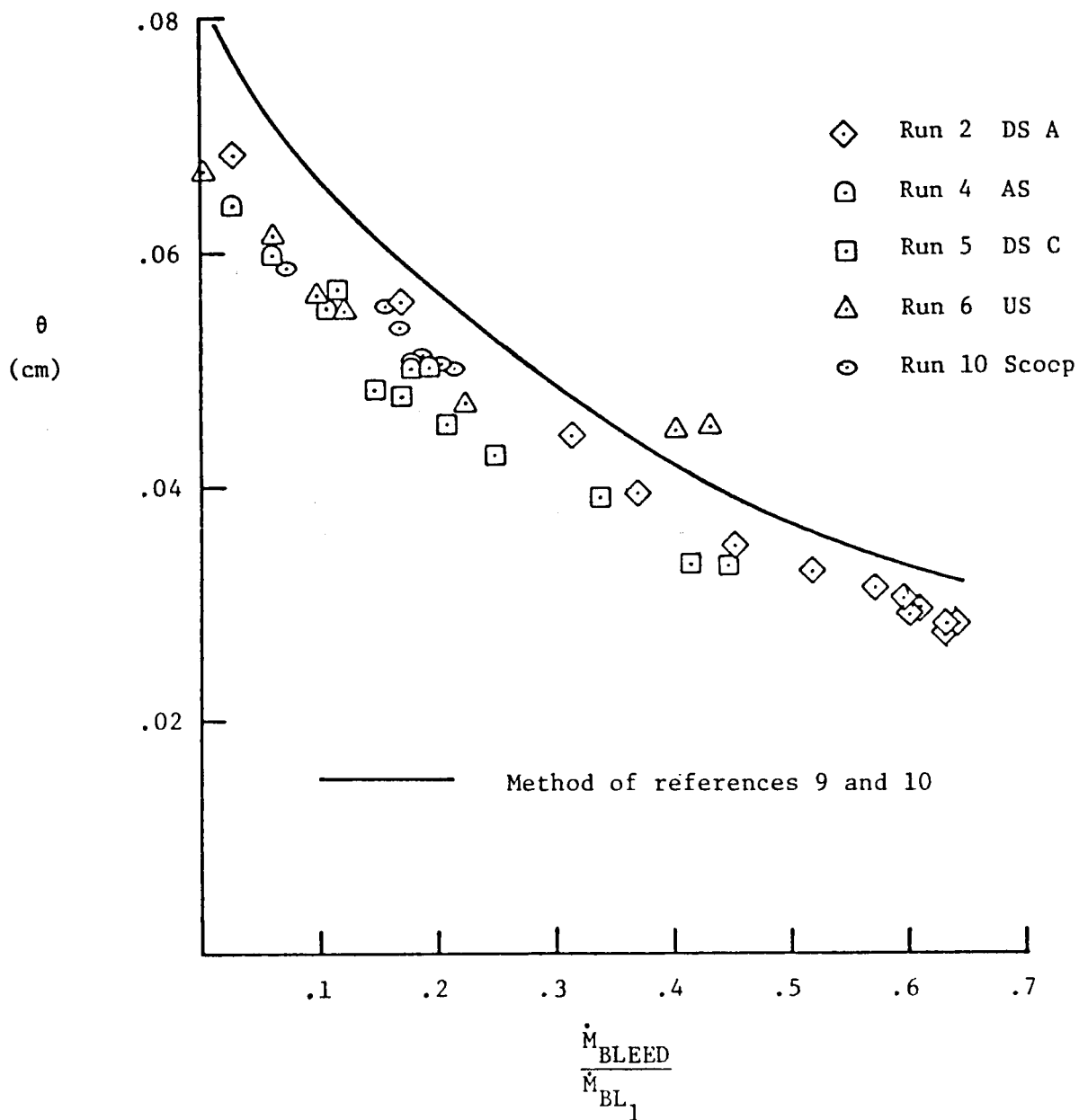
Figure 3.16 θ vs. $\dfrac{M_{BLEED}}{M_{BL_1}}$ at Probe 3
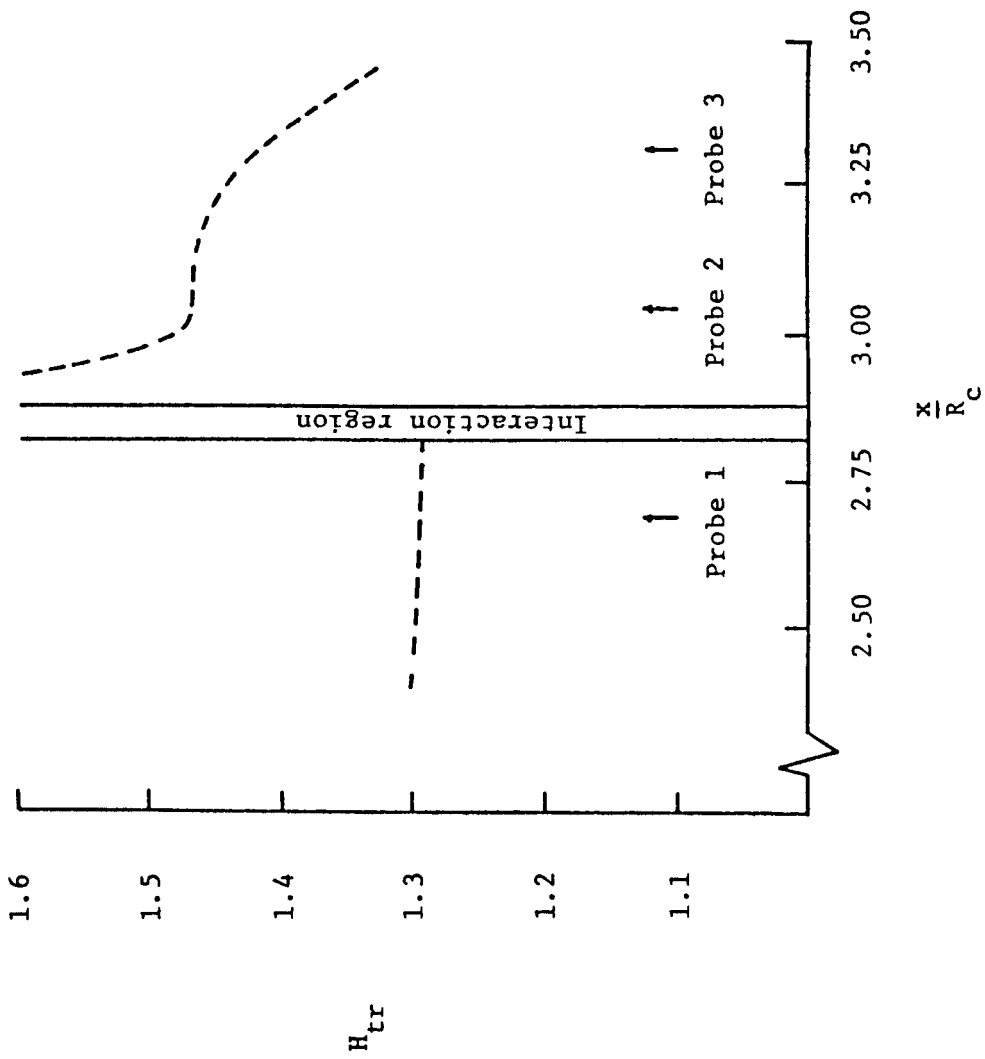
Figure 3.17 Theoretical H_{tr} vs. $\frac{x}{R_c}$ on the Centerbody
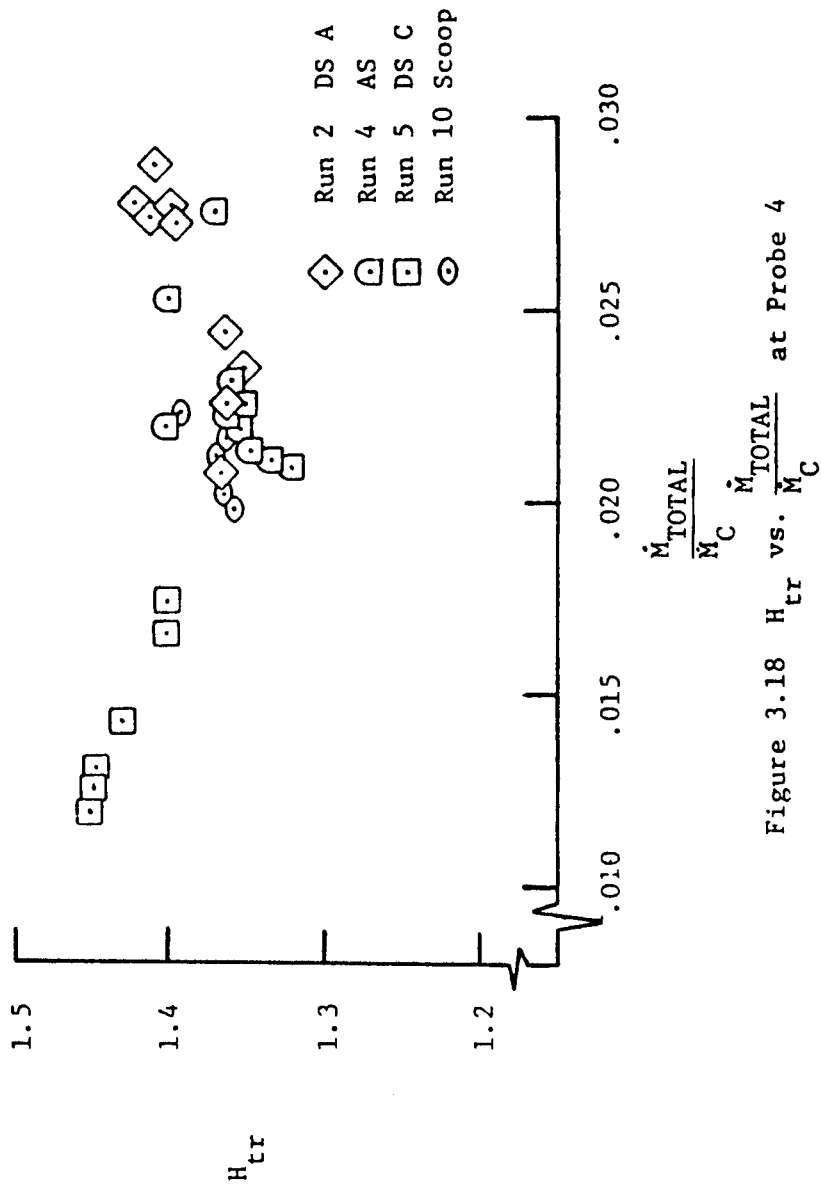
Figure 3.18 H_{tr} vs. $\frac{\dot{M}_{TOTAL}}{\dot{M}_C}$ at Probe 4

99

Figure 3.19 δ^* vs. $\frac{\dot{M}_{TOTAL}}{\dot{M}_C}$ at Probe 4

100

Figure 3.20 θ vs. $\frac{\dot{M}_{TOTAL}}{\dot{M}_C}$ at Probe 4

θ (cm)

Run 2 DS A
Run 4 AS
Run 5 DS C
Run 10 Scoop
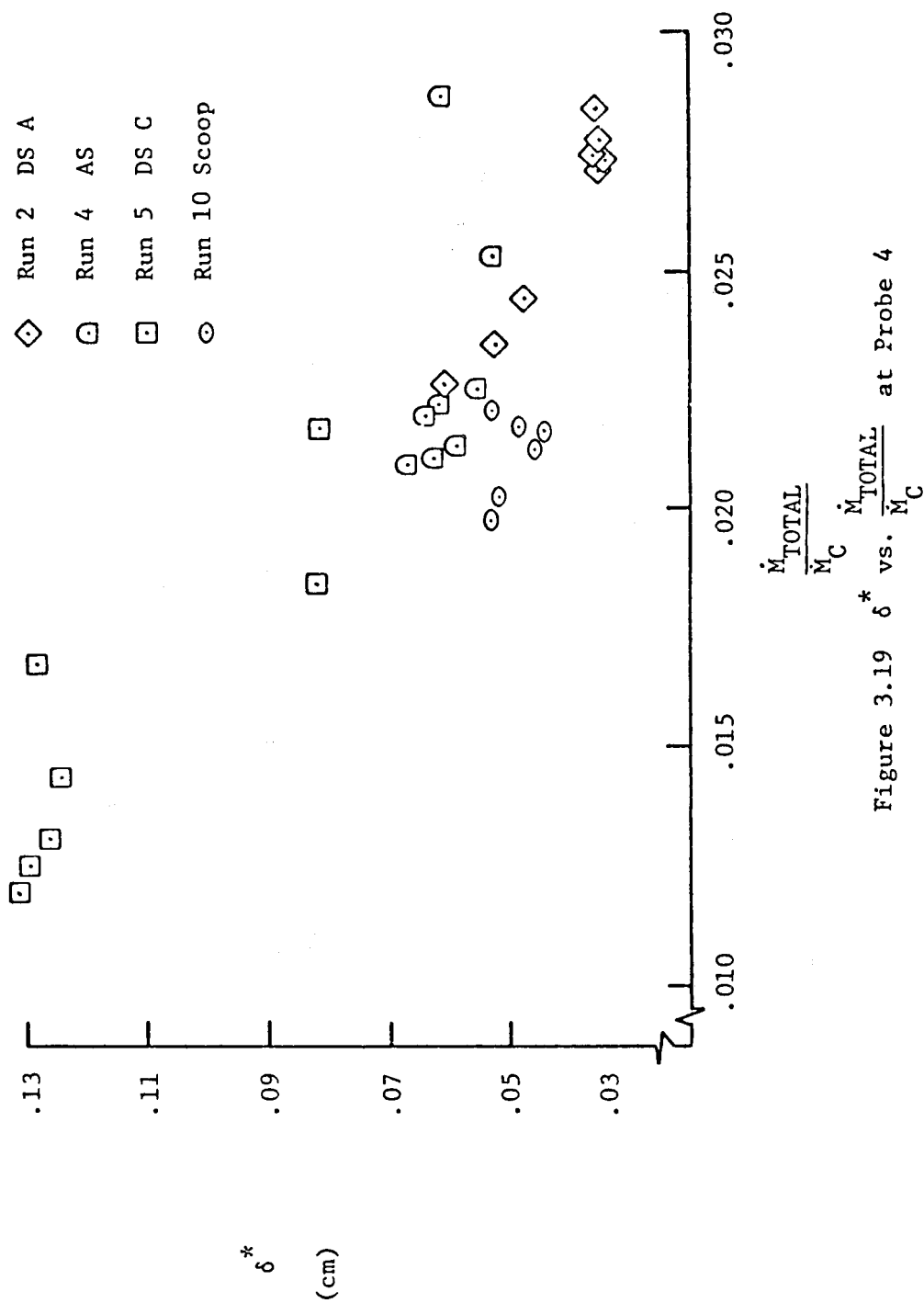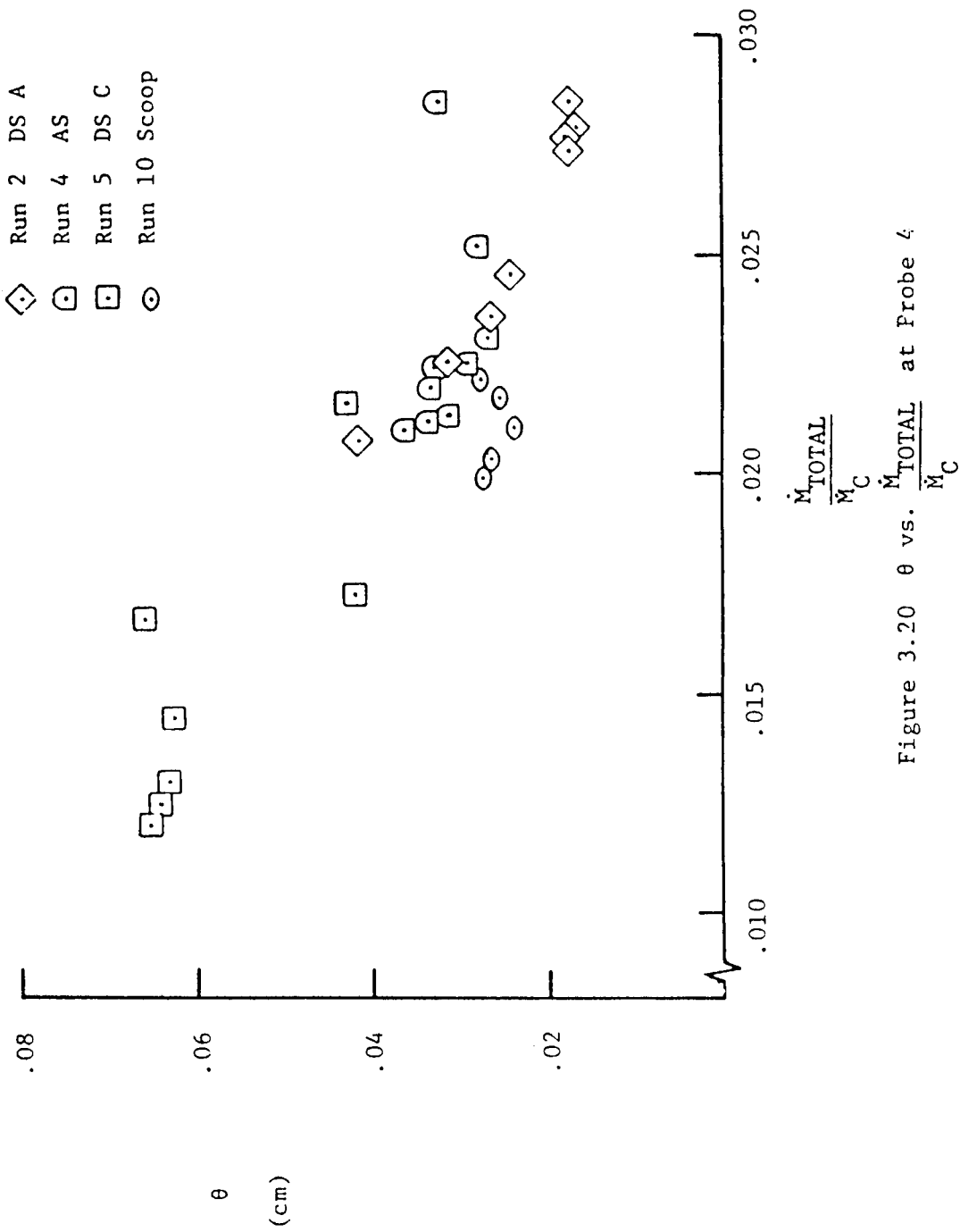
$\frac{\dot{M}_{TOTAL}}{\dot{M}_C}$
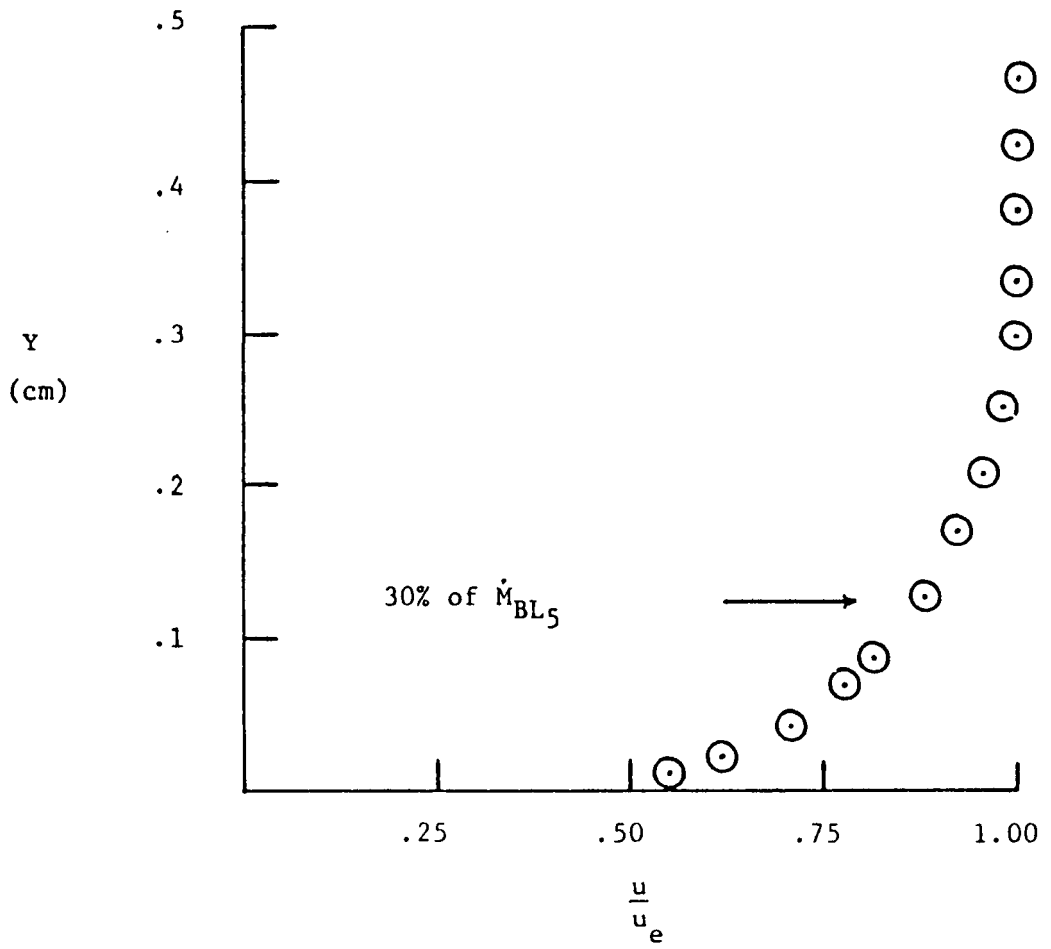
Figure 3.21 Probe 5 Boundary Layer Velocity Profile
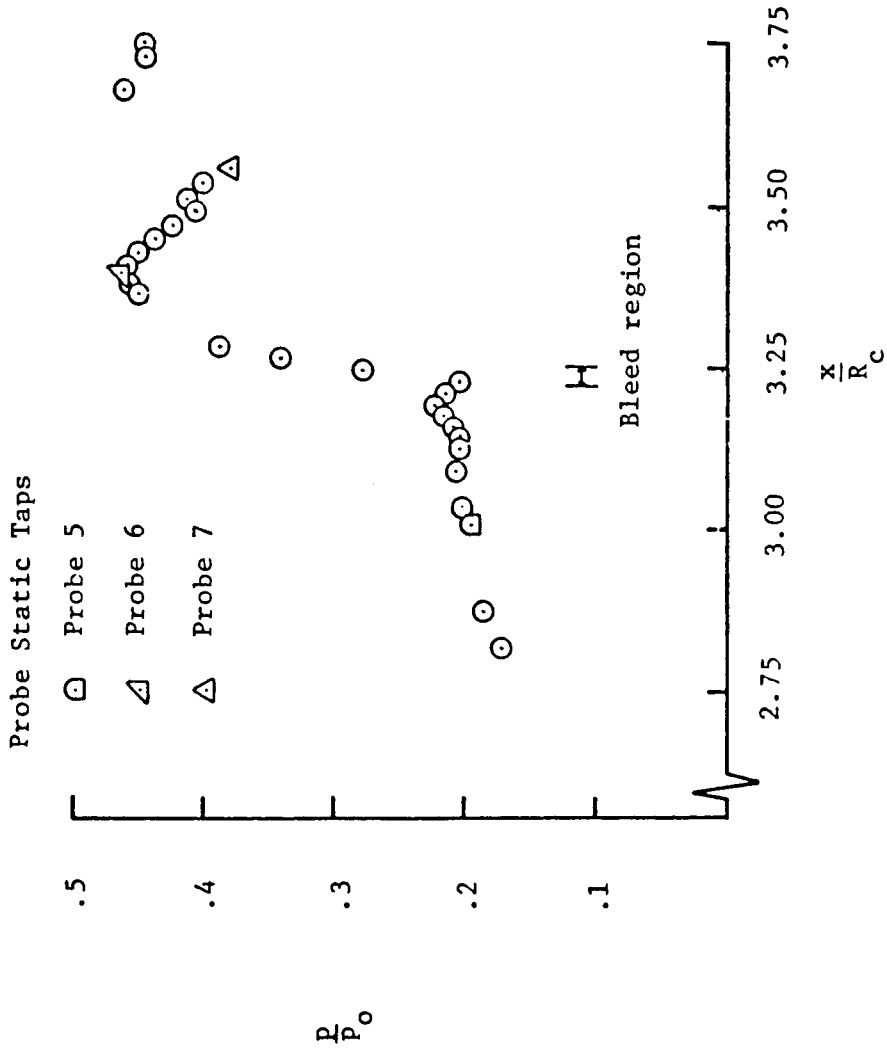
Figure 3.22   Run 2 Cowl Static Pressure Distribution
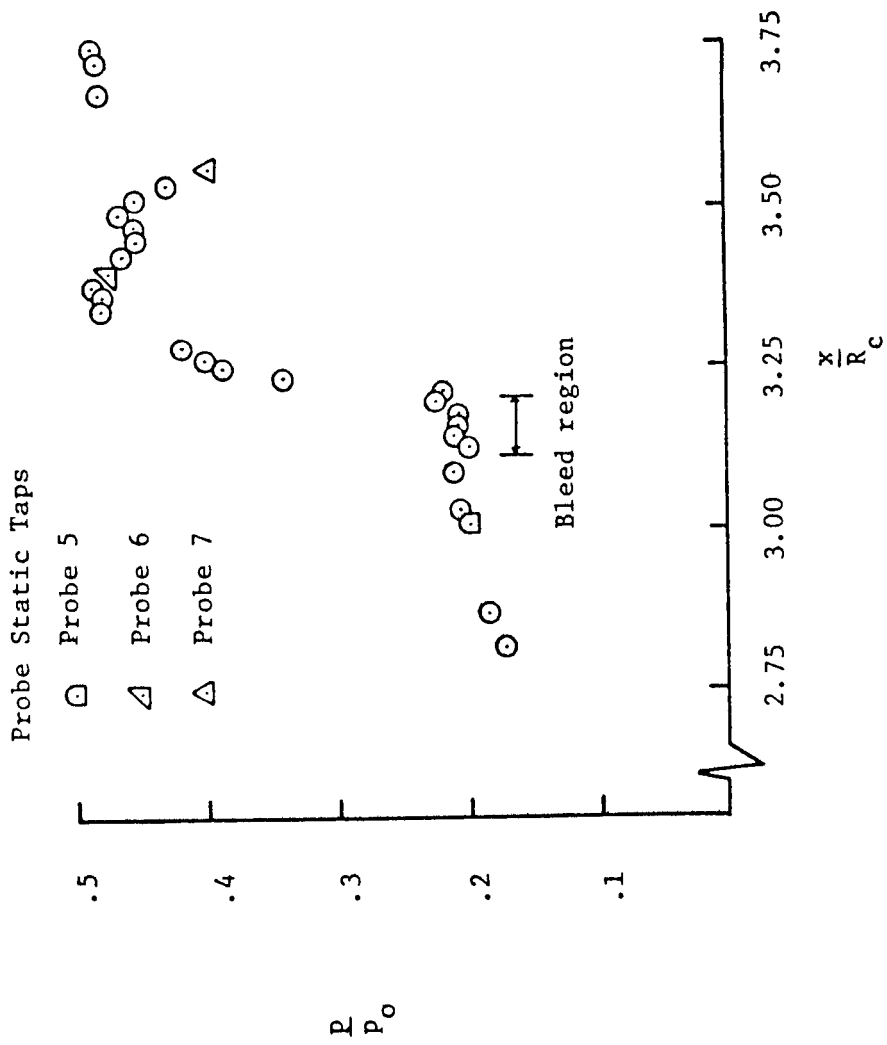
Figure 3.23 Run 4 Cowl Static Pressure Distribution

104
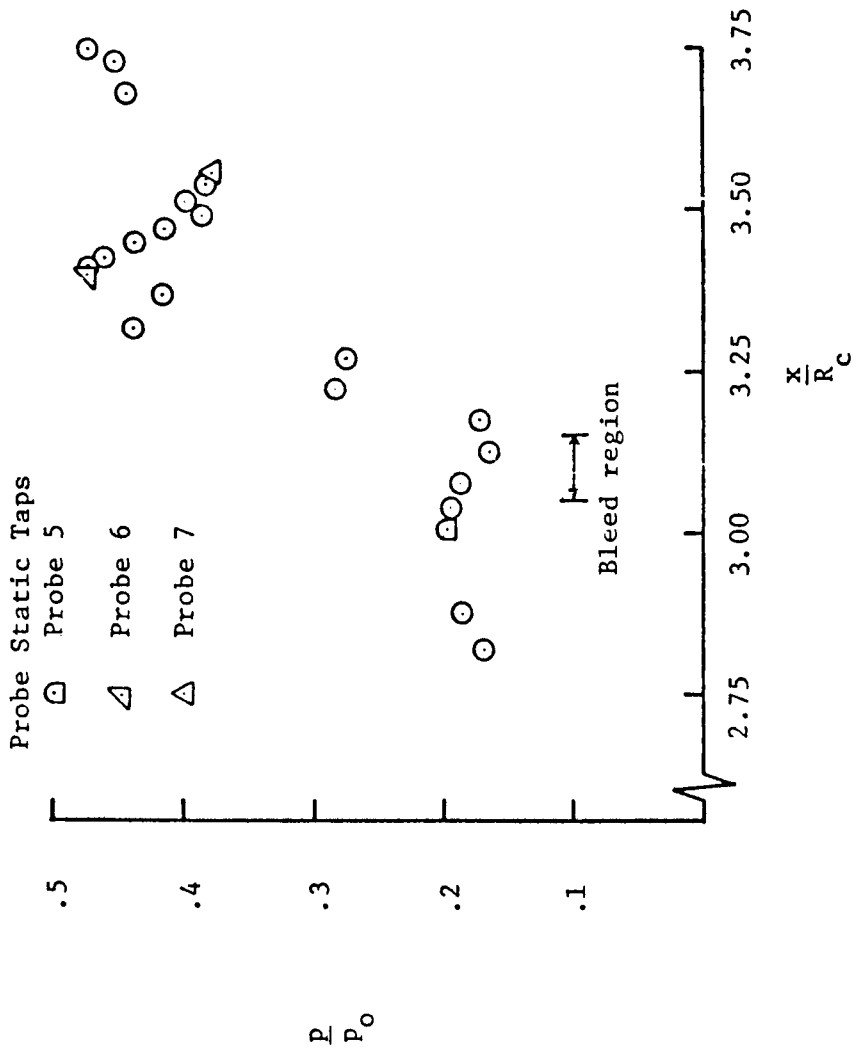
Figure 3.24 Run 5 Cowl Static Pressure Distribution
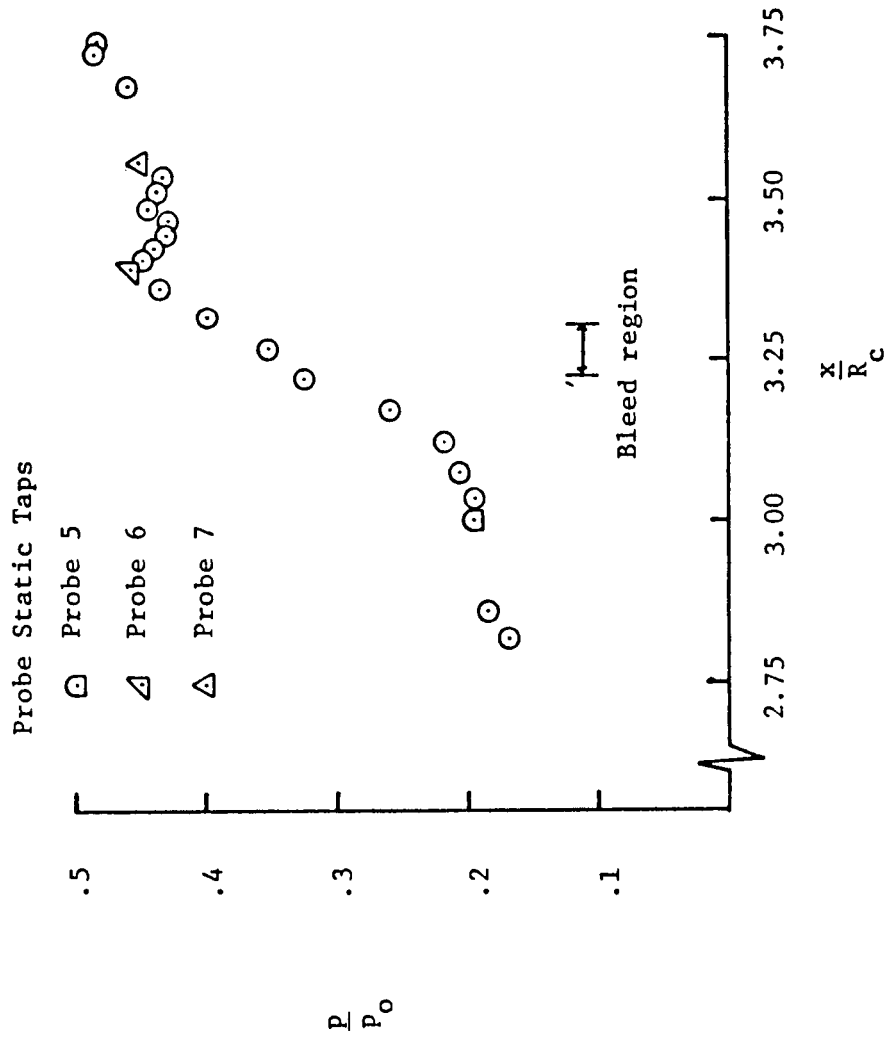
Figure 3.25   Run 6 Cowl Static Pressure Distribution
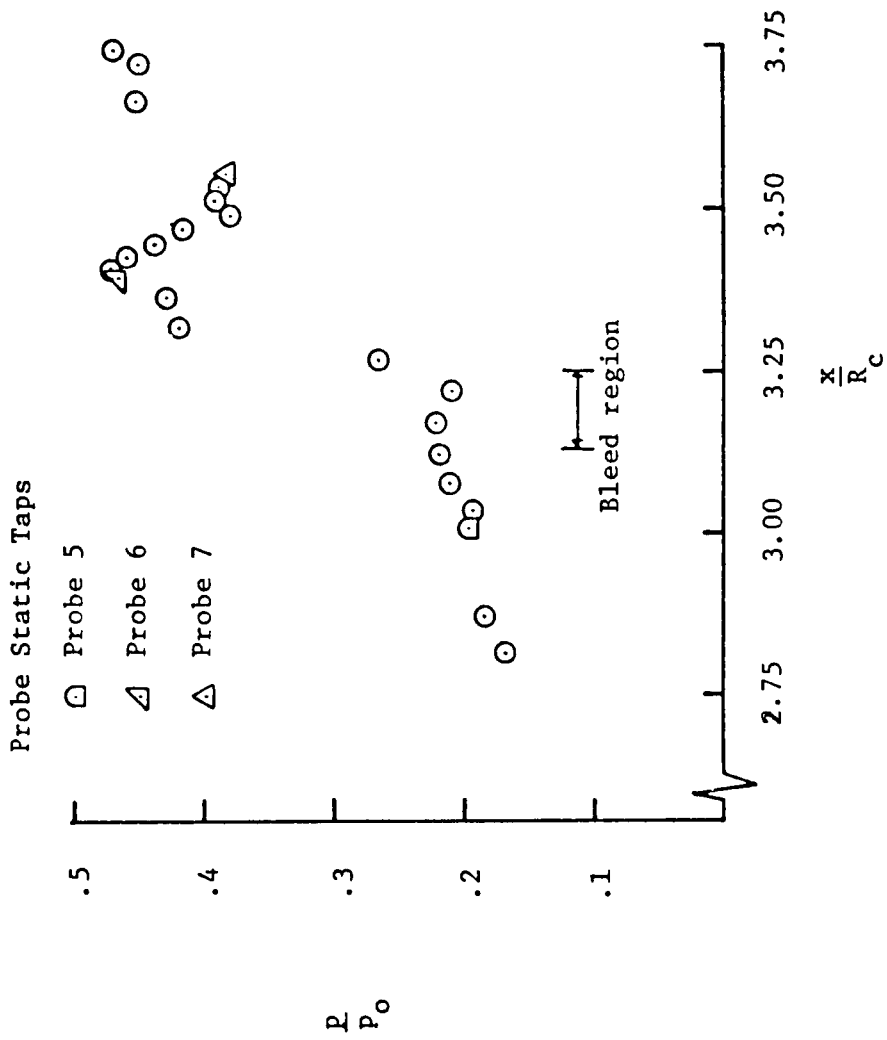
Figure 3.26 Run 7 Cowl Static Pressure Distribution

107
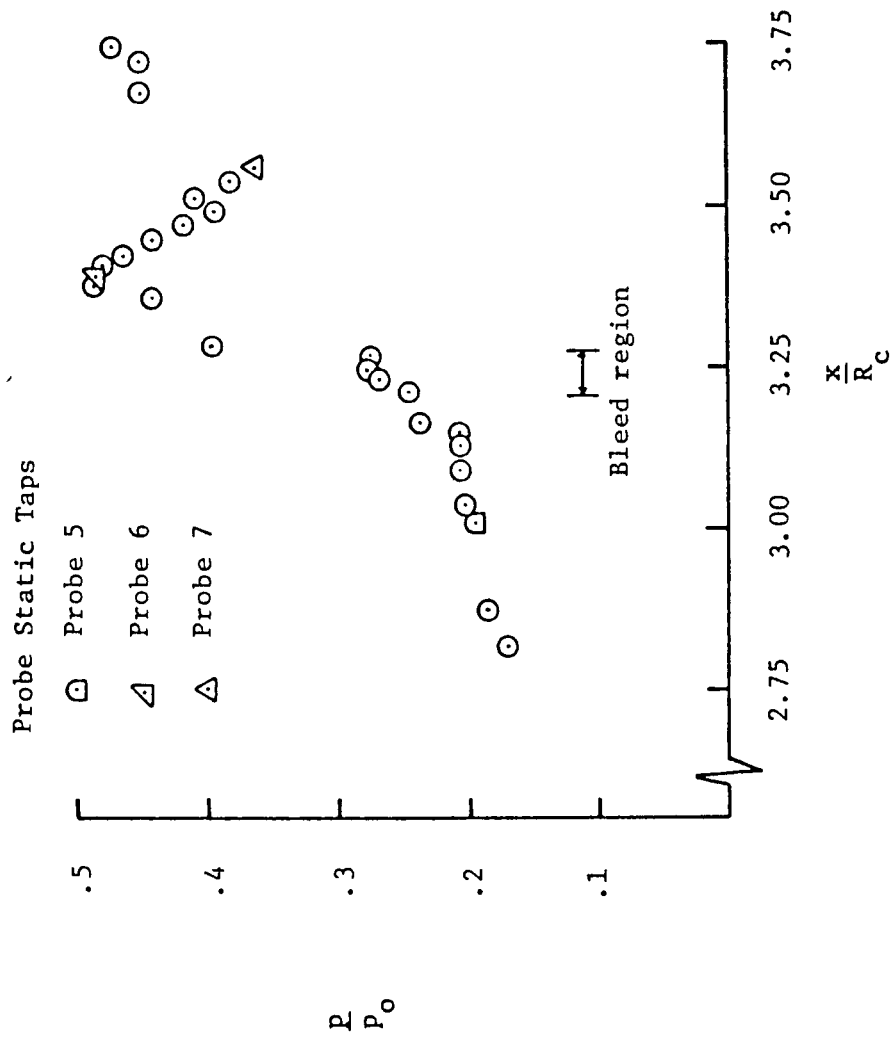
Figure 3.27 Run 8 Cowl Static Pressure Distribution

108
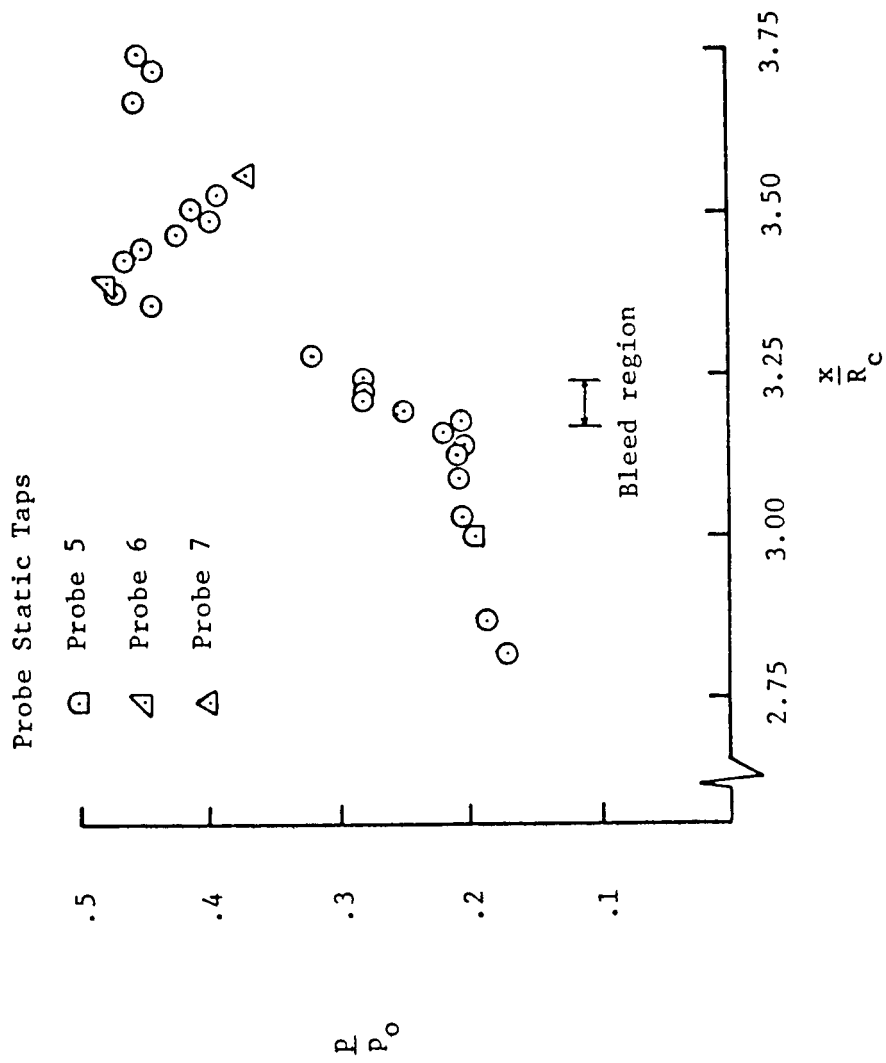
Figure 3.28   Run 9 Cowl Static Pressure Distribution
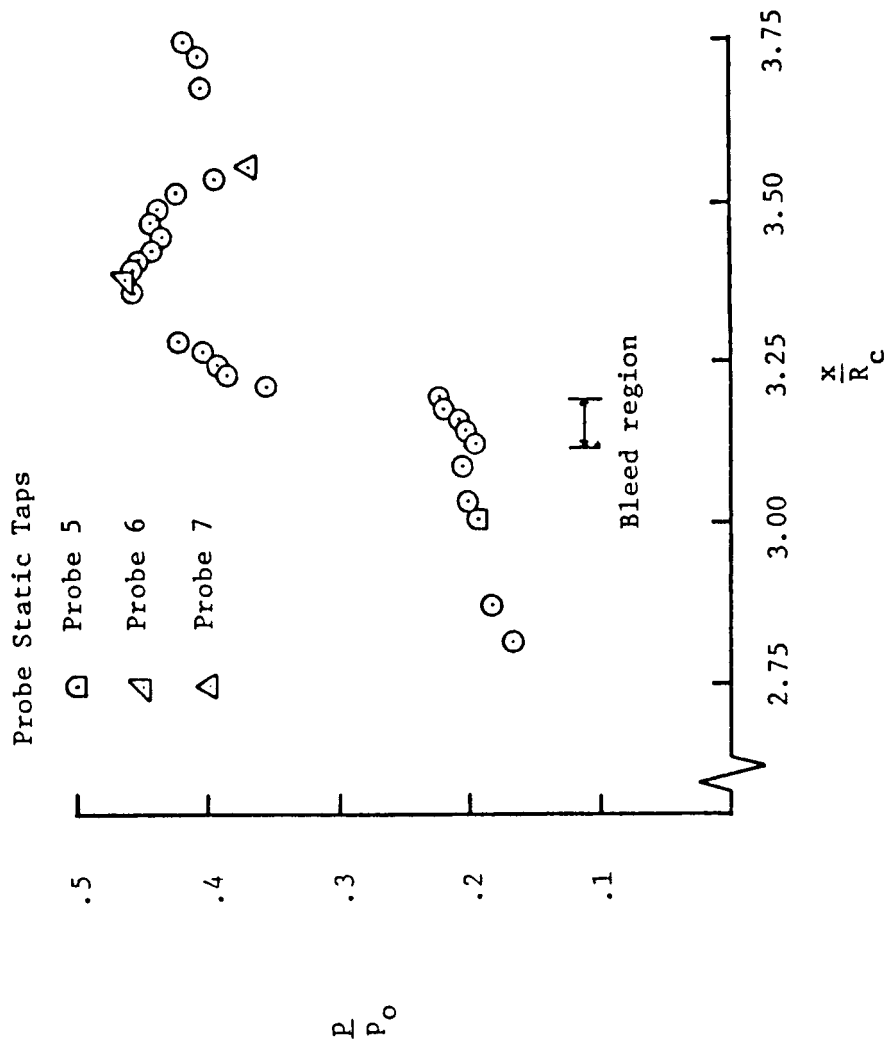
Figure 3.29 Run 10 Cowl Static Pressure Distribution
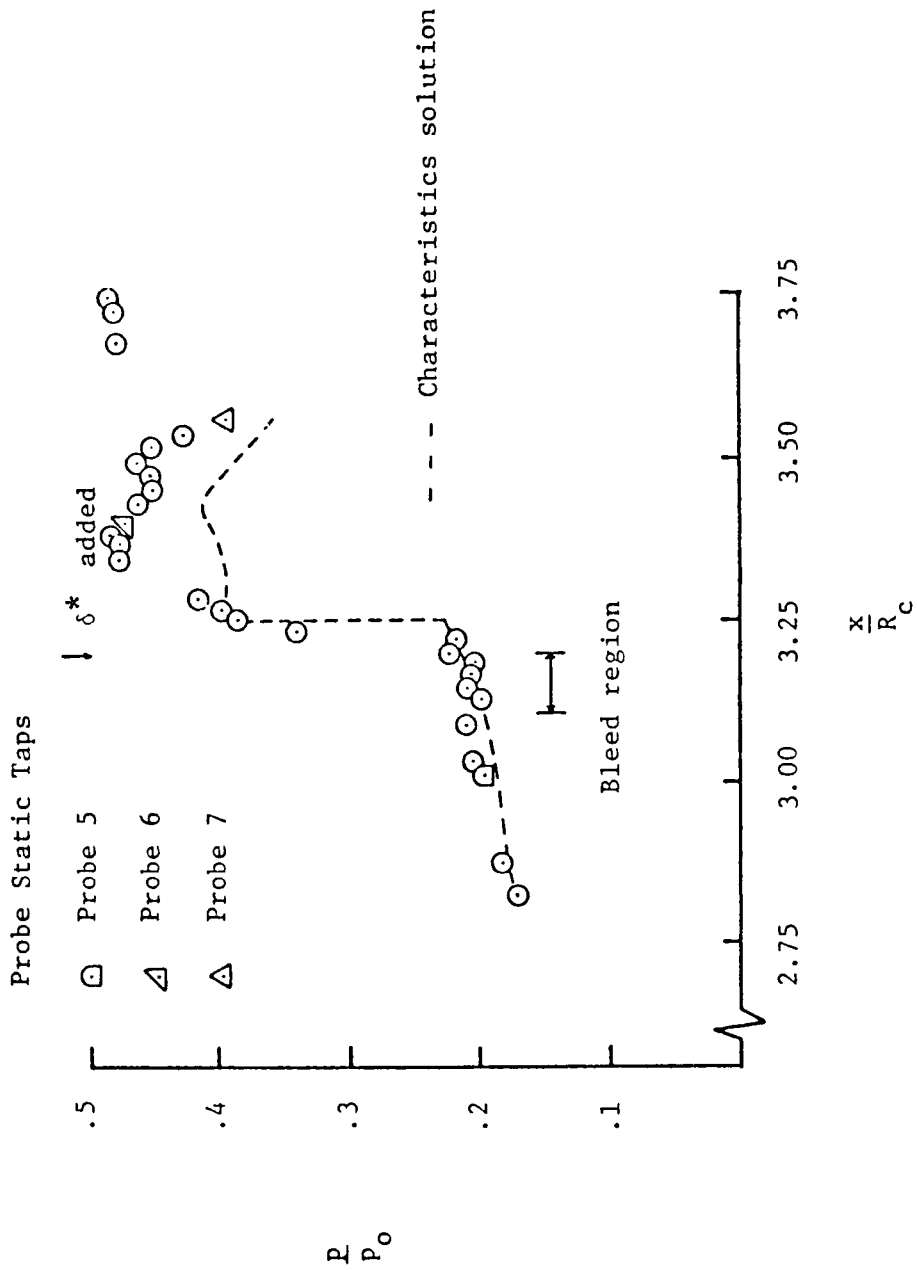
Figure 3.30 Comparison of Run 4 Cowl Static Pressure Distribution with the Method of Characteristics Solution

111
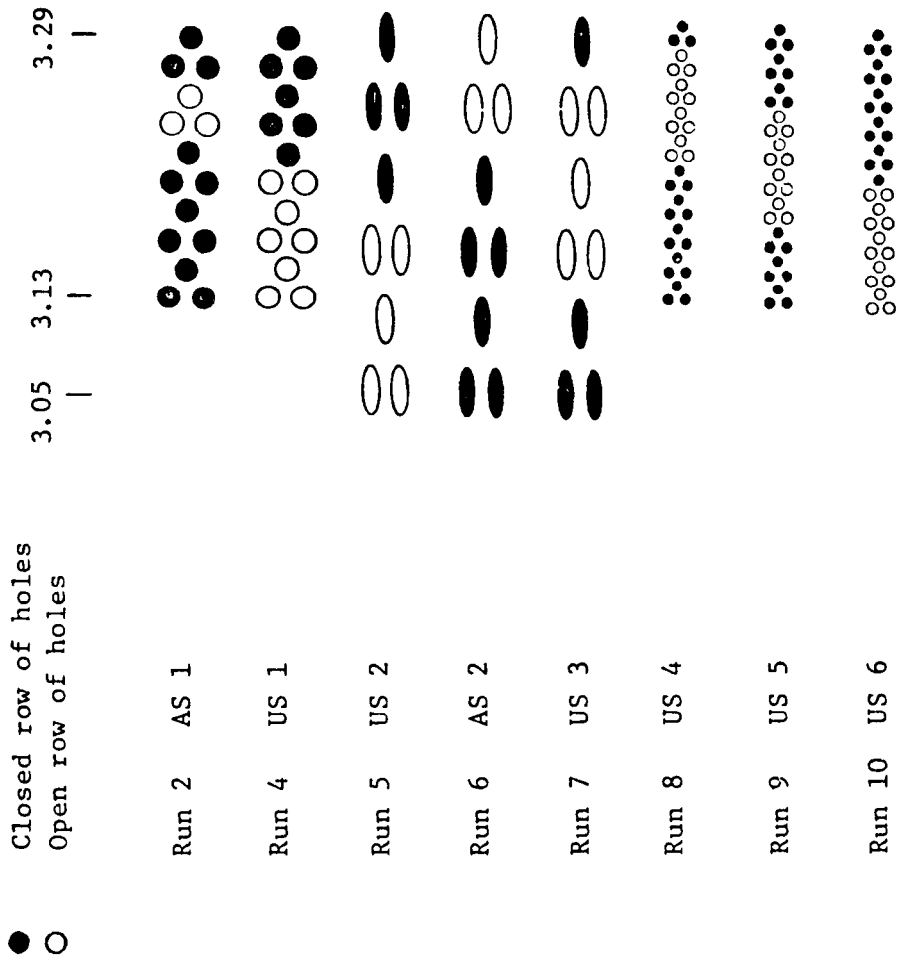
Figure 3.31 Schematic of Cowl Bleed Regions

112
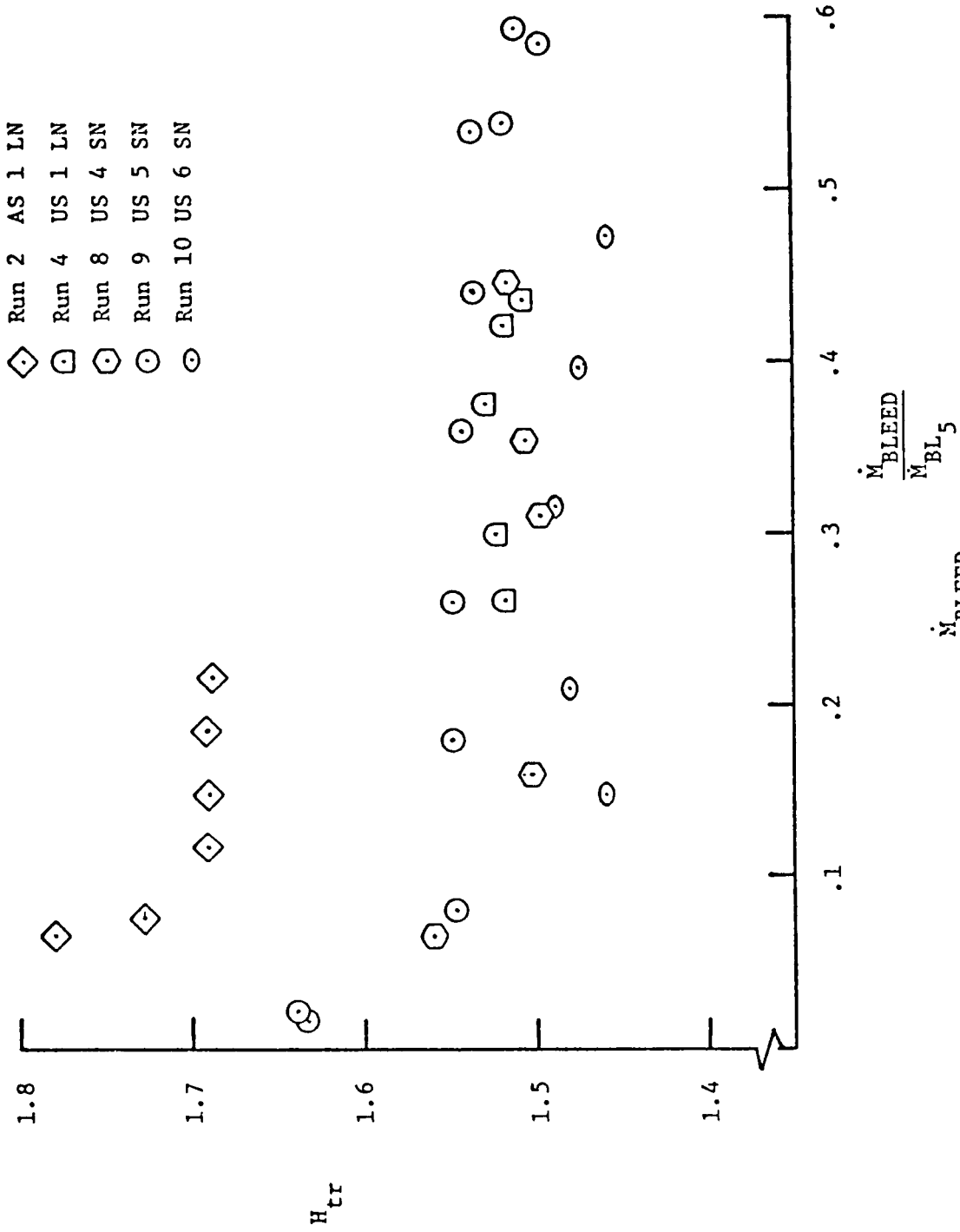
Figure 3.32 H_{tr} vs. $\dfrac{\dot{M}_{BLEED}}{\dot{M}_{BL_5}}$ at Probe 6 for Normal Hole Bleed
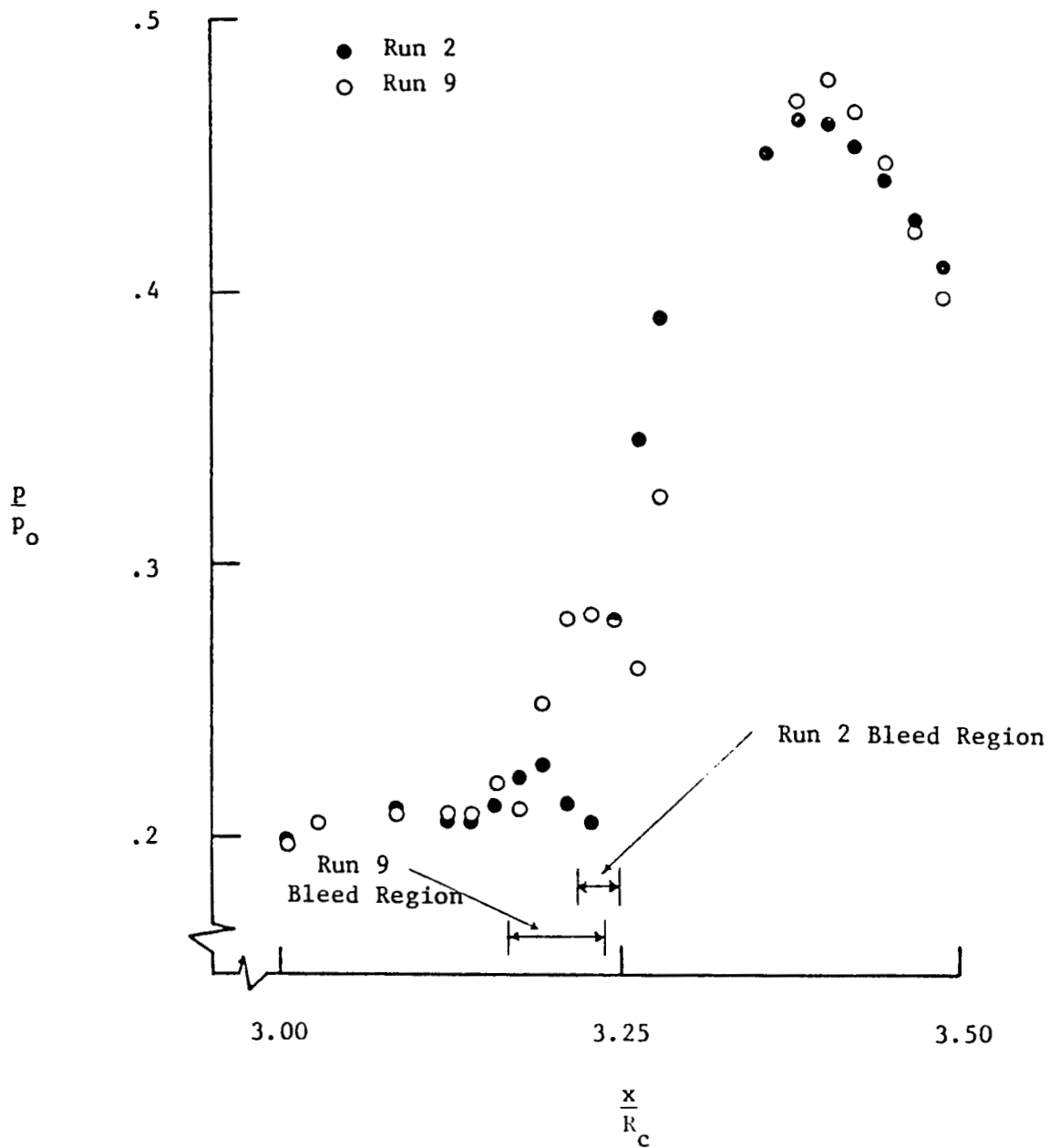
Figure 3.33 Cowl Interaction Region Static Pressure
Distributions for Runs 2 and 9
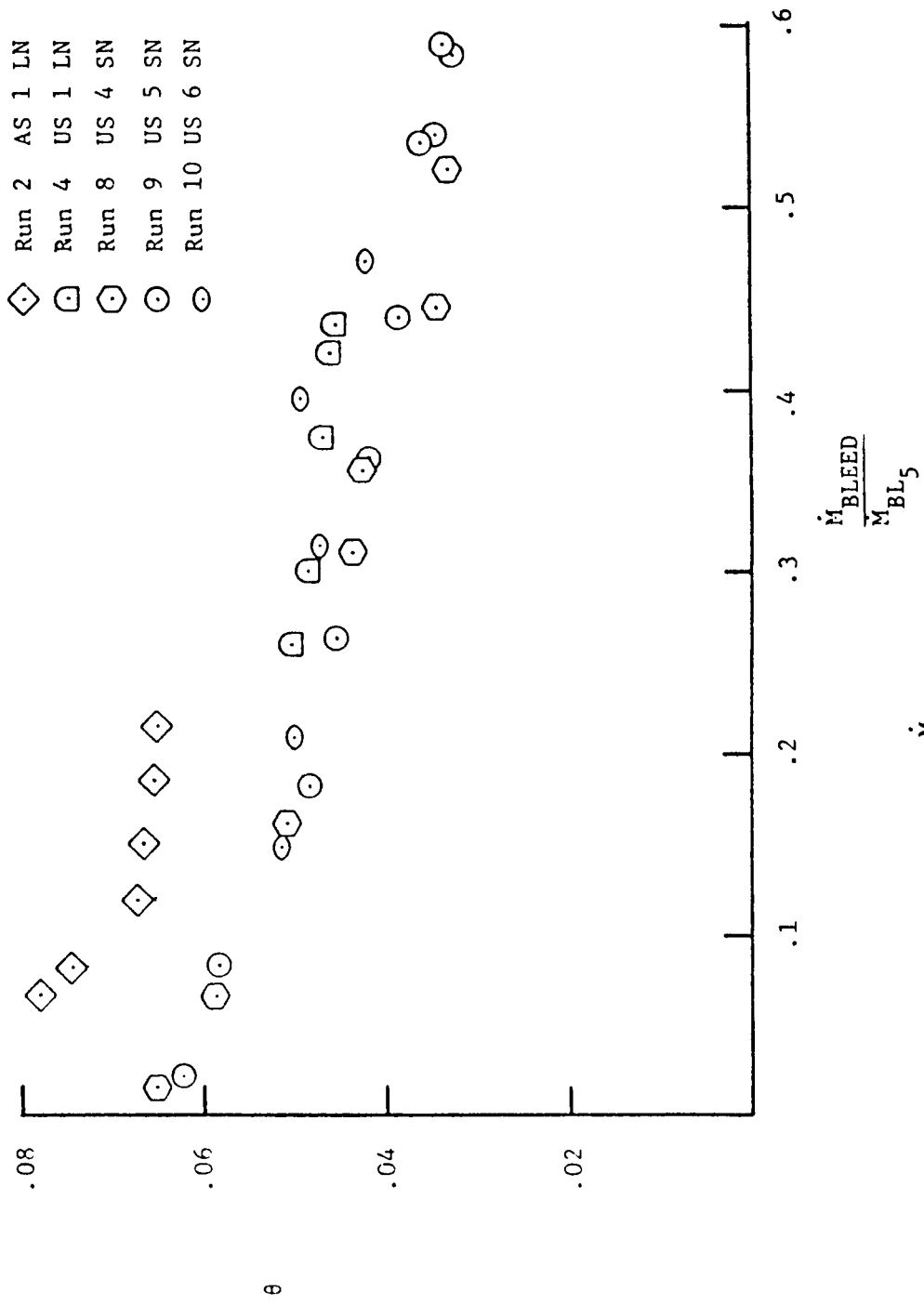
114

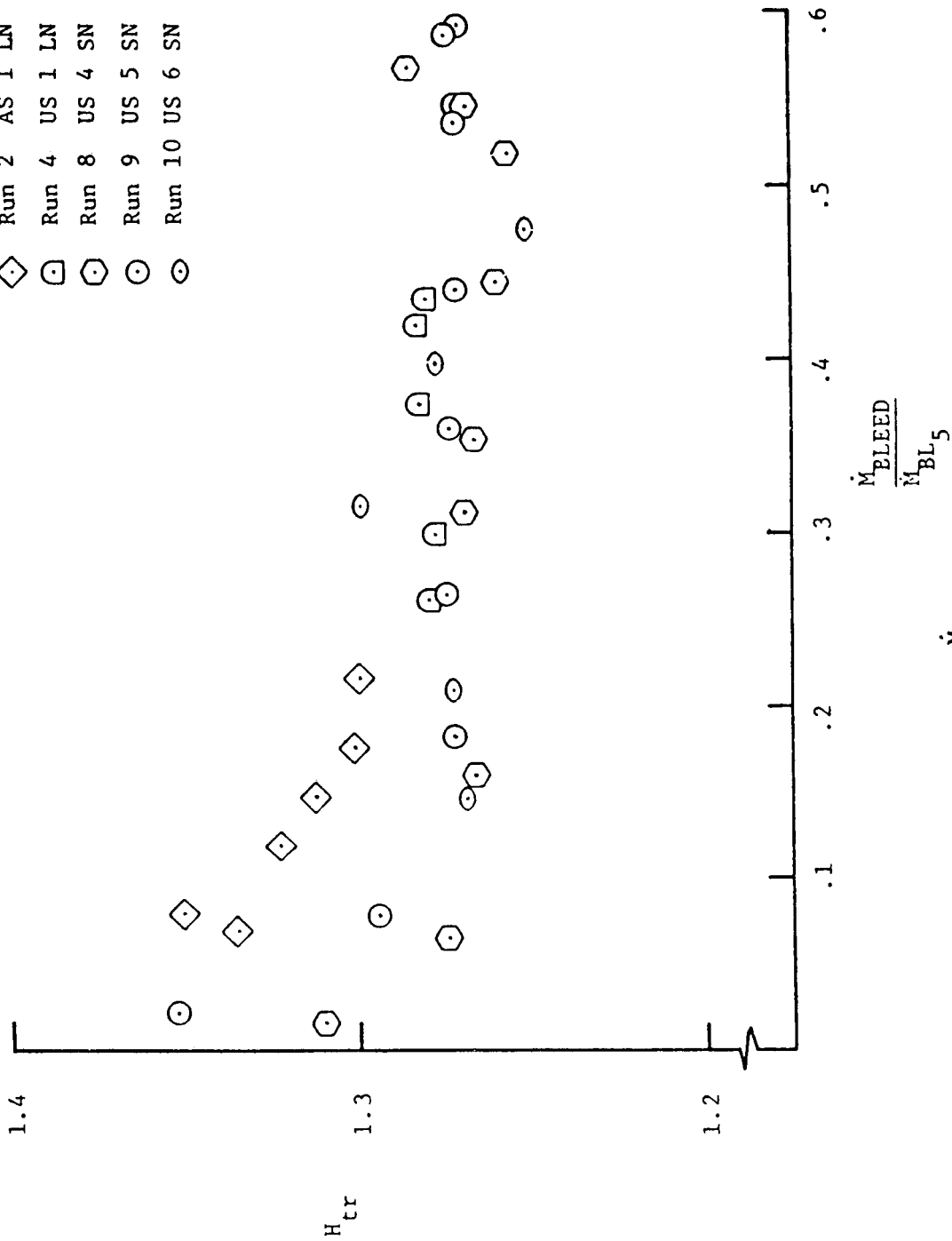Figure 3.34 δ^* vs. $\dfrac{\dot{M}_{BLEED}}{\dot{M}_{BL_5}}$ at Probe 6 for Normal Hole Bleed

Figure 3.35 θ vs. $\dfrac{\dot{M}_{BLEED}}{\dot{M}_{BL_5}}$ at Probe 6 for Normal Hole Bleed

Figure 3.36 H_{tr} vs. $\dfrac{\dot{M}_{BLEED}}{\dot{M}_{BL_5}}$ at Probe 7 for Normal Hole Bleed
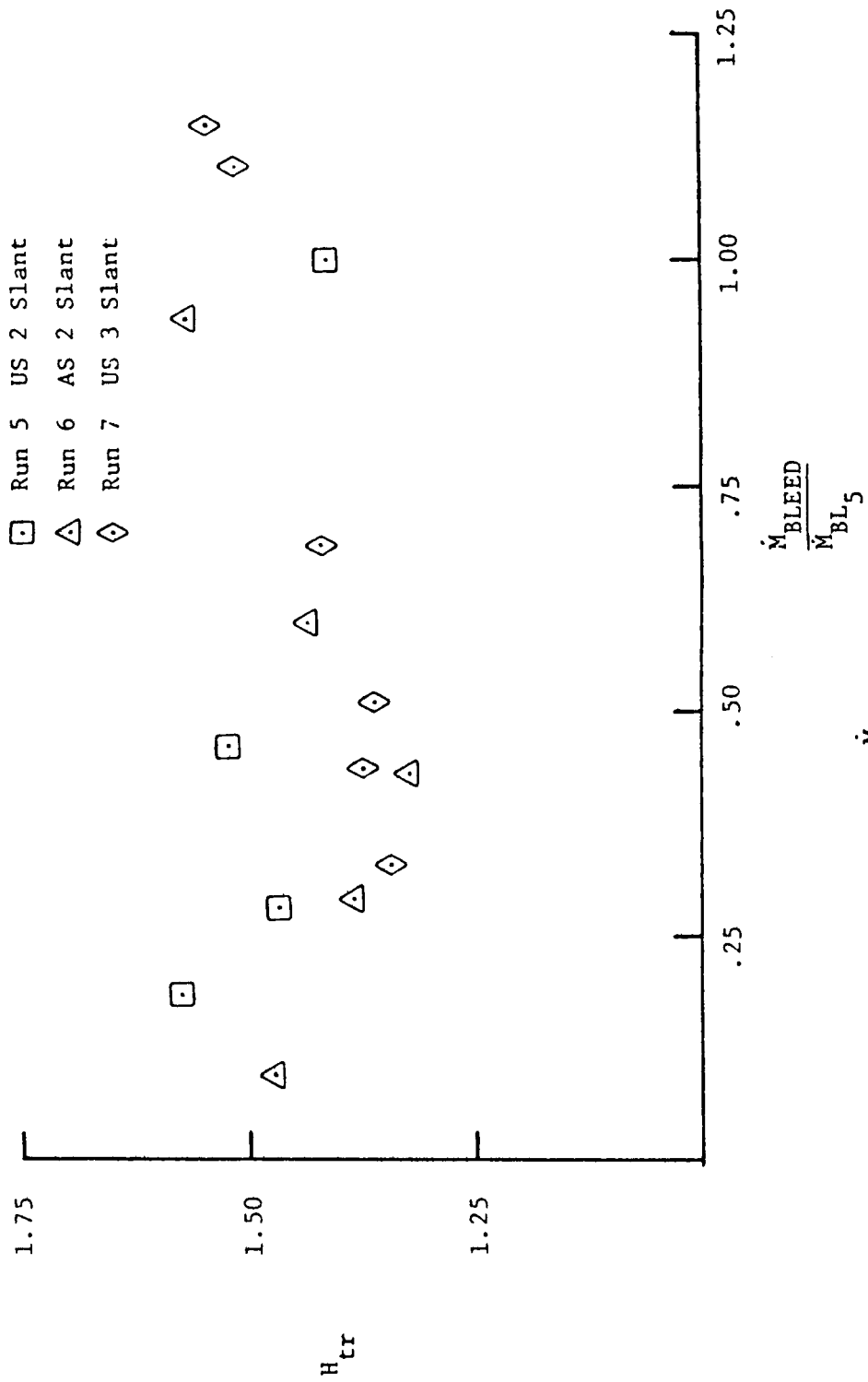
117

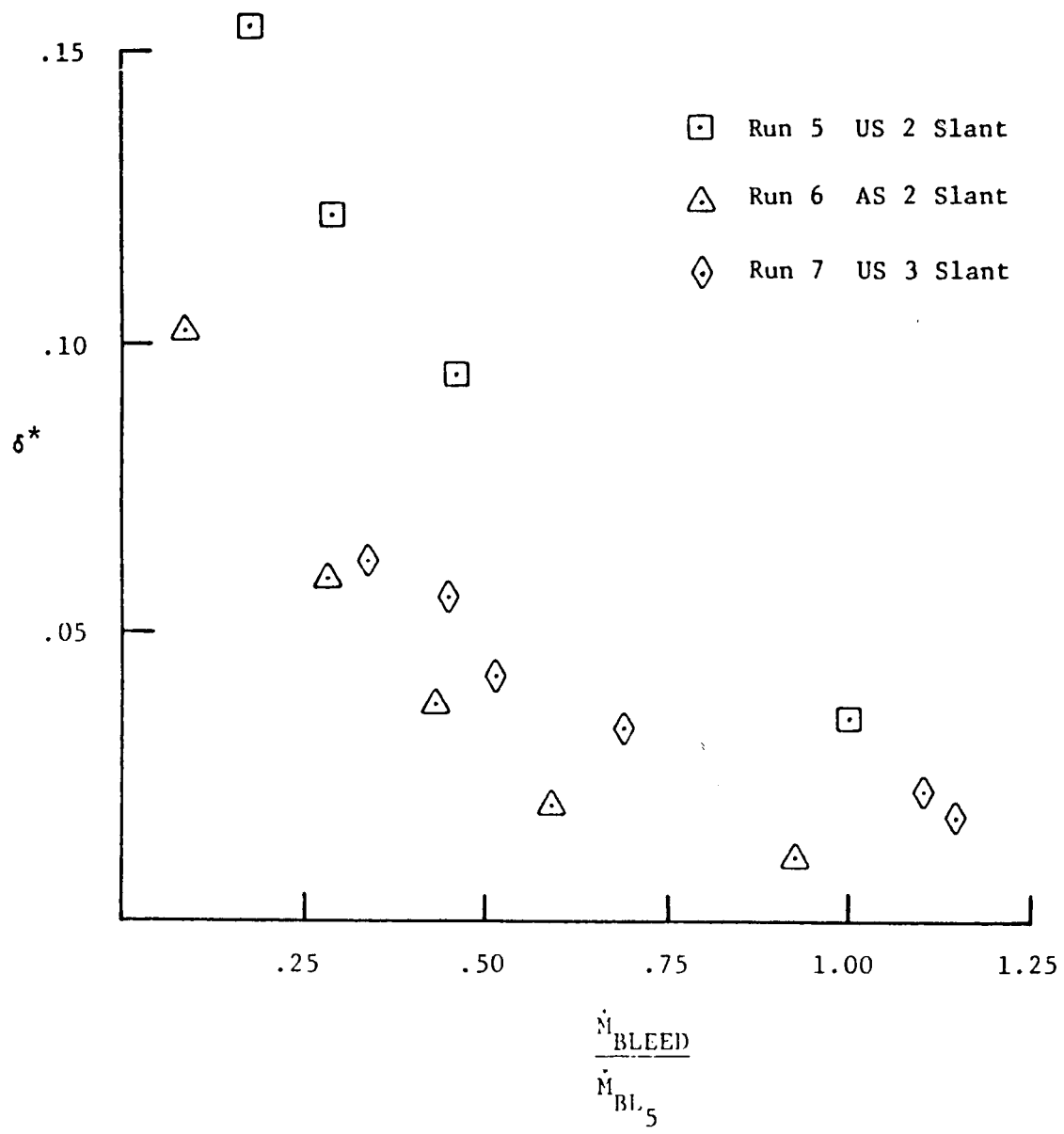Figure 3.39 H_{tr} vs. $\dfrac{\dot{M}_{BLEED}}{\dot{M}_{BL_5}}$ at Probe 6 for Slanted Hole Bleed

Figure 3.40 δ^* vs. $\dfrac{\dot{M}_{BLEED}}{\dot{M}_{BL_5}}$ at Probe 6 for Slanted Hole Bleed

121

Figure 3.41   θ vs. $\dfrac{\dot{M}_{BLEED}}{\dot{M}_{BL_5}}$ at Probe 6 for Slanted Hole Bleed

Figure 3.42 H_{tr} vs. $\dfrac{\dot{M}_{BLEED}}{\dot{M}_{BL_5}}$ at Probe 6 for Runs 6,7 and 8

Figure 3.43 H_{tr} vs. $\dfrac{\dot{M}_{BLEED}}{\dot{M}_{BL_5}}$ at Probe 7 for Slanted Hole Bleed

Figure 3.44. δ^* vs. $\dfrac{\dot{M}_{BLEED}}{\dot{M}_{BL_5}}$ at Probe 7 for Slanted Hole Bleed
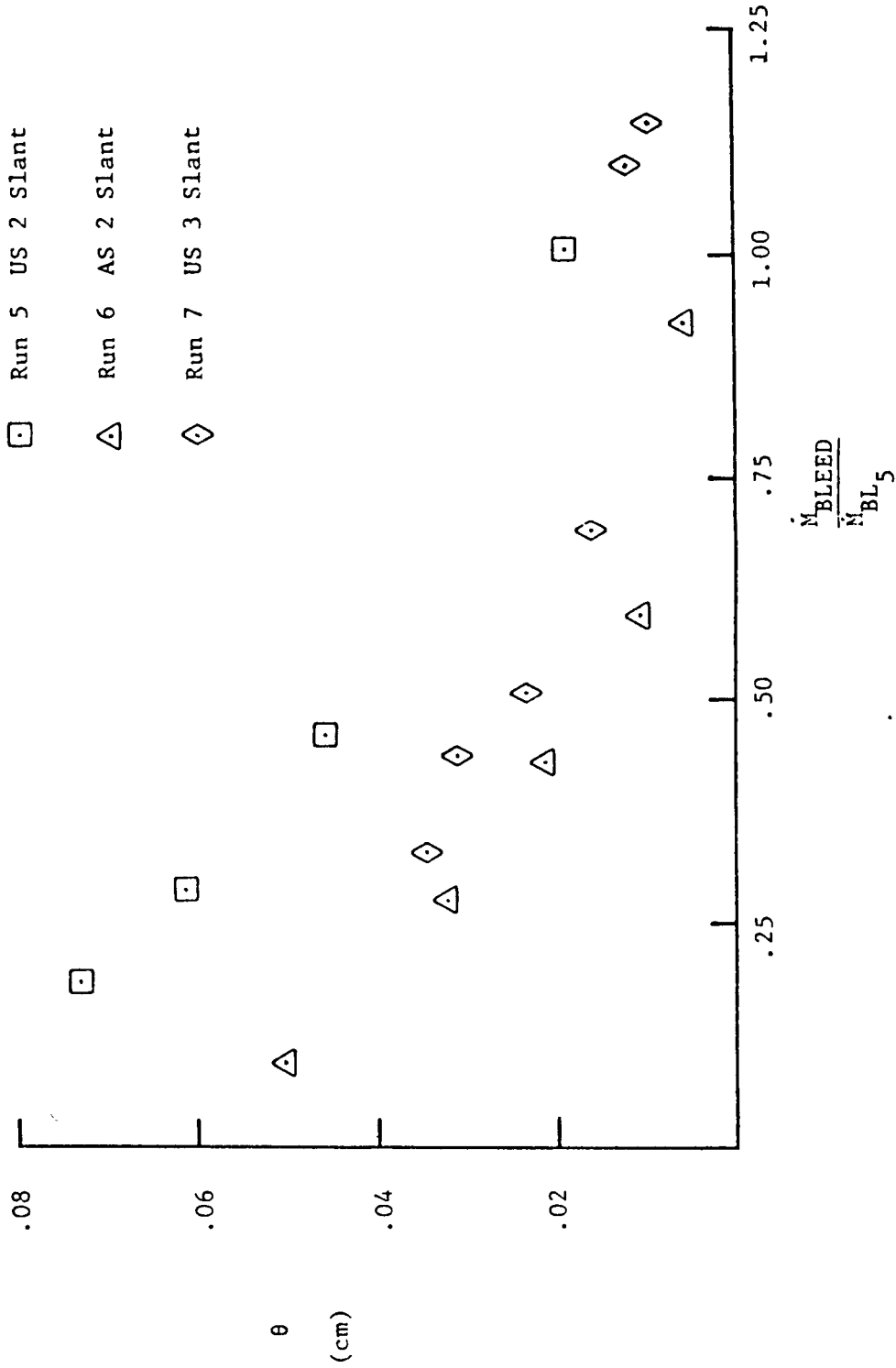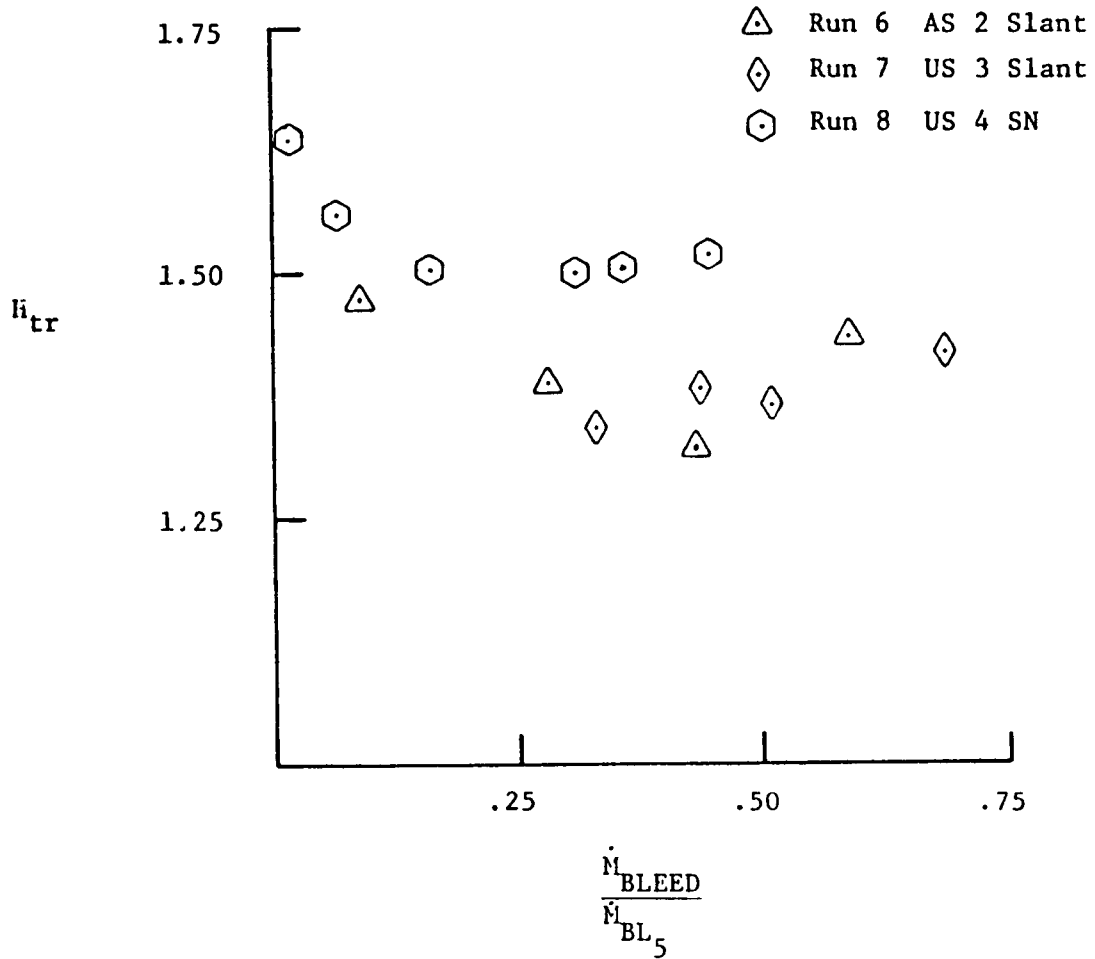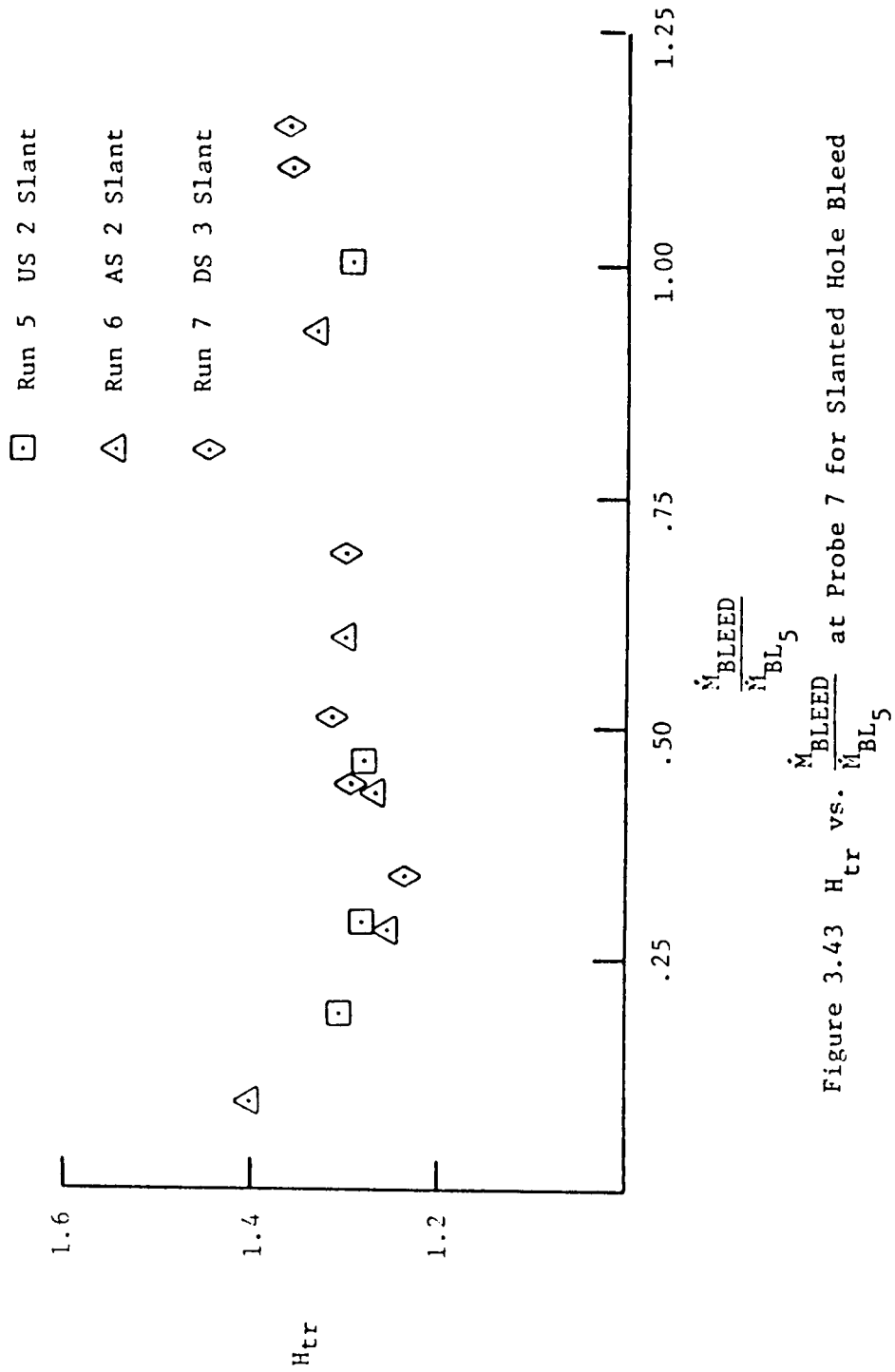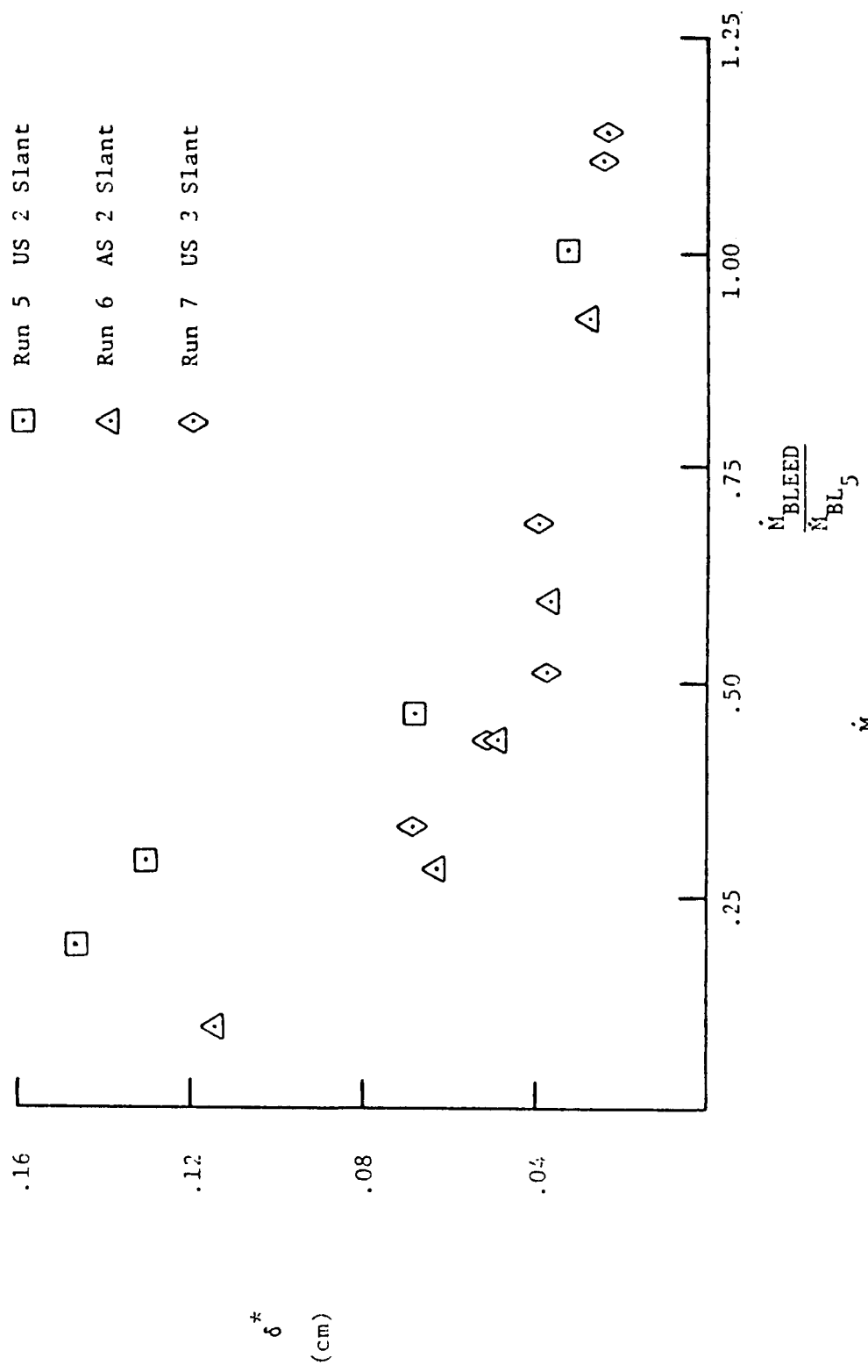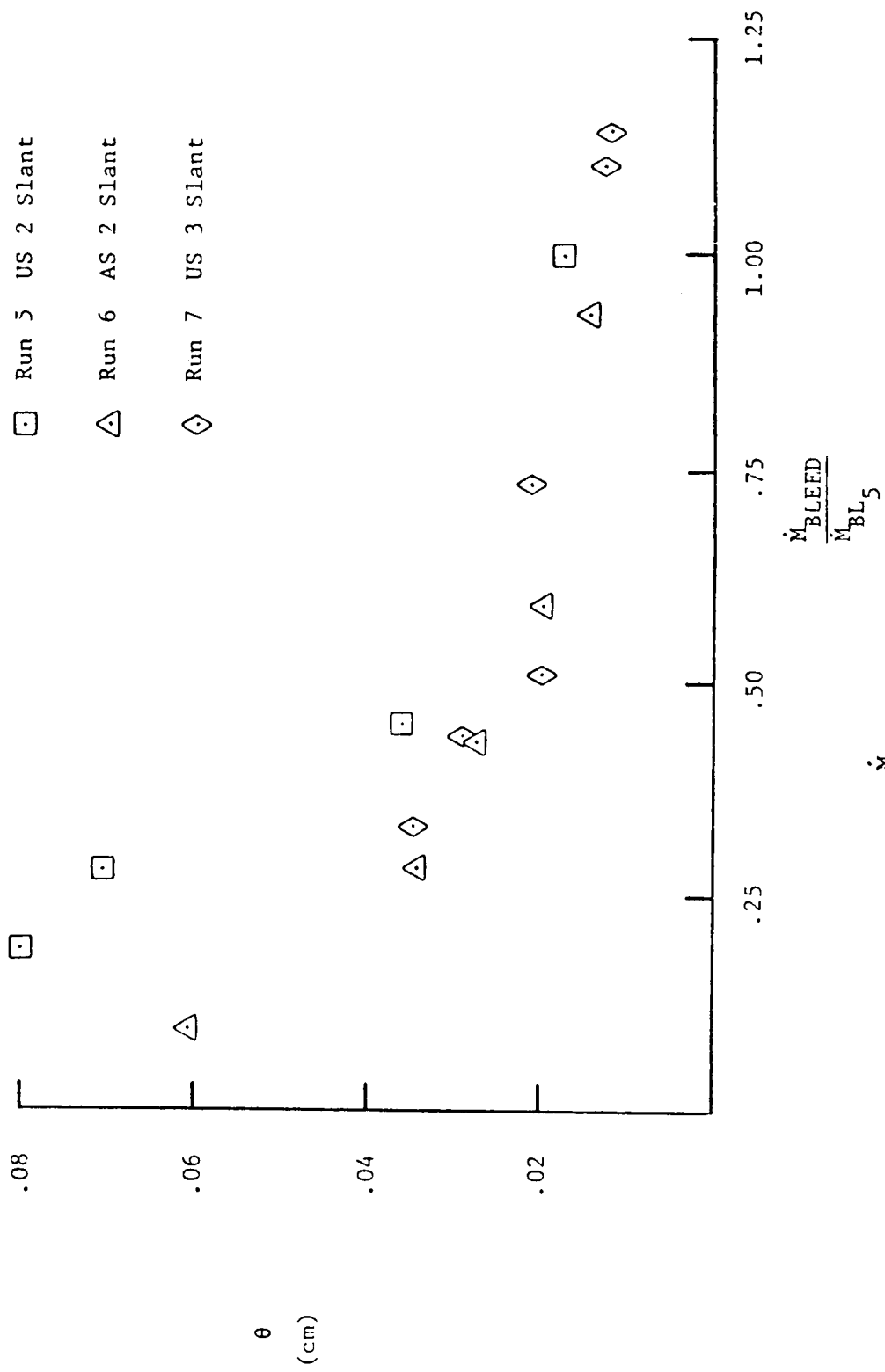
125

Figure 3.45 θ vs. $\dfrac{\dot{M}_{BLEED}}{\dot{M}_{BL_5}}$ at Probe 7 for Slanted Hole Bleed

CHAPTER IV

CONCLUSIONS

An experimental investigation was conducted to determine the effect of bleed on a boundary layer in a shock wave-boundary layer interaction in an axisymmetric, mixed compression, supersonic inlet. The effects of bleed amount and bleed region geometry on the boundary layer after a shock-boundary layer interaction region have been presented. Data have also been presented on compressor face total pressure recovery and distortion in supercritical and critical mode operation.

The results have shown that the transformed form factor, H_{tr}, directly after an interaction region, decreases with increasing bleed until a plateau is reached. The level of the plateau was found to be dependent on the placement of the bleed region relative to the shock-induced pressure rise for a given type of bleed. The plateau H_{tr} was reached within bleed mass flows of 30% to 40% of the boundary layer mass flow before the interaction region except for the slanted hole bleed configurations on the cowl, where plateau transformed form factors were obtained with bleed mass flows of 45% to 50% of the boundary layer mass flow before the interaction region.

The δ^* and θ data have shown that the plateau transformed form factors both on the centerbody and on the cowl were obtained while δ^* and θ were still decreasing. The results strongly indicate that bleed mass flow rates larger than 40% to 50% of the boundary layer mass flow before the interaction region are unnecessary. The effectiveness of bleed for smaller mass flows was dependent on bleed region location and geometry.

A comparison of bleed region configurations showed that the AS bleed configuration, open rows of holes spanning the shock-induced pressure gradient, generally had the worst performance when δ^*, θ and H_{tr} were used as criterions. The relatively large boundary layer parameters may have been due to recirculation in the bleed region. Inlet unstart occurred at low bleed mass flow rates when the AS bleed region with holes normal to the surface was used. For the geometry of this investigation, the AS type of bleed region should be avoided.

Acceptable transformed form factors for critical inlet operation were obtained by the US, DS and scoop bleed configurations. At larger bleed mass flow rates, the DS bleed configurations provided lowest form factors directly behind the interaction regions while the US bleed configurations had the lowest form factors farther downstream of the interactions. This suggested that lower values of H_{tr} obtained with the DS bleed configurations were a local effect. The results indicate somewhat smaller displacement and momentum

thicknesses for DS bleed than for US bleed. There is however not
enough overall difference between US and DS bleed to prefer one
over the other. On the centerbody in the first interaction region,
the scoop bleed configuration was very effective at maintaining
smaller transformed form factors and smaller thicknesses at the lower
bleed rates.

The results comparing the effects of normal and slanted hole
porous bleed sections on the cowl showed that the slanted hole bleed
configurations were much more effective in providing lower form
factors for a fixed amount of bleed. The slanted hole bleed regions
had much lower plateau transformed form factors but the bleed mass
flow needed to reach the plateau H_{tr} was approximately twice that
needed to reach plateau H_{tr} for the normal hole bleed configurations.
In spite of this, the slanted hole bleed regions still had lower
transformed form factors for a fixed amount of bleed.

The result comparing the effects of 0.159 cm and 0.318 cm
diameter normal bleed holes on the cowl showed that there was no
discernable effect of bleed hole size on the boundary layer after
the bleed region.

Compressor face total pressure recoveries of 89% to 90% were
achieved with bleed rates of 3% to 5% of the inlet's capture mass
flow in critical mode operation and no attempt was made to optimize
the bleed configurations for higher total pressure recoveries.
Less bleed could probably have been used with only very slight effects

on the total pressure recovery. The bypass system was not used during
this investigation, utilization of the bypass system would have in-
creased the compressor face total pressure recovery but at the
expense of usable compressor face mass flow.

Since no investigation of bleed geometry and mass flow rate in
the vicinity of the normal shock in critical operation was done, more
work in this area is needed as well as in the optimization of bleed
for maximum inlet performance.

REFERENCES

1. Cubbison, R.W., Meleason, E.T. and Johnson, D.F., "Effect of Porous Bleed in a High Performance Axisymmetric Mixed Compression Inlet at Mach 2.50", NASA TM X-1692, 1968.

2. Hingst, W.R. and Johnson, D.F., "Experimental Investigation of Boundary Layers in an Axisymmetric, Mach 2.5, Mixed Compression Inlet", NASA TM X-2902, 1973.

3. Smeltzer, D.B. and Sorensen, N.E., "Analytical and Experimental Performance of Two Isentropic Mixed Compression Axisymmetric Inlets at Mach Numbers 0.8 to 2.65", NASA TN D-7320, 1973.

4. Kilburg, R.F. and Kotansky, D.R., "Experimental Investigation of a Plane, Oblique Incident-Reflecting Shock Wave with a Turbulent Boundary Layer on a Cooled Surface", General Dynamics/Fort Worth (NASA CR-66841), Oct. 1969.

5. Strike, W.T. and Rippey, J.O., "Influence of Suction on the Interaction of an Oblique Shock with a Turbulent Boundary Layer at Mach 3.0", Rep. AEDC-TN-61-129, Arnold Engineering Development Center, Oct. 1961.

6. McLafferty, G. and Ranard, E., "Pressure Losses and Flow Coefficients of Slanted Perforations Discharging from Within a Simulated Supersonic Inlet", UAC R-0920-1, United Aircraft Corporation, 1958.

7. Smeltzer, D.B. and Sorensen, N.E., "Performance Estimates for a Supersonic Axisymmetric Inlet System", AIAA Paper No. 72-45 presented at the 10th Aerospace Sciences Meeting, San Diego, California, January 1972.

8. Syberg, J. and Koncsek, J.L., "Bleed System Design Technology for Supersonic Inlets", AIAA Paper 72-1138 presented at the AIAA/ SAE 8th Joint Propulsion Conference, New Orleans, Louisiana, Nov-Dec. 1972.

9. Sasman, P.K. and Cresci, R.J., "Compressible Turbulent Boundary Layers with Arbitrary Pressure Gradient and Heat Transfer", AIAA J., Vol. 9, No. 1, January 1966, pp. 19-25.

10. Seebaugh, W.R., Paynter, G.C., and Childs, M.E., "Calculation of Turbulent Boundary Layer Characteristics Across an Oblique Shock Reflection including the Effects of Mass Bleed", J. Aircraft, Vol. 5, No. 5, Sept.-Oct. 1968, pp. 461-467.

11. Sorenson, V.L., "Computer Program for Calculating Flow Fields in Supersonic Inlets", NASA TN D-2897, 1965.

12. Anderson, B.H., "Design of Supersonic Inlets by a Computer Program Incorporating the Method of Characteristics", NASA TN D-4960, 1969.

13. Sanders, B.W. and Mitchell, G.A., "Increasing the Stable Operating Range of a Mach 2.5 Inlet", NASA TM X-52799, 1970.

14. "10-By 10-Foot Supersonic Wind Tunnel, The Lewis Unitary Plan", Lewis Research Center - NASA, 1959.

15. Young, A.D. and Maas, J.N., "The Behavior of a Pitot Tube in a Transverse Pressure Gradient", R. &. M. 1770, British ARC, 1936.

16. MacMillan, F.A., "Experiments on Pitot Tubes in a Shear Flow", R.&M. 3028, British ARC, 1957.

17. Allen, J.M., "Impact Probe Displacement in a Supersonic Turbulent Boundary Layer", AIAA J., Vol. 10, No. 4, April 1972.

18. Wilson, R.E., "Aerodynamic Interference of Pitot Tubes in a Turbulent Boundary Layer at Supersonic Speed", AIAA J., Vol. 11, No. 10, Oct. 1973.

19. Wilson, R.E. and Young, E.C., "Aerodynamic Interference of Pitot Tubes in a Turbulent Boundary Layer at Supersonic Speed", CF 1351 Defense Research Laboratory, Univ. of Texas, Dec. 1949.

20. Green, J.E., "Interactions Between Shock Waves and Turbulent Boundary Layers", RAE-TR-69098, Royal Aircraft Establishment, May 1969.

21. Cubbison, R.W., Meleason, E.T. and Johnson, D.F., "Performance Characteristics from Mach 2.58 to 1.98 of an Axisymmetric Mixed Compression Inlet System with 60 Percent Internal Contraction", NASA TM X-1739, 1969.

22. Choby, D.A., "Tolerance of Mach 2.50 Axisymmetric Mixed Compression Inlets to Upstream Flow Variations", NASA TM X-2433, 1972.

23. Unpublished data obtained at the Lewis Research Center.

24. Hingst, W. R. and Towne, C. E., "Comparison of Theoretical and Experimental Boundary Layer Development in a Mach 2.5 Mixed-Compression Inlet", NASA TM X-3026, 1974.

APPENDIX A

ASSUMPTIONS IN DATA REDUCTION PROCEDURE

When the boundary layer calculations were made, several assumptions were made as the traversing pitot tubes gave only total pressure information. These assumptions were:

(1) $\dfrac{\partial p}{\partial y} = 0$ in the boundary layer

and

(2) the total temperature profile was a Crocco integral distribution (Pr = 1).

$$\frac{T}{T_e} = \frac{T_w}{T_e} + (1 - \frac{T_w}{T_e}) \frac{u}{u_e} + \frac{u_e^2}{2c_p} (\frac{u}{u_e} - (\frac{u}{u_e})^2)$$

where it has also been assumed that

$$h = c_p T$$

Since the wall temperature, T_w, was very close to the adiabatic wall temperature, assumption (2) was thought to be valid. Since the pitot probes were away from the immediate vicinity of the shock-boundary layer interaction region, assumption (1) was also valid.